Experimental assessment of properties for a non-aqueous and precipitating alkanolamine absorption system

by

Erik Robertsson

Department of Chemical Engineering

Lund University

June 2022

Supervisor: **Senior Lecturer Helena Svensson**

Co-supervisor: **Postdoctoral researcher Hanna Karlsson**

Examiner: **Professor Christian Hulteberg**

Postal address
P.O Box 124
SE-221 00 Lund, Sweden
Web address
www.lth.se/chemeng

Visiting address
Naturvetarvägen 14

Telephone
+46 46-222 82 85
+46 46-222 00 00

Acknowledgements

I want to start by thanking my supervisor Helena Svensson for enabling me to do this master thesis project at the Department of Chemical Engineering. Together with my co-supervisor, Hanna Karlsson, you have during this period helped and listened to my concerns, questions, and thoughts around the master thesis project and more. For that, and your support in completing the master thesis, I am very grateful to the both of you.

Moreover, I would like to thank the persons at the Department of Chemistry that have shown an interest in my master thesis project, especially the persons situated on Floor +1. I would also like to thank Mikeal Sjölin and Mats Galbe for their help with equipment on Floor -1. Thanks to Ann-Sofi Jönsson who helped me with the report. I would also like to thank Selda, who I have shared an office space with. It has been nice to share the struggles of writing our respective theses with you, and best of luck moving forward.

Furthermore, I would like to thank my family and my girlfriend Noemi for the immense support they have provided to me when I have struggled, worried, or contemplated over my laboratory work or the writing process. I love you all, and it is thanks to you that I have been able to complete any of this.

I would also like to thank the friends I have made during my studies, especially the two friend groups, the bio-engineering group and the chemical engineering organisation, I have had the pleasure to be a part of through my studies here at Lunds Tekniska Högskola. Good luck to all of you moving forward, and let's make our common future sustainable and bright! Thanks especially to Lucas Werner for all the fun things we have done together during these five years! Best of luck!

Lastly, thanks to my examiner Christian Hulteberg for giving me the suggestion to talk to Helena about a master thesis project on CCS. Thank you for also agreeing to be my examiner!

Erik Robertsson, June 2022, Lund

Abstract

With increasing atmospheric carbon dioxide (CO_2) concentrations, energy efficient carbon capture and storage (CCS) technologies could prove important to enable reductions in the global CO_2 emissions. The aim was to investigate a novel, non-aqueous, and precipitating chemical absorption system of dimethyl sulfoxide (DMSO) and 2-amino-2-methyl-1-propanol (AMP), which forms solid carbamate salt crystals with CO_2. Four properties of mixtures of water, AMP, and DMSO, with or without CO_2, were evaluated experimentally. The four properties were the settling velocities, the freezing temperatures, the densities, and the viscosities.

Higher settling velocities being registered at higher temperatures and for mixtures with larger particles. It was shown that the freezing temperatures of mixtures of water, AMP, and DMSO, both with or without CO_2, were lower than the freezing temperature of pure DMSO or AMP. Another finding was that when the water content increased, the freezing temperature decreased.

The effect of the temperature, the CO_2-loading, and the AMP- and water concentration, on the density and viscosity of the liquid mixtures, were also investigated. The results showed that if the weight percentage of AMP or if the temperature is increased, the density decreased, while the opposite was shown for increasing water content and amounts of absorbed CO_2. Furthermore, the experimentally derived densities for CO_2-loaded mixtures could be well estimated, although slightly underestimated, from experimental values for unloaded mixtures. The viscosity was increased at higher CO_2-loadings, higher water concentration, but also when the AMP concentration increased. Higher temperatures led to lower viscosities of unloaded liquid mixtures. Although less reliable, the results indicate that for the mixtures with high CO_2-loadings and high AMP concentration, much higher viscosities can be expected.

Sammanfattning

Med ökande koncentrationer av koldioxid (CO_2) i atmosfären kan energieffektiva tekniker för koldioxidinfångning (CCS) bli viktiga för att växthusgasutsläppen ska minska. Rapportens syfte har varit att experimentellt bestämma och utvärdera fyra egenskaper hos lösningar av vatten, dimetylsulfoxid (DMSO) och aminoalkoholen 2-amino-2-metyl-1-propanol (AMP) som ska användas i en pilotanläggning. Vid infångningen av koldioxid reagerar den med AMP och bildar ett fast salt. Sedimenteringshastigheten hos saltpartiklarna studerades, och resultaten visade att större partiklar och högre temperatur ökar sedimenteringshastigheten. Det har även visats genom resultaten att frystemperaturen för blandningar av vatten, AMP, DMSO, och CO_2 minskar med högre vattenhalt. Även om bara AMP och DMSO blandas så har blandningen en lägre frystemperatur än de enskilda ämnena, även om koldioxid löst sig i blandningen.

Fyra parametrars påverkan på blandningarnas densitet och viskositet, som är viktiga att veta för beräkningar och för att förutsäga absorptionsegenskaper, studerades. De fyra parametrarna var: mängden absorberad CO_2, blandningens andel vatten respektive AMP, och temperaturen. Resultaten visar att när andelen AMP i blandningen eller temperaturen ökar så minskar densiteten. Däremot så ökar densiteten om andelen vatten eller mängden absorberad CO_2 ökar. Det togs fram en beräkningssätt att uppskatta densiteten för blandningar med CO_2 utifrån de experimentella värdena för blandningar utan CO_2. Uppskattningen blir god, men det experimentellt uppmätta värdet överstiger det uppskattade värdet. Viskositeten ökade när mängden absorberad koldioxid, andelen vatten, eller andelen AMP ökade. Den minskade däremot med ökande temperatur. Trots att få säkra resultat erhölls för blandningar med hög andel AMP och mycket absorberad CO_2 så kunde det ses att mycket högre viskositeter kunde fås vid denna kombinationen av parametrar.

Table of contents

1 Introduction 1
1.1 Background 1
1.2 Aim 3
2 Theory 5
2.1 Chemical absorption of carbon dioxide. 5
2.2 Non-aqueous amine absorption system 9
2.2.1 Research at the Department of Chemical Engineering, Lund University. 9
2.2.2 Pilot plant 12
2.3 Important physical properties 14
2.3.1 Viscosity and Density for Aqueous Alkanolamine Absorption Systems 16
2.3.2 Viscosity and Density for Non-aqueous Alkanolamine Absorption Systems 17
2.3.3 Freezing point 18
2.4 Sedimentation 18
3 Materials and methods 23
3.1 Preparation of stock mixtures 23
3.2 Imaging of carbamate salt particles 24
3.3 Determination of settling velocity 26
3.4 Lamella sedimentation 27
3.5 Freezing temperature 29
3.6 Density 29
3.7 Viscosity 30
4 Results 33
4.1 Settling velocity experiments 33
4.1.1 The stock mixture with a CO_2-loading of 0.38 33
4.1.2 The stock mixture with a CO_2-loading of 0.50 36
4.2 Lamella sedimentation experiment 37
4.2.1 The lamella sedimentation basin 37
4.2.2 Qualitative results concerning the effluent slurry 38
4.2.3 Qualitative results of the microscope study of the bottom slurry 39
4.3 Freezing temperature 40
4.3.1 0H25A75D mixtures 40
4.3.2 5H24A71D mixtures 42

4.3.3 10H22.5A67.5D mixtures 43
4.4 Density 44
4.4.1 Unloaded stock mixtures 44
4.4.2 CO_2-loaded mixtures 47
4.5 Viscosity 50
4.5.1 The Ostwald viscometer 50
4.5.2 The Anton Paar MCR 302e 52
4.5.3 The NDJ-8S Digital Rotary Viscometer 54
5 Discussion 57
5.1 Sources of error associated with stock mixture preparation 57
5.2 Discussion of settling velocity results 57
5.3 Discussion of lamella sedimentation results 59
5.4 Discussion of the freezing temperature results 60
5.5 Discussion of the density results 61
5.5.1 The unloaded stock mixtures 61
5.5.2 The CO_2-loaded stock mixtures 62
5.6 Discussion of the viscosity results 63
5.6.1 The unloaded stock mixtures 63
5.6.2 Comparisons of the results for the CO_2-loaded mixtures 64
6 Conclusions and future work 67
7 References 71

Nomenclature

Abbreviations

AMP	2-amino-2-methyl-1-propanol
DMSO	dimethyl sulfoxide
MEA	monoethanolamine
TEGDME	tetraethylene glycol dimethyl ether
NMP	N-methyl-2-pyrrolidone
EOR/EHR	Enhanced oil recovery/Enhanced hydrocarbon recovery
CCS	Carbon capture & storage/sequestration
BE-CSS	Bioenergy carbon capture and storage
CDR	Carbon dioxide removal
NO_x	a generic term for a set of nitrogen oxides that are common air polluters, such as NO, and NO_2.
SO_x	a generic term for a set of sulphur oxides that are common air polluters, such as SO_2, and SO_3.
WLS	water lean system for chemical absorption of CO_2
NAS	non-aqueous system for chemical absorption of CO_2.
PCS	phase-change system for chemical absorption for chemical absorption of CO_2.
DMOZD	4,4-dimethyl-1,3-oxazolidin-2-one, degradation product of AMP.
SYSAV	Sydskånes Avfallsaktiebolag
VEAB	Växjö Energi aktiebolag
MDEA	N-methyl diethanolamine
MEG/DEG/TEG	mono/di/tri-ethylene glycol
EDA	ethylenediamine
PZ	piperazine
DIPA	diisopropylamine

CARBITOL	diethylene glycol monoethyl ether
RPM	Revolutions per minute
HOI	Height of Interface

Abbreviations for samples

0H25A75D	0 wt-% water, 25 wt-% AMP, and 75 wt-% DMSO
5H24A71D	5 wt-% water, 24 wt-% AMP, and 71 wt-% DMSO
10H22.5A67.5D	10 wt-% water, 22.5 wt-% AMP, and 67.5 wt-% DMSO
0H50A50D	0 wt-% water, 50 wt-% AMP, and 50 wt-% DMSO
5H47.5A47.5D	5 wt-% water, 47.5 wt-% AMP, and 47.5 wt-% DMSO
10H45A45D	10 wt-% water, 45 wt-% AMP, and 45 wt-% DMSO

1 Introduction

At the Department of Chemical Engineering at Lund University, research has been conducted to bring forth a novel chemical alkanolamine absorption system that can be utilized as a carbon capture and storage technology. In a project funded by the Swedish Department of Energy, the research will move from being conducted on laboratory scale to pilot plant scale. In this master thesis report, which has been a small project within the larger project to build and operate the pilot plant, laboratory experimental work has been conducted to determine physical properties of both unloaded and CO_2-loaded stock mixtures of the chemicals that will be utilized within the pilot plant.

1.1 Background

The technological advancement of society that has been ongoing since the advent of the Industrial Revolution has parallel to its success in creating our modern societies also created the most pressing global problem facing mankind, climate change. Through emissions of greenhouse gases, with the main component being carbon dioxide, the radiative forcing on the Earth has increased with the associated effect being increasing global temperatures [1, 2]. The majority of the emissions of carbon dioxide, CO_2, are directly related to the anthropogenic combustion of carbonaceous fossil resources as natural gas, coal, oil, or their derivatives [3]. Problems facing the environment due to climate change and the increasing global temperature range from acidification of the oceans and loss of biodiversity to the risk of droughts and extreme weather [4]. As these, and more, aspects of the environment are disrupted by climate change, which has been brought on by human activity, the Earth will become harder for humans to inhabit.

To ensure human welfare on the planet for the foreseeable future, climate change and its cause, the greenhouse gas emissions, must be combated and limited. Through the Paris Agreement that went into effect in November 2016, the countries of the world committed themselves to reduce the projected increase in global temperature at the end of the century to well below 2 °C above pre-industrial levels [5]. To meet the Paris Agreement, the Swedish Government has committed Sweden to have a zero-net emission of greenhouse gases by 2045 [6]. As of 2019, the industrial sector in Sweden was responsible for a third of the Swedish fossil emission. To achieve the ambitious goals, several technical measures have been suggested. The main ones are electrification of the transportation and industry sectors; replacing fossil resources with bio-based resources; utilizing hydrogen gas originating from non-fossil sources as an energy carrier; and carbon capture and storage[A] (CCS) [6].

The ambition of the last technology, CCS, is to be able to hinder the release of carbon dioxide to the atmosphere after its production within industrial processes. It also seeks to transport and subsequently permanently store the captured CO_2 in geological formations to hinder the CO_2 from entering into the atmosphere. In addition, by combining the technology with

[A] An alternative name for the technology, which is abbreviated the same, is carbon capture and sequestration.

combustion of biomass-based fuels, called BE-CCS[B], the technology could potentially achieve negative emissions[C] of carbon dioxide and work as a carbon dioxide removal (CDR) technology, decreasing the CO_2 levels in the atmosphere instead of contributing to their increase [7-9] .

When it comes to the technological aspects of capturing the carbon dioxide, the carbon capture arrangements are usually divided into two separate branches, the pre-combustion and the post-combustion arrangements [10, 11]. Common for the pre-combustion arrangements is that the separation process whereby CO_2 is removed takes place prior to the combustion. The separation prior to combustion is enabled by turning the fuel into synthesis gas, a gas mixture of hydrogen gas, H_2, and carbon monoxide, CO, and then through the water gas shift reaction converting CO into CO_2 according to reaction equation I [11]:

$$CO + H_2O \leftrightarrow CO_2 + H_2 \qquad \text{I}$$

As can be seen from reaction equation I, the water gas shift reaction also effectively increases the hydrogen production. The reasons for implementing the initial steps prior to combustion is that a higher concentration of CO_2 is obtained compared to what can be expected in the flue gas. Hence, the subsequent removal of the CO_2 can be done with a wider range of separation methods. As the CO_2 is removed, a clean hydrogen fuel is produced that can be used in the combustion process. Thereby, the CO_2 emissions connected with the fossil fuel will also be locally concentrated for capture. [11]

It is although the post-combustion arrangements that have garnered the most attention because they can be implemented onto existing facilities without large retrofitting efforts to the existing equipment [10]. In a post-combustion arrangement, the carbon dioxide is removed from the flue gases leaving the combustion chamber prior to its release to the environment. The lower CO_2 concentration has made aqueous alkanolamine absorption systems the most common separation method. In aqueous absorption systems, the alkanolamine reacts with the CO_2 after it has been dissolved into the water, which increases the absorption rate [10, 11].

The obstacle for widespread usage of aqueous alkanolamine absorption systems on existing facilities is the high added energy penalty, in the range of 20 – 30% of the plant energy output, accompanying the technology [12]. Therefore, research into novel technologies with lower energy footprints is critical in accelerating implementation of CCS technology. At the Department of Chemical Engineering at Lund University, research has been conducted on a novel system utilizing the sterically hindered alkanolamine 2-amino-2-methyl-1-propanol (AMP). Instead of utilizing the alkanolamine dissolved in an aqueous solution, the research was focused on whether there are benefits with instead using non-aqueous solvents, such as

[B] BE-CCS stands for Bioenergy Carbon Capture and Storage. The carbon fuel source is not fossil. Instead, the fuel can either be biomass or a bio-based fuel such as bio-ethanol or bio-diesel.
[C] The used definition of negative emissions corresponds to the definition in "Vägen till en klimatpositiv framtid". In the review report, negative emissions are defined as anthropogenically instigated reductions in carbon dioxide concentration that exceed the natural reductions achieved through the carbon cycle.

N-methyl-2-Pyrrolidone, NMP, and dimethyl sulfoxide, DMSO. The research has been fruitful. In non-aqueous systems, CO_2 can react with AMP to form a solid carbamate precipitate. The next stage of research at the Department involves the construction of pilot plant utilizing the novel, non-aqueous, and precipitating absorption system of AMP and DMSO. The master thesis project presented herein has been conducted during the initial parts of the pilot plant project. [13, 14]

1.2 Aim

The aim of the master thesis project was to evaluate properties of mixtures of the organic solvent DMSO and the sterically hindered alkanolamine AMP. In addition, tertiary mixtures containing small amounts of water were also studied. In the studied system, CO_2 is captured by forming a solid carbamate salt through a series of reaction steps between AMP and CO_2. The influence of different CO_2-loadings was also investigated.

The properties examined can be divided into two categories, physical properties and properties related to the separation of carbamate particles. Several separation methods can be used, as for example filtration, centrifugation, and sedimentation. Sedimentation was studied in this work and settling velocity was therefore the separation property studied. The evaluated physical properties were the freezing temperature, the density, and the viscosity. Ethical considerations concerning the work is found in Appendix G.

The effects upon the studied separation property, the settling velocity, for two parameters, the CO_2-loading and the temperature, were investigated. Furthermore, a qualitative analysis was done of lamella sedimentation utilizing a lab-scale lamella sedimentation basin. Experiments were also conducted to determine how the physical properties varied due to changes of up to four different parameters. The first parameter was the CO_2-loading, which is often denoted with the α-number. The α-number[D] represents the molar ratio of absorbed carbon dioxide to the AMP initially present within the stock mixture [13]. The second parameter was the water content, as water infiltration will happen over time in the real system. Water infiltration happens due to the presence of water in the flue gases and the hygroscopic nature of DMSO, the utilized organic solvent [15]. These two parameters were the only parameters whose effect were investigated for the freezing temperature. The third parameter studied was the weight percentage of AMP. Finally, for the viscosity and the density experiments, the influence of the temperature of the mixture was also investigated.

The first research question for the project was to determine and evaluate how the properties vary with the studied parameters. To answer the first research question, experimental work was conducted, evaluated, and discussed.

The second research question was to determine how the investigated properties are influential to the design of the pilot plant. To answer the second research questions, a literature review was conducted, with the findings presented in the Theory section of the report.

[D] The definition of the α-number can also be seen in equation 1.

2 Theory

2.1 Chemical absorption of carbon dioxide.

The utilization of an aqueous amine[E] scrubbing systems, where the main unit operations are the absorption- and stripping columns, for removing CO_2 from gaseous streams is a technology dating back to the 1930s [12, 16]. The main purpose of using the technology has throughout the years not been to capture CO_2, but instead to purify gas streams either containing natural gas, ammonia, and hydrogen gas

The usage of the amine scrubbing technology over a long duration of time has made it a mature technology, where a 30 wt-% aqueous solution of monoethanolamine (MEA) is considered the benchmark technology. Numerous advanced configurations of the stripping- or regeneration column are presented in the literature, all with the aim to make greater use of the heat input used in the regeneration of the aqueous amine absorption solution, thereby diminishing the large energy penalty related to technology [17]. The reader is referred to the literature for discussions on the performance of these process configurations [17, 18]. Instead, it is the most common schematic process configuration for amine scrubbing that will be presented herein. A schematic and common process configuration when employing amine scrubbing for CCS purposes can be seen in Figure 2.1. The absorption- and the stripper columns seen in Figure 2.1 are either packed or trayed columns arranged in counter-current configurations.

The flue gas, which has been previously treated to remove most of the particulate matter, nitrogen oxides, referred to as NO_x, and sulphur oxides, referred to as SO_x, is cooled in a water wash unit operation prior to entering the absorption tower to a temperature between 40 – 60 °C [19]. Particulate matter, NO_x and SO_x must be removed effectively as they, primarily NO_x, degrade the MEA solvent. The degradation can, among others, result in the formation of nitrosamines, which are a set of compounds that have potentially carcinogenic and mutagenic effects. Another component present within the flue gas, oxygen, also degrades the amine within the absorber. The degradation can result in greater emissions of ammonia, but also the formation of organic acids, that react further to heat stable salts. Degradation increases the need for make-up amine solution as regeneration of the amine are hard to regenerate. Furthermore, the presence of degradation products can change the solvent properties, and affect the design by increasing the rate of corrosion and fouling. [20, 21]

[E] What is referred to as amines in much of the literature, and in this paper, should, to be correct, be referred to as alkanolamines. The alkanolamine compounds are compounds that have, as the name suggest, an alkane structure of the carbon backbone. The alkane structures are attached to a central amine group. It is the amine group that enables the reactions with CO_2 to take place. Furthermore, for all alkanolamines, at least one hydroxyl group is present on the alkane backbone, which provides the compound with an increased solubility in water and a lower volatility.

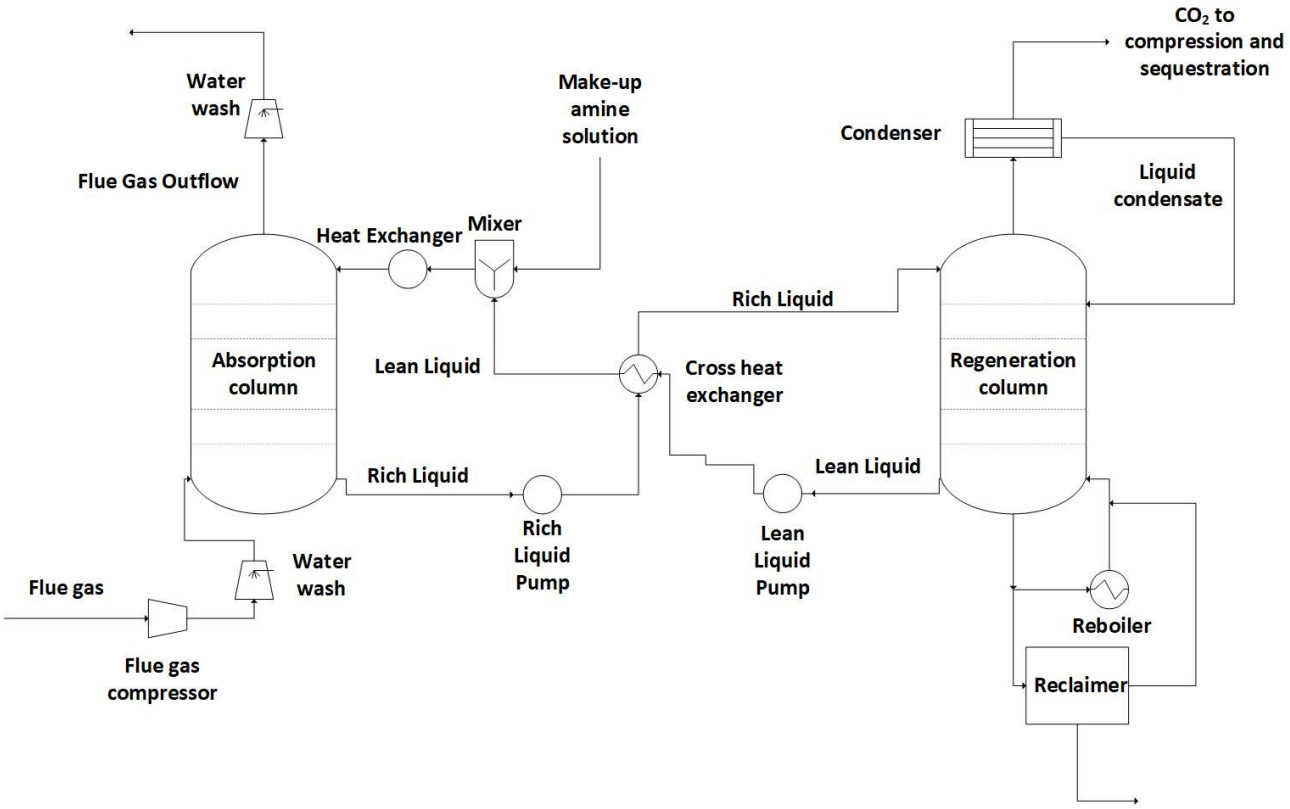

Figure 2.1. A common process configuration for CCS with aqueous amine solutions, shown as a process flow diagram. Adopted from Sanku [17].

In the absorption column, CO_2 that become physically absorbed from the gas phase into the solvent reacts with the amine, RNH_2, forming a zwitterion, RNH_2+COO-. The zwitterion can then go through further reaction with another amine, forming a carbamate, $RNHCOO^-$, or a reaction with the present water. The reaction with water produces bicarbonate, HCO_3^-, which can also be produced if the carbamate reacts with water, whereby the alkalinity in the water is affected. The reaction mechanism is summarized in the reaction equations II-VI, with the tag *(sol)* denoting that the compound is present in the liquid solution. [14, 17]

$$CO_2(g) \leftrightarrow CO_2(sol) \qquad \text{II}$$

$$CO_2(sol) + RNH_2(sol) \leftrightarrow RNH_2^+COO^-(sol) \qquad \text{III}$$

$$RNH_2^+COO^-(sol) + RNH_2(sol) \leftrightarrow RNH_3^+(sol) + RNHCOO^-(sol) \qquad \text{IV}$$

$$RNH_2^+COO^-(sol) + H_2O(sol) \leftrightarrow HCO_3^-(sol) + RNH_3^+(sol) \qquad \text{V}$$

$$RNHCOO^-(sol) + H_2O(sol) \leftrightarrow HCO_3^-(sol) + RNH_2(sol) \quad \text{VI}$$

The solvent, water, is also able to participate in an additional reaction with the amine, which will produce hydroxide ions. Hence, the water autoprotolysis reaction can also occur. Water and hydroxide ions will also react with the dissolved CO_2 to produce bicarbonate through two different reactions. The overall reaction equations for these reactions are summarized below as reaction equations VII-X. [14]

$$RNH_2(sol) + H_2O(sol) \leftrightarrow RNH_3^+(sol) + OH^-(sol) \quad \text{VII}$$

$$H_2O(sol) \leftrightarrow H^+(sol) + OH^-(sol) \quad \text{VIII}$$

$$CO_2(sol) + OH^-(sol) \leftrightarrow HCO_3^-(sol) \quad \text{IX}$$

$$CO_2(sol) + H_2O(sol) \leftrightarrow HCO_3^-(sol) + H^+(sol) \quad \text{X}$$

The prevalence of bicarbonate formation from the zwitterion in comparison with carbamate formation depends on the stability of the formed carbamate. MEA gives rise to the formation of a highly stable carbamate. Therefore, bicarbonate formation in aqueous mixtures of MEA can be disregarded and the overall reversible reaction mechanism during absorption and stripping of CO_2 with MEA can be simplified to reaction equation XI. The overall absorption process is exothermic. [14]

$$CO_2(g) + 2RNH_2(sol) \leftrightarrow RNHCOO^-(sol) + RNH_3^+(sol) \quad \text{XI}$$

The gas stream enters through the bottom of the absorption column, while the aqueous MEA solution is fed to the top, and trickles down the column. Simultaneously, CO_2 is transferred over the interface between the two phases from the gas to the liquid, with the chemical reaction moving from left to right in reaction equation XI [1]. Due to the overall reaction being exothermic, the temperature of the liquid solvent is increased before it leaves the absorption column rich in CO_2-derived reaction products[F] [22]. The exiting gas from the absorption column is passed through a water wash step to lower the outgoing flue gas temperature and hinder gas

[F] The stream will from here on be referred to as the rich stream in accordance with the literature.

emissions of the amine [17]. The rich stream passes through a cross heat exchanger, where it meets the lean aqueous MEA solution stream leaving the bottom of the stripper column [17].

In the stripper column, the reverse reaction, moving from right to left in equation XI, takes place [17]. Absorption is enhanced with keeping low operational temperatures, and high operational pressures, while stripping is instead favoured by decreasing pressure and increased temperature [11]. Hence, stripping can either be done through pressure- or temperature swing operation. The latter is more widely employed for aqueous amines scrubbing, and stripping is achieved by keeping a higher operating temperature, in the range between 100 - 120 °C when utilizing MEA in the stripping column [18, 23]. Water vapour, which works as a stripping agent, is produced in the reboiler in the bottom of the stripping column [23]. A reclaimer is also placed in the bottom, where degradation products can be removed [23]. The utilized amine can, in addition to oxidative degradation and degradation due to the presence of residual NO_x, also be degraded through thermal degradation. Thermal degradation primarily takes place if the stripper temperature becomes excessively high, especially in the reboiler where the highest temperatures are achieved [24]. MEA is thermally degraded following a reversible reaction where the MEA-derived carbamate is converted into oxazolidinone, a compound that subsequently reacts with another MEA molecule to form a MEA-derived dimer [24]. The degradation rate is although acceptable at 120 °C [24].

The gas leaving the through the top of stripping column consists of the stripping agent, water vapour, and the CO_2. By condensing and recycling the water to the stripping column, a high purity CO_2 gas stream is achieved. The lean aqueous solution leaving the stripper is passed through the cross-heat exchanger, and possibly also through an additional heat exchanger. The aqueous solution is then once again fed, along with make-up solution to account for the degradation of the amine over time, to the absorption column. [14, 17]

The aqueous amine scrubbing system utilizing MEA has the advantages of low production costs for the aqueous solution, resistance against thermal degradation, and high chemical reactivity with CO_2 [1, 16]. The CO_2 loading (α), which is the molar amount of absorbed CO_2 divided by molar amount of initially added amine to the solution, is shown in equation 1 [13]. Because of the lack of bicarbonate formation, the theoretical CO_2 loading that can be achieved through chemical absorption is limited to 0.5 [14].

$$\alpha = \frac{(CO_2)_{abs}}{(C_{amine})_0} \qquad 1$$

Values around the theoretical value of the CO_2 loading can be achieved during the rich loading in the absorption column, and lean loadings of 0.2 is usually obtained after stripping [17]. Hence, the cyclic capacity of the MEA amine scrubber system is often around 0.3 mol CO_2/mol MEA, a low absorption capacity [16]. Other disadvantages with operating the benchmark technology are a high parasitic power demand, in the range of 20-30 % of the output from a conventional power plant, when the CO_2 also needs be compressed to enable its transportation [12]. The energy requirement of the CO_2 compression is comparable to the most energy demanding part of the design presented in Figure 2.1, which is to transfer heat with low-pressure steam in the reboiler and often accounts for 70 –80 % of the operational costs, although can extend up to 90 % [1, 12]. Furthermore, the high enthalpy for the regeneration,

much due to the high heat of vaporization of water, is a negative aspect when it comes to decreasing the required energy input [1, 16, 17]. Lastly, the corrosiveness of concentrated MEA solutions forces the design to utilize more expensive design materials such as stainless steel.

2.2 Non-aqueous amine absorption system

2.2.1 Research at the Department of Chemical Engineering, Lund University.

The inherent disadvantages of the current state-of-the-art absorption system for carbon capture, with the main one being the high energy demand of the reboiler, has led to research into better alternatives. Alternatives, such as other amines, mixtures of amines or something else, to fill the CO_2-capturing function of MEA in the aqueous solution is widely investigated. In parallel, advanced stripper configurations as the advanced flash stripper, the interheated stripper, and the lean vapour compression stripper have been proposed to improve the energy performance of the simple stripper configuration in Figure 2.1 [17, 18, 22]. The details of these advanced stripper configurations can be found in the literature. What they all manage to accomplish in contrast to the simple stripper configuration is to diminish the substantial reduction in the energy efficiency of the stripper caused when the condensation of water vapour occurs without recovering heat. Connected to the high reboiler duty is also the chosen solvent, water, and its high heat of vaporization and heat capacity. Diminishing the initial amount of water used as solvent, or using another solvent entirely, has also been proposed as ways to arrive at a more energy efficient process. A system where another solvent has partially replaced water is called a water-lean system (WLS). A non-aqueous system (NAS) is a system where water is not present to begin with and another solvent is utilized. However, over time water can accumulate to some extent within the system, as it is present in small concentrations within the flue gas stream. [17]

Although stripping is a necessary step for regenerating the amine solution, employment of another separation step prior to the stripping, where the rich stream to the stripper could be reduced in magnitude, would also lower the energy requirement of the stripper column. A phase-change system (PCS), is a system where another phase is formed in addition to the amine solution. The other phase can either be another liquid with a low solubility in the primary solvent, or a solid. If the compound that must go through regeneration is concentrated to one phase, phase separation prior to the stripper would reduce the amount that has to be regenerated in the stripper. Heterogeneous phase mixtures can often be separated into the respective phases with a completely different set of separation methods than those applicable for homogeneous phase mixtures. [17]

The Department of Chemical Engineering at Lund University has conducted research into novel absorption systems utilizing the sterically hindered amine AMP. As a sterically hindered amine. As AMP is sterically hindered, CO_2 will primarily react to form bicarbonate in an aqueous AMP system through the reaction mechanism expressed in reaction equations II-VI [14]. The overall reaction formula can hence be described by reaction equation XII [14]:

$$CO_2(g) + RNH_2(sol) + H_2O(sol) \leftrightarrow HCO_3^-(sol) + RNH_3^+(sol) \qquad \text{XII}$$

From reaction equation XII, it can be seen that AMP has a high theoretical absorption capacity with an α-number of 1. Investigations have also suggested that the energy requirement for regeneration is comparatively low. [14]

The research started out as part of the doctoral thesis by Svensson on investigating new technologies for gas upgrading of gaseous biofuels, where, among other things, CO_2 is separated from the gaseous biofuel. In her work, the novel amine solutions of AMP mixed with the non-aqueous solvents N-methyl-pyrrolidone (NMP), and triethylene glycol dimethyl ether (TEGDME) were investigated to determine their suitability for CO_2 removal. The organic solvents, NMP and TEGDME, were chosen after an initial screening. The search criterion during the screening was that AMP should be regenerated in the temperature interval of 70 – 90 °C. Regeneration in the stripper in the stated temperature interval enables that the reboiler duty could be satisfied with low-grade heat. At a temperature of 75 °C, CO_2 was completely desorbed for a 25 wt-% AMP and 75 wt-% NMP solution. The same was observed for a 25 wt-% AMP and 75 wt-% TEGDME solution, but at 90 °C. [13]

Furthermore, it was found that the novel amine solutions produce a precipitate through the chemical absorption reactions. In a non-aqueous solution, the reaction mechanism for AMP is instead as described by reaction equations XIII-XVI. Reaction equation XVI shows the formation of a solid, a carbamate salt, which is possible with the utilization of a non-aqueous solvent. Reaction equation XVII shows the overall reaction equation resulting in the formation of the precipitate $RNH_3^+RNHCOO^-$. [13]

$$CO_2(g) \leftrightarrow CO_2(sol) \quad \text{XIII}$$

$$CO_2(sol) + RNH_2(sol) \leftrightarrow RNH_3^+COO^-(sol) \quad \text{XIV}$$

$$RNH_3^+COO^-(sol) + RNH_2(sol) \leftrightarrow RNH_3^+(sol) + RNHCOO^-(sol) \quad \text{XV}$$

$$RNH_3^+(sol) + RNHCOO^-(sol) \leftrightarrow RNH_3^+RNHCOO^-(s) \quad \text{XVI}$$

$$CO_2(g) + 2RNH_2(sol) \leftrightarrow RNH_3^+RNHCOO^-(s) \quad \text{XVII}$$

The formation of the precipitate, $RNH_3^+RNHCOO^-$, is due to the steric hindrance of AMP. As bicarbonate formation cannot occur without the presence of water, the CO_2-loading is theoretically limited to 0.5, as can be seen in reaction equation XVII. Lastly, experimental data on the solubility and the heat of absorption was determined. The solubility and heat of

absorption was determined at 25 and 50 °C respectively for two concentrations of the amine in the respective organic solvent with varying CO_2-loading. [13]

The research initialized by Svensson was thereafter extended through two doctoral theses on non-aqueous and precipitating system with AMP by Sanku and Karlsson. Both performed further studies of the CO_2 solubility in solutions of AMP and NMP [14, 17]. Sanku also investigated the possibility to model non-aqueous systems in addition to developing a thermodynamical model for estimating the crystallization kinetics for systems with all three phases present. Through the thesis, several conclusions regarding solutions of AMP and NMP could be drawn. The first conclusion was that a similar cyclic capacity of 0.3 could be achieved as for the benchmark MEA technology, although shifted towards lower loadings, using a 25 wt-% AMP and 75 wt-% NMP solution. Lower loadings often entail a smaller corrosive effect. The second conclusion that was identified was that stripping of the CO_2 without a stripping agent could be achieved to very low loadings at atmospheric pressure. It was also concluded that under normal operation, with a flue gas temperature of 40 °C and a CO_2 partial pressure of 20 kPa, using a 25 wt-% AMP and 75 wt-% NMP solution would result in a precipitating system. However, if the amine concentration is lower, 15 wt-%, the ingoing temperature would have to be lowered to 25 °C to get a precipitating system. Finally, by changing the amount of time whereupon the system was determined to have reached equilibrium from 30 minutes to 330 minutes for the solubility experiments, it was concluded that the CO_2 solubility increased and that precipitation could occur for lower CO_2 loadings. If intermittent operation would take place during the operation of a CCS plant with the novel amine system, it would result in a higher solubility of CO_2 due to the extended contact time for the gas and the amine solution. [17]

Karlsson expanded upon the initial screening done by Svensson by examining the absorption conditions for AMP in seven different organic solvents, in order to find an alternative without the reproductive toxicity of NMP. Another criterion for the screening was that a suitable candidate should have similar precipitating properties as NMP. An additional promising candidate to the AMP / NMP system was found, namely a system where AMP is dissolved in the organic solvent DMSO. The newly discovered AMP system showed a higher solubility of CO_2 than the original NMP system at all studied temperatures, while simultaneously have similar precipitating trends. The solubilities of CO_2 for the two novel non-aqueous absorption systems are lower than for the benchmark aqueous 30 wt-% MEA solution. However, the presented experimental data tells that it still will be possible to achieve similar cyclic capacities under appropriate absorption conditions. The suitable absorption conditions previously stated for when NMP is used as the organic solvent were also appropriate with DMSO. Suggested advantages with the novel absorption solutions are that the regeneration can be made using low-grade heat, often available within the industry, and without the use of a stripping agent at atmospheric pressures. The last conclusion drawn specifically for the CO_2 solubility was that higher amine concentrations increases the solubility, while also enabling precipitation at higher temperatures and lower CO_2 loadings. [14]

Another property that was investigated for the novel absorption solution was the heat of absorption. It was found that the heat of absorption reaches higher values when precipitation occurs. Furthermore, the experiments showed that supersaturation of the solution takes place prior to precipitation, which is an exothermic reaction, as significantly high values for the heat

of absorption were measured at the onset of precipitation. The phenomena could give rise to problems with hot spot formation within the absorption column, where the temperature could locally become very high, effectively shifting the equilibrium towards desorption. Higher values for the heat of absorption will mean that the temperature increase down the absorption column is likely to increase, which is further aggravated by the lower heat capacities of the studied organic solvents in comparison to water. NMP and DMSO also have higher boiling points than water, meaning that less vaporization of the solvent, will take place. It was stated that intercooling, or further cooling of the flue gas prior to the absorption column, will probably be necessary to enable precipitation to occur along the entire height of the absorption column. [14]

As DMSO is a hygroscopic solvent, water accumulation can become a problem, and hence the influence of water on the absorption capacity was investigated [15]. It was concluded that water accumulation up to a molar ratio of 2:1 between water and AMP did not hinder precipitation and that a regeneration temperature of 88 °C would still be sufficient. A too high water content is although still believed to be able to hinder precipitation due to the alternative CO2 reaction route to bicarbonate. In the dissertation, it was further speculated that the presence of water can be advantageous to some extent. By having water present, the temperature rise in the absorption column could potentially be limited, due to its high heat capacity and greater volatility. In addition, it is reasonable to expect that the freezing point of the amine solution will decrease, a trend that has been seen for increasing water content in pure DMSO. Bicarbonate formation will also be possible, meaning that higher CO_2 loadings could be achieved. Through ^{13}C NMR studies, the findings of the potential degradation product 4,4-dimethyl-1,3-oxazolidin-2-one (DMOZD) could be interpreted as that amine degradation occurs quicker with water present. [14]

Given the promising research done at the Department, a project in collaboration with Växjö Energi AB (VEAB), Sydskånes Avfallsaktiebolag (SYSAV), Öresundskraft, and Midroc[G] was initiated with funding from Energimyndigheten in 2021 [25]. Through the project, a pilot plant will be constructed by Granitor and operated sequentially at VEAB, SYSAV, and Öresundskraft to test in practice the novel amine absorption system consisting of AMP and DMSO.

2.2.2 Pilot plant

A schematic illustration of the proposed process configuration for the pilot plant is showed in Figure 2.2. There are notable differences between the proposed process configuration for the pilot plant and the common process configuration for amine absorption technologies utilized for carbon capture and storage that was presented in Figure 2.1.

[G] MIDROC Europe changed their name to Granitor in January 2022.

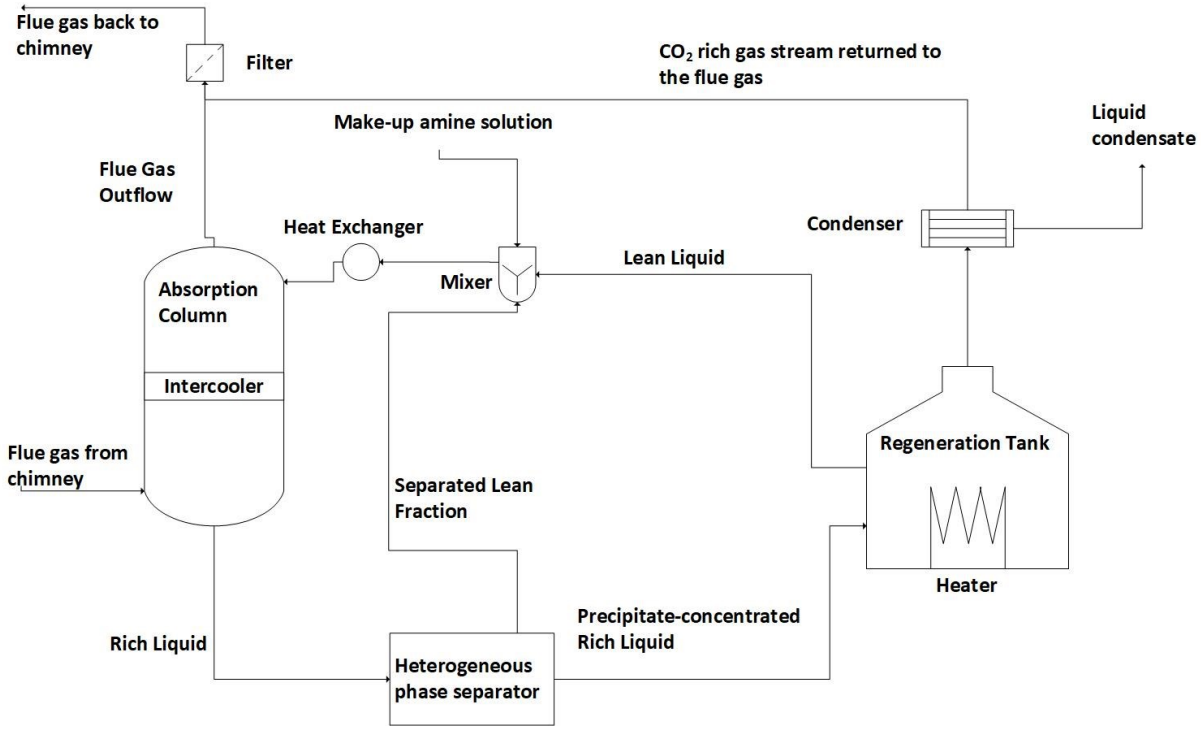

Figure 2.2. The proposed process configuration of the pilot plant, which differs to the common process configuration for carbon capture and storage utilizing amine absorption that was depicted in Figure 2.1. The most notable difference with the process configuration is the presence of the heterogeneous phase separator. Pumps, sample ports, and other instrumentation needed to successfully operate the pilot have not been included.

During operation, the pilot plant will be supplied with low temperature flue gases originating from the chimney of one of the three partners where the pilot plant will be placed. The flue gases will enter through the bottom of the absorption column, which is a randomly packed column. As the flue gas passes through the column, the flue gas will come in contact with the lean amine solution that enters through the top of the absorption column. The absorption column will also have an intercooler, that could be used to reduce the temperature increase of the liquid caused by the absorption of CO_2 from the flue gas.

The outgoing rich liquid from the absorption column, will be passed through a heterogeneous phase separator. One of the discussed alternatives for performing the heterogeneous separation is lamella sedimentation. The heterogeneous phase separator will split the rich liquid into two outgoing streams, one concentrated with the precipitate and one with a lower concentration of precipitate, which will be recycled back towards the inlet of the absorption column. The precipitate concentrated rich liquid will enter into a regeneration tank, instead of a regeneration column. The tank will be heated to reverse the absorption reaction, thereby releasing CO_2 and regenerating the amine. Both a gaseous stream and a liquid stream will leave the regeneration tank. The lean liquid will be recirculated back towards the absorption column. It will be mixed with make-up amine solution and the separated lean fraction before it will be fed to the absorption column. The mixture will also pass through a heat exchanger prior to entering the absorption column to obtain the correct feed temperature. The outgoing gas from the regeneration tank will pass through a condenser, with the liquid condensate

being removed from the plant. Due to the scale of the plant, the CO_2 rich gas stream will not be concentrated, purified, pressurized or stored. Instead, it will be mixed with the outgoing flue gas from the absorption column, filtered, and then returned to the chimney.

2.3 Important physical properties

Three physical properties will be investigated through the project, being the viscosity, the density, and the freezing point of the slurry mixture. The properties are affected by the composition of the slurry mixture, and hence dependent on the relative amount of water, AMP, DMSO, and the amount of absorbed CO_2.

The first of these properties, the viscosity, is closely related to the flow characteristics of the liquid medium. When external forces in the form of shear stress is applied to a liquid, the volume of liquid cannot tolerate the deformation that the shear stress generates, and it will therefore start to flow. As the fluid starts to flow along a geometric object, for example a pipe, different liquid layers will over time obtain different velocities. The rate with which the difference in velocities arises is termed the shear rate. Frictional or viscous forces will also arise due to the difference in velocities between the layers. For Newtonian fluids, the shear rate and the shear stress are linearly related through the dynamic viscosity of the liquid. For non-Newtonian fluids, the relation is not necessarily linear, but a higher shear stress does correspond to a higher shear rate. [26]

The Reynolds number is a dimensionless number arising from the Navier-Stoke equation, which assumes a Newtonian fluid, and the size of the Reynolds number describes the characteristics of the flow [27]. The expression with the dynamic viscosity for the Reynolds number is given in equation 2 and the expression with the kinematic viscosity is given in equation 3.

$$Re = \frac{\rho * v * X}{\mu} \qquad 2$$

$$Re = \frac{v * X}{\vartheta} \qquad 3$$

Low values of the Reynolds number indicate that the flow is laminar, meaning that the flows is structured into layers with varying velocity with little to no mixing perpendicular to the flow. This was also the flow characteristic described above. The structuring of the flow is due to the viscous forces that dampens out local variations in fluid velocity [28]. When the Reynolds number increases, the viscous forces become too small to quench the local variations in velocity and kinetic energy, and hence the flow becomes unstructured, full of turbulent eddies, and local velocity gradients [28]. For increasing Reynolds numbers, the flow first enters the transition zone, and then into the fully turbulent flow zone. The irregularity of turbulent flow is beneficial in that it increases the three diffusivities, mass, heat and momentum, of the

liquid. The diffusivities all have the same unit, which in SI-units is m^2/s, and the momentum diffusivity corresponds to the kinematic viscosity [27]. Beneficial general effects that accompany larger values for the diffusivities are effects such as superior mixing and greater rate of heat transportation.

The viscosity is an interesting parameter for the pilot plant, since the slurry mixture will continuously flow between the different unit operations. Furthermore, the composition of the slurry mixture will be different at different locations within the design and the composition can be expected to change time as a result of water accumulation. To achieve a certain flow of slurry mixture within the plant, which will be set by the amount and composition of the slurry, the anticipated cyclic capacity, and the desired capture rate of CO_2, appropriate process equipment, in the form of pumps, must be chosen. Given a desired flow on a mass or molar basis, to obtain the volumetric flow, it will also be necessary to know, or estimate accurately from experimental data, the density of the slurry mixture at the composition of interest. The pumps must be able to provide the required work needed to achieve the desired flow, which will be influenced by the flow characteristics and hence the viscosity [14]. The characteristic of the flow will also determine the rate of heat transportation achieved in the heat exchanger between the rich and lean stream [14]. For the absorption and desorption processes themselves, the viscosity is also of importance. The rate of absorption is affected by the diffusivities, which also changes with the characteristics of the flow [14]. Absorption is a chemical process that takes place over the interface between the liquid phase and the gas phase. Therefore, the interfacial area, over which the mass transport of CO_2 from the gas to the liquid takes place, is hence very important. Though it is hard to estimate the interfacial area, the degree of wetting of the packing can serve as an indication, and it is also affected by the viscosity of the liquid. The rate of heat transfer is also affected by the flow characteristics. The *h*-value, which for the film theory describes the heat transfer coefficient between the bulk fluid and the wall of the heat exchanger, depends on the dimensionless Nusselt number. Several factors, such as the geometry and the flow characteristics, affect how the Nusselt number depends on the Reynolds number. However, the value of the viscosity will greatly impact the heat transfer. [29]

Due to the climate in which the pilot plant will be situated, the freezing points of the different slurry mixtures will be of importance. As pure substances, DMSO has higher freezing temperature than water at 18.5 °C, and AMP is a semi-solid mixture with a melting interval between 24-28 °C [15, 30]. As make-up amine slurry will have to be available to compensate for the degradation and emissions of AMP during the continuous operation, the higher freezing temperatures would be a disadvantage. The high freezing temperatures can limit the range of acceptable temperatures of the chemical storage facilities, and the unit operations for mixing of the slurry. To maintain acceptable storage temperatures, given the range and frequency of outdoor temperatures below the desired storage temperature, it will be necessary to design the storage with a reliable form of heating.

However, depending on whether the chemicals will be stored separately or will be mixed prior to storage will be off importance. When a solute, which could be another liquid, is mixed into a pure solvent, the chemical potential of the solvent will, in principle, be decreased, reducing the vapour pressure of the solvent. Therefore, the vapour pressure of the liquid and the solid phase will become equal at a lower temperature, meaning that the freezing point will be depressed [31]. If the depression is substantial, it could enable outdoor storage as an alternative.

Furthermore, it will also be of importance to determine the extent of freezing point depression to set lower temperature limits for cooling, for example in the intercooler in the absorption tower. If the slurry mixture would freeze during the heat transfer operations, solid would form on the heat transfer surfaces, which will alter the heat transfer coefficient. The plausible effect would be a decrease in the efficiency of the heat transfer operation, with the results being insufficient intercooling. Lastly, high freezing point values can also be problematic during start-up, shutdown or maintenance. If the process must be stopped and is kept interrupted for a long period of time, problems can occur with freezing of the slurry mixture within the pipes. The scenario can happen if the average outdoor temperature over the time period of the shutdown is lower than the freezing point, which will complicate and delay the process from being restarted.

In addition to determining the volumetric flow, both the density and the viscosity are necessary to have knowledge about from an engineering point of view, since they are required to be able to carry out key design calculations [32]. For example, knowledge or estimations of expected values for the physical properties will be required to do calculations that aim to dimension the pipes, storage, and aspects of the other unit operations, such as the diameter and the pressure drop of the absorption column [32]. Even in later stages of the pilot plant project, for instance after data collection has been done extensively, it might be desired to simulate the process. The experimental physical data could in that case be used to find a suitable existing physical property model that can be utilized for simulating the absorption system [29]. However, it could also showcase the need for developing a novel model for the physical properties. Furthermore, both the density and the viscosity are physical properties that greatly affect the sedimentation process, which will be mentioned again and expanded upon in section 2.4.

2.3.1 Viscosity and Density for Aqueous Alkanolamine Absorption Systems

As the physical properties, with an emphasis on the viscosity and the density, are important for absorption systems, research has been conducted to determine the properties for both the benchmark 30 wt-% MEA absorption system as well as other novel mixtures with water.

Although having been widely utilized, it was first in 2009 that density and viscosity measurements were done specifically for CO_2-loaded mixtures of MEA & water over the temperature range 25 – 80 °C. Amundsen et al extended the work initiated by Weiland et al where the density and viscosity had been experimentally determined for loaded solutions at 25 ° C. The initial paper had also presented correlations for the density and viscosity for aqueous alkanolamine mixtures. The conclusions from the experimental work by Amundsen et al was that the values predicted by the correlations of Weiland et al were in accordance with the experimental results obtained. For the aqueous 30 wt-% MEA solution, the dynamic viscosity increased from 2.6 mPa·s for an unloaded solution at 25 °C to 3.9 mPa·s when the CO_2 loading increased to 0.5. At the same time, the density also increased from 1.0280 g/cm^3 to 1.1211 g/cm^3. At 50 °C, the corresponding values were instead 1.4 and 2.1 mPa·s , and for the density 1.0160 and 1.1080 g/cm^3. The maximum relative deviation of the value predicted by the correlation to the experimental data was found to be 10 %. Another conclusion that was drawn was that an increasing CO_2-loading results in increasing densities and viscosities for all temperatures. [32, 33]

Alongside the work in investigating the physical properties of the benchmark technology for amine absorption, research was conducted to determine the physical properties for other aqueous amine absorption systems. The density and viscosity have also been investigated for the secondary or tertiary amines.[16]. Certain secondary and tertiary amines showcase greater resistance to degradation than MEA, while others have the advantage of not requiring the same amount of energy for regeneration [16]. The negative aspects of utilizing secondary and tertiary amines over primary amines are that their reaction rates are lower, especially for the tertiary amines [16]. Amine blends, where different alkanolamines are mixed in different proportions, has had the aim to reach an optimal middle ground. Investigations of the density and viscosity has for example been done for N-methyl diethanolamine, a tertiary amine abbreviated as MDEA. The investigations have been conducted by several research groups for both aqueous solutions of MDEA, and for MDEA blends with a wide-ranging number of other amines. The results showed that the viscosity can be modelled well with an NRTL-DVIS property method for both unloaded and loaded aqueous MDEA solutions over a wide range of temperatures [29]. An increasing weight percentage of MDEA in unloaded solutions increases the viscosity, and for temperatures below 50 °C, a maximum registered viscosity was reached for mixtures with a molar percentage of MDEA of around 70 % with the highest registered viscosity being 112.140 mPa·s at 20 °C [29]. Loaded solutions of 50 and 60 wt-% MDEA aqueous solutions were tested for their viscosity, and the obtained experimental data, and data from Weiland et al, was used to find the suitable parameters for the NRTL-DVIS property method [29, 33]. Although the model under-predicted the viscosity of the 50 wt-% MDEA solution at 20 °C, the derived model overall agreed well with the experimental results [29]. Both the model and the experimental results showcase that an increased viscosity can be expected with increased CO_2 loading, at many temperatures well described by linear functions [29]. Experimental data of how the viscosity and density changes for MDEA blends has also been done. For example, unloaded MDEA blends with AMP and diisopropylamine, DIPA, have lower densities but higher viscosities than solutions with only MDEA, at the same weight percentage of amines to water, between 30 to 90 °C. With increasing temperature, both the density and the viscosity decreased. Upon loading of both blends with CO_2, both the viscosity and the density instead increased. The largest percental increase is seen for the viscosity, not the density. With greater amounts of experimental data becoming available, some researchers have focused on compiling and analysing the data and have thereby developed estimation tools for the density and viscosity for several blends. [34]

2.3.2 Viscosity and Density for Non-aqueous Alkanolamine Absorption Systems

With the idea of utilizing water-lean and non-aqueous absorption systems, the effect of the solvent substitution on viscosity and density has also been investigated. Substitution of half of the weight of water in unloaded, aqueous 30 wt-% MEA solutions with any of the four organic solvents mono/di/tri - ethylene glycol (MEG/DEG/TEG) or diethylene glycol monoethyl ether, known as CARBITOL, resulted in increasing viscosity and density [35]. At 25 °C, the largest increase in viscosity and density came with the substitution of water for TEG, whereby the viscosity increased from 2.7 mPa·s to 11.3 mPa·s and the density increased from 1.010 to 1.062 g/cm^3. Recently, research presenting viscosity measurements of CO_2-loaded non-aqueous phase-changing solutions have been presented. Solid carbamate precipitates are formed during CO_2 absorption with the diamines ethylenediamine (EDA) and piperazine (PZ) with ethanol as solvent, with decomposition temperatures of around 90 °C [36]. The lower observed decomposition temperature corresponds well with the temperature

interval for regeneration of AMP carbamates found by the researchers at the Department of Chemical Engineering at Lund University [13]. At 30 °C, EDA solutions with varying amine concentrations between 0.2 – 1 kmole/m^3 and a CO_2 solubility ranging from 0.0962 down to 0.0901 kmole/m^3 had viscosities ranging between 1.053 mPa·s to 1.178 mPa·s . The results indicate that increasing amine concentration increases the viscosity for similar CO_2–loadings. [36]

Previous studies on non-aqueous AMP, that will be utilized in the novel absorption system studied in this work, has also been conducted. Karlsson and Svensson has studied the viscosity of two unloaded solutions of AMP in NMP, the wt-% of AMP being 15 and 25 respectively, for temperatures between 20 and 80 °C [37]. Decreasing temperatures and increasing amine concentration resulted in greater dynamic viscosity values of the mixtures [37]. Density studies of AMP mixtures has mainly been restricted to its utilization in aqueous absorption mixtures in amine blends with MEA [38]. Although carried out at an elevated pressure of 4 bar, research showed that increased CO_2 – loading increases the density for three studied amine concentrations [38]. The viscosity is also increased due to increased intermolecular interactions caused by the presence of charged ions following the reactions between CO_2 and the amines [38]. However, increasing temperatures decreased the viscosity for all studied CO_2 loadings and compositions of MEA and AMP [38].

Studies of the how the density and viscosity of mixtures with DMSO changes with the composition have for example been done with the following mixing agents: water, monoethylene glycol, and tetraethylene glycol [39-41]. For the two ethylene glycols, the effect of the temperature on density and viscosity were also studied within a small temperature interval [39, 40].

2.3.3 Freezing point

Experiments to determine the freezing point of liquid mixtures, and in particular mixtures with solid salts, have not been widely conducted for either DMSO or AMP. Havemeyer investigated the freezing point of mixtures of DMSO and water in 1966, finding that the freezing point could decrease down towards –140 °C when the mole fraction of DMSO was around 0.3. Furthermore, for mole fractions of DMSO ranging between 0.2 to 0.4, a glassy amorphous solid was formed instead of solid crystals. Prior to freezing, these samples also showed increased viscosity of the liquid for a large temperature interval. [42]

2.4 Sedimentation

If the chosen technology for separating the heterogeneous phase mixture becomes settling[H], the density and viscosity are properties that will also greatly affect the separation [43]. Settling processes can either employ centrifugal forces to separate the particles or gravitational forces [44]. In this work, whenever settling is referred to from here on, settling by gravitational forces will be implied Settling is a separation process that can either be utilized for clarification, thickening, or both [11, 45]. In clarification steps, the focus is on the liquid phase and the aim is to acquire a liquid phase without, or with a substantially lower concentration, of solid

[H] The terms settling and sedimentation are closely related. In the paper, the term settling will be reserved for the process whereby solids descend through a liquid. The term sedimentation refers to the final state after a completed settling process.

particles [11]. Thickening operations instead have the purpose of producing a slurry with a higher concentration of solid particles [11]. If settling is utilized within the pilot plant design, both the clarification and thickening effect from the settling process would be desirable. The reason for experimentally investigating the settling velocity for the solid carbamate salt particles is since the settling velocity will give an insight into the appropriate size required for a lamella settler. The size of the lamella settler, and other factors such as the spacing and the number of plates, will determine the possible velocity of the flow through the settler and must be chosen correctly relative to the settling velocity. The relative size of the two velocities will be imperial to determining the separation efficiency that can be expected for the equipment. The desirable effect with having a high separation efficiency at the pilot plant will be that the rich slurry stream entering the regeneration column will become more concentrated with the carbamate salt than the rich slurry leaving the absorber. The implication of getting a rich slurry more concentrated with the carbamate salt will be that a lower amount of solvent will have to pass through the energy-demanding regeneration step during each cycle. Possible disadvantages could be that the transportation of the concentrated rich slurry becomes more energy-demanding, and has to be conducted with more complicated, and expensive, process equipment.

The physical properties that are utilized to accomplish sedimentation are the density of the solid particle and the density of the surrounding fluid. When the settling process is studied for an individual particle, it can either proceed in unsteady state or steady state with respect to the momentum balance [45]. In unsteady state, which often occurs when the particle initially starts to settle, the particle will accelerate downwards through the liquid medium due to its gravitational force [46]. However, two forces will work in the opposite direction on the particle, eventually stopping the acceleration as steady state is achieved, whereby the particle will get a constant settling velocity [45, 46]. These forces are the buoyancy force caused by the particle displacing the liquid medium and frictional drag force caused by the particle movement through the fluid [45]. The steady state equation of the momentum balance is given in equation 4 [45].

$$\rho_p * \frac{\pi * d^3}{6} * g = \rho_f * \frac{\pi * d^3}{6} * g + C_D * \frac{\pi * d^2}{4} * \frac{\rho_f * v_T^2}{2} \qquad 4$$

Rearranging the equations, the terminal settling velocity can be calculated from equation 5, which shows that for settling to occur, there has to be a difference in density between the particles and the fluid through which settling occurs. [45]

$$v_T = \sqrt{\left(\frac{4 * g * d}{3 * C_D}\right) * \left(\frac{\rho_p - \rho_f}{\rho_f}\right)} \qquad 5$$

For non-spherical particles, the equations are slightly altered, as the expression for the volume and the lateral surface are different. As mentioned, the viscosity does also affect the settling process, although it is not immediately obvious from equation 5. However, the drag coefficient, C_D, depends on the Reynolds particle number, equation 6, which is a dimensionless number similar to the Reynolds number presented in equations 2 and 3 [11].

$$Re_p = \frac{\rho_f * v * X_p}{\mu} \qquad 6$$

Hence, the Reynolds particle number depends linearly on the inverse of the viscosity. The size of the Reynolds particle number tells within which flow regime the flow resides, being either in the laminar-, in the transition-, or the fully turbulent region [45-47]. Within each region, empirical correlations relate the drag coefficient to the Reynolds number and these correlations and their ranges of applicability can be found within the literature. [11, 45]

If the solid particles can settle as distinct particles, the abovementioned theory is suitable. However, as the concentration of particles increases, the settling process will be better described as another class of settling. In total, settling processes, which are most often used industrially for water- and wastewater treatment, are commonly divided into four classes. The first, known as Class I or distinct particle settling, is the one that has previously been discussed. Class II is also known as flocculant settling, while Class III and IV are known as hindered settling[I] and compression settling respectively. During Class II settling, the particles flocculate[J], whereby the particle shape and size are altered throughout the process. Specifically, small particles, which have large surface areas relative to their volume, tend to flocculate. [46, 47] When the concentration of particles increases further, being in the range of 1,000 mg solids, as particles, per litre of liquid medium, hindered settling and compressing settling will also start to occur [46, 47]. Due to the high particle concentration, the difference in settling velocities that the particles would have during discrete particle settling is suppressed. Slower particles are accelerated to higher settling velocities though collisions with faster particles, which they simultaneously retard [46, 47]. The effect of the collisions and transfer of momentum is that the particles maintain their relative position to each other, hindering faster particles from overtaking slower particles [48]. Therefore, a clear interface is often formed between a layer with a very low concentration of solid particles and a zone with a very high concentration of them [48]. The zone characteristically moves downwards with a constant velocity, called the hindered settling velocity, which is also dependent on the concentration of particles [48]. As the zone moves closer towards the bottom, a layer of particles just above the bottom will start to form a compressed layer with a smaller porosity. Compression settling is caused by additional mechanical support as the particles approach the bottom of the settling

[I] Hindered settling is also known in the literature as zone settling.

[J] The term flocculation is ambiguously used in the literature. It can either be used to solely refer to the physical process whereby particles come in contact with each other. When this definition is used, the term coagulation is used for the processes enabling the particle to conglomerate, an example being the removal of surface charges. However, flocculation can also encompass both the physical and the chemical processes and that is the definition used within the report.

basin [45]. The weight of the solid particles in contact with the particles in bottom layer, which increases with time, pushes the liquid upwards and the particles themselves become part of the compressed bottom layer [46, 47]. An intermediate class of settling can also be observed between hindered- and compression settling, known as transition settling [48].

Ideal settling theory, which in addition to assuming Class I settling also assumes the presence of a distinct settling zone with even distribution of flow both to and from it, was presented by Camp in 1936. Camp also assumed the distribution of the solid particles along the depth of the settling zone to be uniform. The result, which applies to a rectangular, horizontal-flow sedimentation tank without lamella plates, is that the settling velocity does not depend on the depth of the sedimentation tank, but instead on the surface area, A_{basin}, over which the settling process occurs with a volumetric flow Q. [47]

According to the ideal theory, particles with a settling velocity, v_0, fulfilling the mathematical inequality in equation 7

$$v_0 \geq \frac{Q}{A_{basin}} \qquad 7$$

will thereby be removed through the settling process [47]. In the equation, v_0, is defined as the particle settling velocity. The equality holds when v_0 is the minimum settling velocity of a particle, meaning that the particle just has time to reach the bottom of the sedimentation tank prior to the horizontal flow leaving the sedimentation tank. Although being an economical way of achieving solid-liquid separation due to their low energy demand, settling processes have the disadvantage of often requiring long separation times to get high efficiencies of particle removal [43]. A method to further enhancing the removal efficiency for a given sedimentation time, or decreasing the required retention time for a given efficiency, is to utilize lamella settlers [49]. By inserting several parallel plates on a 45° – 60° angle within the settler, the settling device utilizes the Boycott's effect [43, 48, 49]. A.E. Boycott noted in 1920 that if he held tubes containing blood droplets at an angle, the sedimentation process proceeded faster [50]. The reason is that the settling distance for the particles decreases, and they will encounter the plates in a shorter time [49]. When having struck the lamella plates, most solids will slide down along the plates towards the bottom of the settler, a process that proceeds quicker than settling under high concentrations of particles or droplets [49].

According to the ideal settling theory, it is the additional horizontal settling area provided for deposition by the lamella plates that reduces the required settling velocity of the particles, and thereby increases the efficiency of removal [49]. However, the assumptions of the ideal theory are often not valid during actual operation. For lamella settlers, equal flow distribution between the formed channels is often the major problem, along with hindering particles sliding down the channels from being resuspended [48, 51]. These factors are also connected, as the fate of deposited particles on the lamella plates can affect the flow distribution [51]. If, illustrated with an example from wastewater treatment, biological mass sticks to the lamella

plates, specific channels can over time become clogged, which will lead to uneven flow distribution [51].

Lamella settlers can be configured in three ways, counter-currently, co-currently, or cross-currently, which are presented schematically in Figure 2.3 [48]. The three names indicate the relation between the liquid flow pattern and the sliding motion of the solids along the plates. The most common configuration is the counter-current mode. New equations for the settling velocity, given an ideal settling process, are acquired, which will depend on the tilt angle against the vertical axis, the perpendicular distance between the lamellas and the length of the lamellas. Corresponding equations to equation 7 for each configuration can be found in the literature. [52]

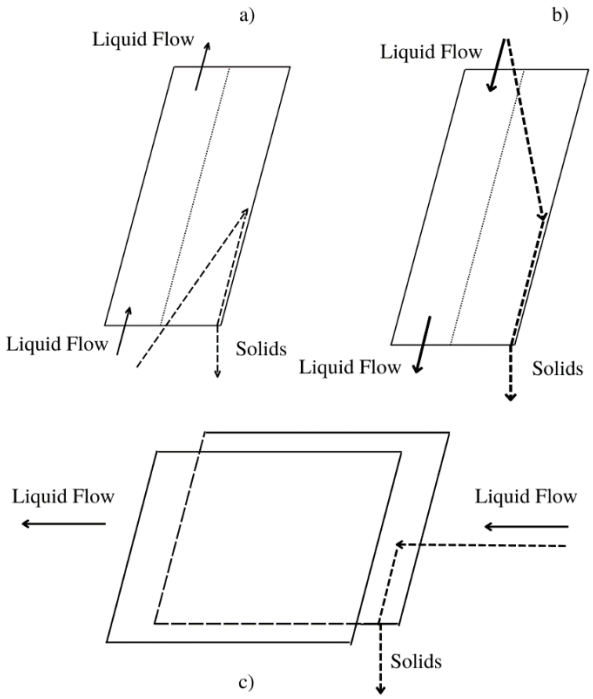

Figure 2.3. The three types of configurations that lamella sedimentation basins can configured in with respect to the flow pattern. The schematic images showcase the liquid flow through the plates. The images also showcase examples of the movement of the solids, and how they are captured and slide down the lamella plates and are hence separated away from the liquid phase. Subimage a) showcases the counter-current configuration, b) the co-current configuration, and c) the cross-flow current configuration. Adapted from Metcalf & Eddy [48].

3 Materials and methods

3.1 Preparation of stock mixtures

Materials

The main chemicals used in this study was DMSO (99.9 %, Acros Organics) and AMP (99 %, Thermo Fisher Scientific). Both chemicals were utilized without further purification. For mixtures with added water, deionized water was used. Gaseous carbon dioxide (99.99 %, AGA) was used to obtain the CO_2-loaded samples. Additionally, 1-pentanol (99 %, Sigma Aldrich) was used as a reference for some of the viscosity experiments.

Preparation of stock mixtures

In order to carry out the desired experimental work and investigate how the CO_2-loading and the water content affects the physical properties, stock mixtures with varying composition were prepared. The stock mixtures containing water, AMP, and DMSO were prepared by weight. The stock mixtures can be divided into two groups. In the first group, the ratio between the weight of DMSO and AMP was three, while in the second group, the ratio was one. The abbreviations used to denote the stock mixtures are found in Table 3.1, together with the weight percent of each component. The letter H refers to water, A refers to AMP, and D to DMSO. The numbers in the abbreviations correspond to the weight percentage of the chemical within the stock mixture, rounded to the closest half or whole percentage. The tested CO_2-loadings (α) of the stock mixtures, which describes the molar ratio of CO_2 to AMP initially present within the mixture (see equation 1), are also listed.

Table 3.1. Mixtures included in the experimental investigation. The table also indicates the composition of water, dimethyl sulfoxide, and 2-amino-2-methyl-1-propanol of the liquid mixture prior to CO_2-loading. The composition is written as weight percentages. The investigated CO_2-loadings (α) are indicated, i.e. the ratio, on a molar basis, between CO_2 absorbed and the initial amount of amine in the mixture.

First Group	Water (**wt-%**)	AMP (**wt-%**)	DMSO (**wt-%**)	**α** (mol CO_2/mol AMP)
0H25A75D	0	25	75	0, 0.2, 0.38, 0.5
5H24A71D	5	24	71	0, 0.2, 0.38, 0.5
10H22.5A67.5D	10	22.5	67.5	0, 0.2, 0.38, 0.5
Second Group				
0H50A50D	0	50	50	0, 0.2, 0.38, 0.5
5H47.5A47.5D	5	47.5	47.5	0, 0.2, 0.38, 0.5
10H45A45D	10	45	45	0, 0.2, 0.38, 0.5

The compositions of the stock mixtures within the first group were chosen based on the amine solution that will be fed to the pilot plant, 25 wt-% AMP and 75 wt-% DMSO, following the research by Karlsson [14]. Karlsson has also done experiments with similar water compositions [14]. The second group of stock mixtures has a higher AMP concentration, and was chosen as some of the DMSO will be separated before the regeneration step in the pilot design. Similarly, the expected CO_2-loading for the rich liquid leaving the absorption column is 0.38,

which is why it was investigated specifically. The other investigated CO_2-loadings were chosen within the interval of possible CO_2-loadings, as the actually achieved CO_2-loading for the pilot plant might differ from the expected.

The total amount of stock mixture that needed to be prepared was decided based on the amount needed for the different experimental measurements. Then, the necessary amounts of AMP to achieve the desired final weight was calculated. A transparent screw cap reagent bottle was first weighed with the cap on to get its tare weight. The cap was then removed and replaced with a funnel, and the digital scale was tared again. AMP was then poured into the reagent bottle. From the added weight of AMP, the required amount of DMSO was calculated to achieve the correct relation between the weights of the two chemicals for the given stock mixture. Next, if the stock mixture was to contain water, the desired weight of deionized water was calculated and added. Lastly, the funnel was removed and the cap was screwed on tightly. For unloaded stock mixtures, the stock mixtures were complete after following the abovementioned procedure.

The CO_2-loaded stock mixtures were prepared by bubbling gaseous CO_2 into the mixtures of water, AMP and DMSO. The starting weight of the sealed reagent bottle was noted. The weight of carbon dioxide that had to be added, to achieve the desired CO_2-loading, was calculated. The cap was taken off and the tube from the CO_2 bottle was put into the mixture. The flow of gas from the gas tube was opened carefully until carbon dioxide bubbled through the mixture. When the desired final weight had been achieved, the flow of gas was turned off and the cap was put back on. The sealed reagent bottle was then allowed to cool down at room temperature, as the temperature of the stock mixture increased due to the exothermic absorption reactions. The utilized equipment was washed with deionized water, with the wash water being disposed of in a designated container for chemical waste, as AMP is toxic to aquatic life [30].

3.2 Imaging of carbamate salt particles

A microscope, Nikon Optiphot, with a Nikon E Plan 10X/0.25 160/- Ph 1 DL objective was used for image capturing of carbamate salt particles. Before the first studies were carried out, satisfactory performance and interplay between the camera, the computer, and the microscope was tested by observing a 1/100[K] millimetre microscope calibration slide with distinctive marking. The phase used on the microscope was Phase 4. A standard setting, denoted as PM0, with P standing for plus and M for minus, was marked out with tape on the smallest rotor for adjusting the plate height on the microscope. As the rotor changed the distance between the objective lens and the sample, the effective magnification changed when it was rotated. Hence, the microscope was calibrated against the calibration slide at different relative positions of the height adjuster rotor. The results of the microscope calibration can be found in Appendix A.

Positive, or plus, rotations of the rotor resulted in an increased distance between the lens and the sample, as can be seen in Figure 3.1. Negative, or minus, rotations of the rotor resulted in a decreased distance between the lens and the sample, as can be seen in Figure 3.2. After

[K] On a 1/100 millimetre slide, there are 100 markings, with 10 large markings, over the total distance of 1 millimetre.

capturing an image, see Figure 3.3 of the calibration slide, the VisiCam software allowed the user to manually enter a calibration line. The distance between two adjacent large lines was chosen as the calibration basis for all rotor positions. The calibration line was drawn along the top of the smaller lines to correctly place the start – and end point of the calibration line. After drawing the calibration line, the software asks the user to enter the actual length of the calibration line. As a 1/100-millimetre microscope calibration slide was used, the distance between adjacent large lines is 100 µm, which was entered into the software. Calibrations were done for all rotor positions, including no rotation, relative to the standard setting for which the calibration slide could be clearly visualized.

For the investigations of sample mixtures with the microscope, a single droplet of the desired mixture was transferred to a clean microscope slide with the aid of a flat spatula after thorough mixing. A cover glass was put on top of the liquid droplet. The slide was then placed under the objective, the light was adjusted, as was the relative position of the height adjuster rotor towards the standard setting. When the crystals could be visualized, the location studied within the droplet could be changed with the rotors encircled in green in Figure 3.2. The relative position of the height adjuster rotor was noted. After an image had been captured, the relevant calibration was selected from the calibration table and the image could be processed within the VisiCam software.

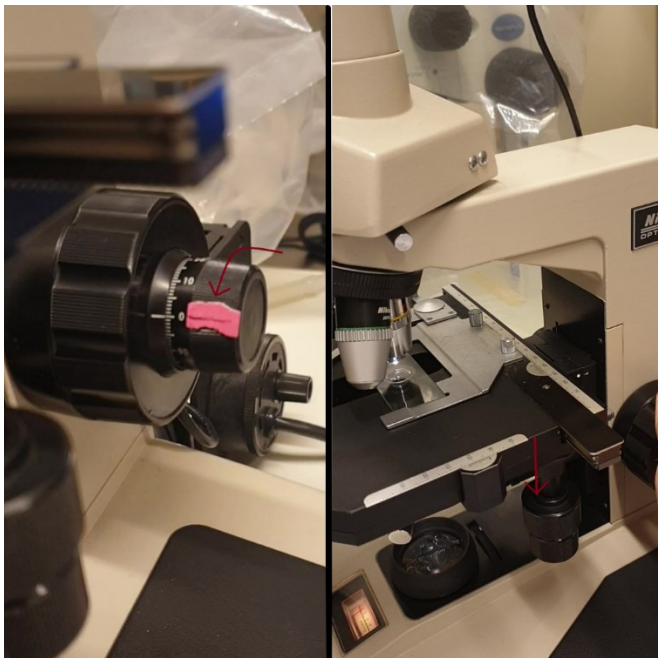

Figure 3.1. Definition, and effect, to the left and right respectively, of a positive rotation of the height adjuster rotor.

Figure 3.2. Definition and effect, to the left and right respectively, of a negative rotation of the height adjuster rotor. The green encircled rotors can change the studied position on the microscope slide.

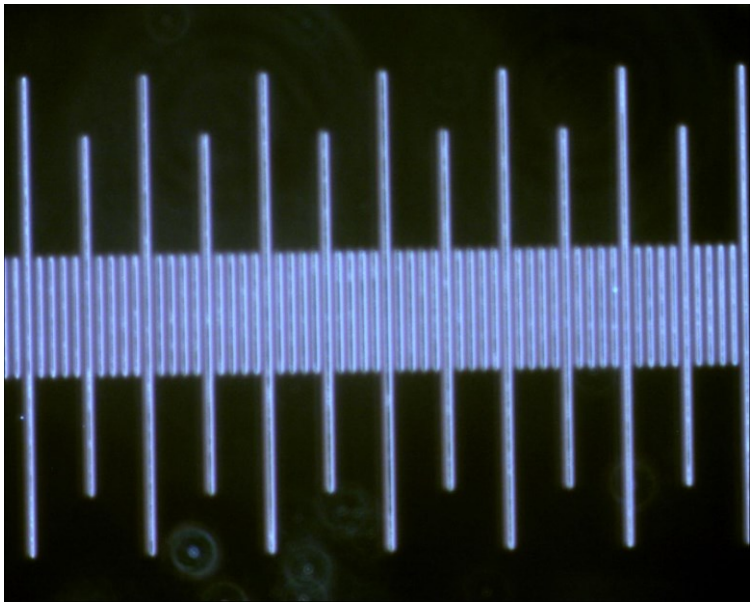

Figure 3.3. An image of the utilized 1/100 mm calibration slide with the standard magnification and the height adjuster rotor in position PM0. By drawing a straight line between two adjacent lines of the largest visible line, with the line being drawn along the top of the smallest lines, a correct calibration could be made within the software, enabling the distance to be calculated for other images utilizing the same magnification and position of the height adjuster rotor.

3.3 Determination of settling velocity

The settling velocity experiments were conducted using measuring cylinders (50 mL), which were either kept at room temperature or at an elevated temperature within a water bath. Prior to transferring the stock mixture into two measuring cylinders, the stock mixture was rigorously shaken. Plugs were put into the measuring cylinders, which were then wrapped tight in Parafilm to hinder water infiltration. One of the measuring cylinders was put into a

furnace at 50 °C. A water bath was set up, consisting of a two-litre beaker, a hotplate stirrer, a magnetic stirrer, and a metal retort stand with a ring clamp. The two-litre beaker was filled with deionized water, which was heated to 50 °C. When the correct temperature had been reached, the ring clamp was placed around one of the measuring cylinders. The metal retort stand was put in a position whereby the mixture-containing part of the measuring cylinder became fully submerged in the water. Two adjustable stands were utilized to elevate the GoPro camera and the other measuring cylinder to same elevation as the measuring cylinder in the water bath. The two measuring cylinders were rigorously shaken and were then placed simultaneously at their respective positions in front of the camera.

The experimental results gained from the experimental setup were sets of snapshots from the camera of each measuring cylinder. The snapshots showed how far down from the top of the liquid pillar within the measuring cylinder that the precipitate front had moved. The camera captured an image every sixty second. From the set of snapshots corresponding to an experimental run, the height of interface, abbreviated as HOI, for the stock mixture could be determined and compared to a reference level. The reference level used was the interior bottom of the measuring cylinder. The distance between the lines on the measuring cylinder was determined to be 1.35 mm. The HOI were then plotted as a function of time and the settling velocity was determined as the slope of the linear regression.

3.4 Lamella sedimentation

The utilized stock mixtures for the lamella sedimentation experiment were prepared in accordance with the procedure described under section 3.1. However, due to volume necessary for the experiment, the slurry mixtures were prepared in plastic waste containers, not in glass reagent bottles. Two of the waste containers were put into a brown plastic container after having been prepared. The brown plastic container was filled partly with cold water, and during their cooling within the water-filled container, the containers were at times shaken vigorously. The three other waste containers were not put into the water-filled container, with the aim of treating the waste containers differently being to get a distribution of particle sizes.

After the slurry mixtures had been prepared, the experimental setup was constructed. A Plexiglas lamella sedimentation basin, visualized in Figure 3.4, was placed within a large transparent plastic container. Six sheets of Plexiglas were put into specific position in the basin, visible in Figure 3.4, forming lamella plates. Thereafter, six double-sheet constructions of extra inclined plates were put in place between the Plexiglas sheets with steel wire.

Figure 3.4. Image of the utilized lamella sedimentation basin. To the very right, the Plexiglas plates are shown, and the additional plates can be seen between the lamella sedimentation basin and the Plexiglas plates.

A metal container was put below the outflow of the lamella sedimentation basin, as a secondary collection vessel for the outgoing mixture. Within the metal container, a glass container was put, serving as the primary collection vessel. Its placement within the metal meant that the glass vessel could be emptied without the risk of mixture being spilled. At the inlet to the lamella sedimentation basin, the setup to provide a liquid flow to the basin was constructed. Two adjustable trays were utilized to hold a five-litre container at the necessary elevation. A compatible glass stopcock, seen in Figure 3.5, was greased with vacuum grease and attached to the outflow pipe of the five-litre container. The connection was wrapped with Parafilm to hinder potential leakage of the stock mixture.

Figure 3.5. The utilized glass stopcock, which enabled the inflow to the lamella sedimentation basin to be regulated.

Thereafter, a suitable position for capturing the experiment was found for the camera and the image capturing was initiated. Three waste containers, approximately 14 litres, of stock mixture were poured into the inlet zone of the lamella sedimentation basin. An additional container was poured into the five-litre container. The stopcock was turned to produce an outflow that would give the desired residence time. The slurry mixture within the five-litre container was mixed manually with a rod, after poor performance of the utilized magnetic stirrer was noted. The poor performance of the magnetic stirrer led to sedimentation within

the five-litre container. Therefore, collected outgoing fluid was returned to the five-litre container three times during the experiment to provide liquid to get out the remaining settled particles from the five-litre container. After the experiment, two slurry mixture samples were collected from the experimental setup. The first was taken from the bottom of the lamella sedimentation basin and was called *Bottom slurry*. The second slurry mixture sample was taken from the glass container after it had been emptied three times, and was called *Effluent slurry*.

3.5 Freezing temperature

The freezing temperature of the stock mixtures, where the weight ratio between DMSO and AMP was three, was measured as the melting temperature of a frozen sample. For the first procedure, a volume around 30 mL was poured with the aid of a funnel into reagent bottles from the stock mixtures with the desired compositions. The cap was screwed on tightly and then, the samples of the stock mixtures were put into a freezer, either at -20 °C or -80 °C. After a sample had frozen, the reagent bottle was taken from the freezer. The content of the reagent bottle was monitored at room temperature until a liquid phase started to form. As soon as the tip of the thermocouple, a model $K^{L,53}$ thermocouple equipped to Anritsu Anritherm Digital Handheld Thermometer, could be inserted into the formed liquid without touching the solid phase or the walls. The thermocouple tip was placed in the middle of the volume of formed liquid and the melting temperature was read. After measuring, the thermocouple was cleaned. For each stock mixture, at least three individual experiments were carried out on different consecutive days.

Another procedure was also tried, where the thermocouple was placed within the sample as it went into the freezer. When the frozen sample was taken out from the freezer, the temperature registered with the thermocouple was measured over time. Ideally for the graph of the temperature over time, a plateau should have appeared when the melting temperature was reached. In theory, at the melting temperature, the entire sample would have to transition from solid to liquid before the temperature could continue to increase. But as several sources of error affected the method, and since the rate of melting could not be controlled, no plateau was achieved. Therefore, no reliable estimation of the melting temperature could be conducted. It was also deemed that the procedure relied too much on the reaction speed of the person conducting the experiment. Therefore, no results with the second procedure will be reported.

3.6 Density

The density of the stock mixtures was measured through two different methods. The first method was conducted with a range of hydrometers spanning densities of 0.7 – 2.0 g/cm^3. To utilize the hydrometers, the stock mixtures had to be poured into a 500 mL measuring cylinder. A clamp was tightened around the measuring cylinder and attached to a ring stand, in order to prevent the measuring cylinder from falling over, and it was also placed within a waste bucket. The studied liquid or liquid mixture was thoroughly mixed and poured into the measuring cylinder with the aid of a funnel. A thermometer was used to check the

[L] A thermocouple of model K, is made of the two nickel alloys chromel and allumel, was utilized during the experiments. The tolerance for Model K thermocouples is 1.5 °C up to temperatures of 375 °C.

temperature of the sample in the bottom, middle, and the top of the measuring cylinder. Thereafter, the density could be measured by reading where the liquid interface placed itself on the graded stem of an appropriate hydrometer. Five consecutive readings were done, with manual mixing and complete removal of the hydrometer taking place between each reading.

In the second method, the densities of the stock mixtures were determined through a gravimetric approach. In the first step of the procedure, a 50 mL volumetric flask was weighed three times. Then, the same was done for a cap to the volumetric flask. Next, the utilized stock mixture was thoroughly mixed. For unloaded stock mixtures, mixing was achieved thorough shaking of the container with the stock mixture. Then, the unloaded stock mixture was poured into the volumetric flask with the aid of a beaker and a funnel. When the liquid interface within the volumetric flask almost touched the line indicating 50 mL, the funnel was removed. To get the meniscus of the liquid exactly on the line indicating the correct volume, a Pasteur pipette was used to transfer the last droplets into the volumetric flask. Then, the cap was put on the volumetric flask, and it was weighted three times. Lastly, the liquid temperature was registered with a thermometer. The employed procedure was similar for the CO_2-loaded stock mixtures. However, mixing was achieved through manual stirring with a lab spatula, as vigorous shaking of the CO_2-loaded stock mixtures resulted in the formation of a layer of foam, which had distinctly different properties to the stock mixture, making the sample unrepresentative. The temperature measurement was also done with a model K thermocouple instead of a thermometer.

3.7 Viscosity

Three different methods were employed to determine the viscosity of the unloaded stock mixtures. However, only one of the three methods, the last described, was also employed for CO_2-loaded stock mixtures.

The first method employed an Ostwald viscometer, visible in Figure 3.6 where the kinematic viscosity of a liquid mixture can be related to the kinematic viscosity of a reference liquid. Deionized water was chosen as the reference liquid. In order to diminish temperature fluctuations during the experiment, the Ostwald viscometer was placed within a water bath. Within the glass beaker, mixing occurred with the aid of a magnetic stirrer and a stirrer plate. Two thermometers were placed into the measuring cylinder to enable the temperature to be read at two different positions, outside the reservoir bulb and the measurement bulb, respectively. The reservoir bulb is the bulb encircled in Figure 3.6, while the measurement bulb is the bulb surrounded with the test lines. Next, a funnel was put into the reservoir opening of the Ostwald viscometer. A volume of 5.4 mL of thoroughly mixed mixture was transferred with a measuring pipette to the reservoir tube of the Ostwald viscometer. Onto the other opening, a laboratory hose, which was connected to a plastic syringe, was put. For each experimental attempt, the syringe was used to draw the liquid sample from the reservoir bulb, up through the capillary and past the measurement zone. After being drawn past the measurement zone, the laboratory hose was removed, whereby the liquid started to fall down the capillary and the measurement zone. When the liquid interface passed the upper line, a time measurement was initiated. The time was stopped when the same interface crossed the lower line. Five consecutive measurements were done according to the abovementioned procedure. After the measurements were done, the Ostwald viscometer was emptied appropriately, washed clean, and dried.

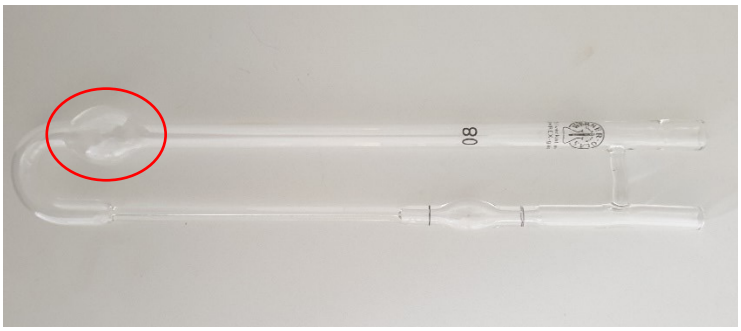

Figure 3.6. The employed Ostwald viscometer, where the two test lines are visible on both sides of the measurement bulb. Encircled is the reservoir bulb of the Ostwald viscometer.

The second method for evaluating the viscosity of the liquid samples used an Anton Paar Modular Compact Rheometer, with the accompanying bob, and cup. A computer with the necessary software to run the instrument was also imperial to the completion of the experiments. The first thing that was done within the software was to initialize the rheometer. Thereafter, within the software, the parameters for conducting and evaluating an experiment could be chosen. The most relevant parameters were the operating temperature, the tolerance against temperature deviations, the number of data points, the span of shear rates to be investigated, and the time spent measuring the shear stress for each of the respective shear rates. The operating temperature was the sole of these parameters which was changed for different experimental runs, with the others being kept constant. The temperature was allowed to deviate +/- 0.2 °C from the desired operating temperature. In addition, the experiment was not allowed to start unless the instrument managed to hold the operating temperature within the desired temperature interval for at least one minute. For each experiment, forty shear rates were tested between 0.1 s^{-1} to 1,000 s^{-1}. The forty data points were spaced out using the ramp logarithmic alternative within the software. The measurement time increased, utilizing the ramp logarithmic alternative, from 1 second for the first data point to 20 seconds for the last data point, to diminish the runtime of each experiment. The decision was supported by previous operational experience, which had concluded that worse, unrepresentative results was often obtained for smaller shear rates. After having set the correct settings, the desired bob and the matching sample container were chosen. A liquid volume of 6.5 mL, was then transferred to the sample container after thorough mixing. Then, the bob and the sample container were placed within the rheometer, and the experiment could be initiated from the software.

For the third and final method, which was used to investigate the viscosity of both unloaded and CO_2-loaded stock mixtures, an NDJ-8S Digital Rotary Viscometer was used. A sample volume of 25 mL of either a thoroughly mixed pure liquid, an unloaded or a CO_2-loaded liquid mixture was transferred to the instrument-associated, metal, measuring beaker. Before the measuring beaker was connected to the instrument, the temperature of the slurry mixture sample was measured with a model K thermocouple. A rotor, with an appropriate viscosity working range, was chosen from the available set of rotors and was screwed onto the centre of the viscometer housing. The appropriate rotor was chosen from a lookup table, within the instrument manual, over the working ranges of each rotor given each rotational speed setting. Thereafter, the instrument-associated housing extension was attached to the perimeter of the viscometer housing with a screw. Then, the measuring beaker was attached to the housing extension with another screw. Finally, the instrument could be turned on. From the digital interface, different rotation speeds could be chosen, and measurements initiated. Alongside

showing the dynamic viscosity after a measurement time period, the percentage value of the maximum dynamic viscosity possible with the chosen rotor and setting was also displayed. If the percentage value was outside the 10 -100 % range, the measurement value was deemed not fully reliable.

4 Results

4.1 Settling velocity experiments

The settling velocity experiments were conducted for two CO_2-loaded 0H25A75D stock mixtures, see Table 3.1. It is a 0H25A75D mixture that will be fed to the pilot plant, and therefore, it was the only composition for which the settling velocity was investigated. Furthermore, a CO_2-loading of 0.38 is expected for the rich liquid entering the separation unit, which motivates its investigation. A stock mixture with a CO_2-loading of 0.50 was also investigated to determine the influence of the CO_2-loading upon the settling velocity. It corresponds to the theoretical maximum loading capacity, and is an upper boundary for the CO_2-loading, which is why it chosen for the tests. Experiments were performed at both 21 and 50 °C. Three experiments were performed with two stock mixtures having a CO_2-loading of 0.38 and 0.50, respectively. Figure 4.1 shows the average values obtained for the settling velocity, for the CO_2-loaded mixtures at both 21 and 50 °C. In Figure 4.1, it can be seen that the average settling velocity was more than 12 times greater at the CO_2-loading of 0.50 than at 0.38 for both temperatures. Furthermore, when the temperature was increased from 21 to 50 °C, the settling velocity roughly doubled for both CO_2-loadings. The explanation to this increase in settling velocity can likely be traced to effect of the temperature on the viscosity and the density. With increasing temperature, both the viscosity and the density tend to decrease, which is beneficial for the settling velocity. The CO_2-loaded mixtures were also investigated using a Nikon Optiphot microscope in order to evaluate if the particle size of the precipitate differed between the different samples. The found characteristics of the stock mixtures, and the details behind the averaged values in Figure 4.1, will be presented next.

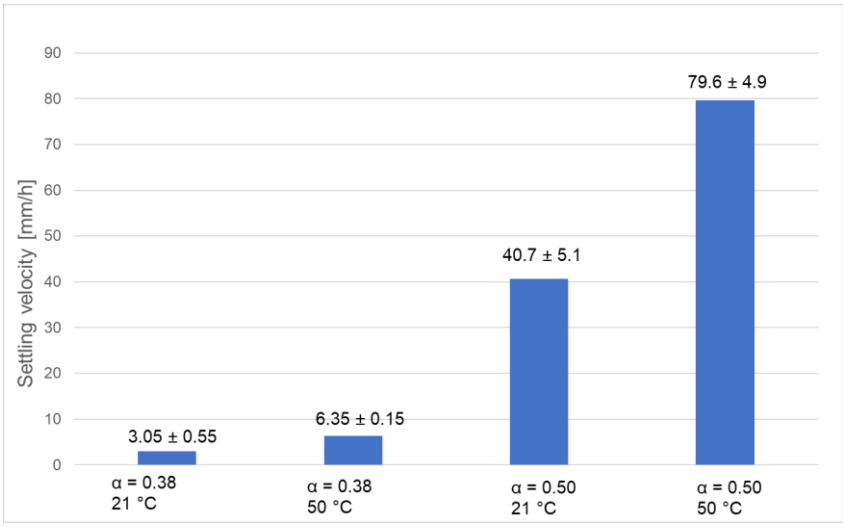

Figure 4.1. Average settling velocity for the stock mixtures containing 25 wt% AMP and 75 wt% DMSO with CO_2-loadings of 0.38 and 0.50, at 21 and 50 °C. Detailed sedimentation data is found in Appendix B.

4.1.1 The stock mixture with a CO_2-loading of 0.38

Two experimental runs were conducted for each mixture at both temperatures. During each experimental run, two measurements were simultaneously captured with a GoPro camera. One measurement was done at 21 °C and one in a water bath at 50 °C, which can be seen in Figure 4.2. Between the first and second experimental run, the measuring cylinders were

heavily mixed. The positions of the measuring cylinders were also switched, meaning that the measuring cylinder that had been tested at 21 °C during the first experimental run was tested at 50 °C during the second experimental run, and vice versa.

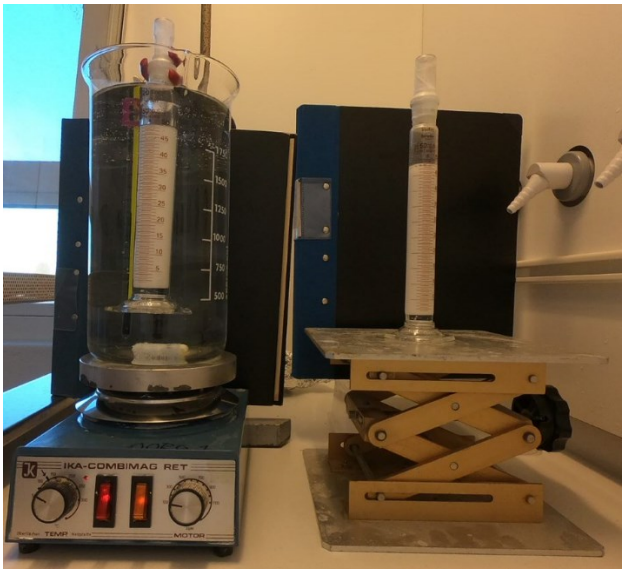

Figure 4.2. Image showing the experimental setup used for determination of the settling velocity.

For three out of the four experiments, reading of the height of interface was initially visually obstructed. The obstruction was caused by the formation of a small carbamate salt particle layer on the surface of the liquid within the measuring cylinders. This obstruction can be seen in Figure A.3 to Figure A.5 in Appendix B as a drastic decrease in HOI as the carbamate salt on the surface was no longer obstructing the actual height of interface from being read. Between the two attempts at 21 °C, the variation in settling velocity was large, which can be seen from the standard deviation in Figure 4.1. During the first attempt, the settling velocity was 2.5 mm/h, while for the second attempt it was 44 % greater at 3.6 mm/h. The results at 50 °C were much closer in magnitude, with the registered settling velocities being 6.2 and 6.5 mm/h, respectively. Two additional settling velocity experiments were also conducted using an old solution, stored approximately 8 months, with a similar CO2-loading of 0.38. During these attempts, no settling velocity could be obtained as the sedimentation proceeded extremely fast, without the presence of a clear front[M].

After the settling velocity experiments, the stock mixtures was investigated with the Nikon Optiphot microscope. Clear crystals were observed, seen in Figure 4.3, when utilizing the standard magnification and as the height adjuster rotor was in the reference position PM0. The distance per pixel differs for different positions of the height adjuster rotor. A calibration of the microscope was conducted between positions P30 and M30, with the results presented in Appendix A. Within this range, the size of the crystals could be determined with the VisiCam software. The top image was taken at the edge of the droplet, and the white section at the top of the image is the interface of the cover glass. As the height adjuster rotor was within the range of the calibration, the particle side lengths could be determined. A distribution of particle sizes could be observed, with side lengths starting around 3µm and going up to

[M] With front, what is meant is a defined interface with the slurry of the solid precipitate particles on one side and transparent solvent on the other.

around 23µm.The bottom image was less representative of the overall distribution of particles for the studied droplet, but shows that also larger crystals were present, with side lengths as large as 42.4 µm being observed. It should be noted that no attempts were made to determine the particle size distribution in the samples.

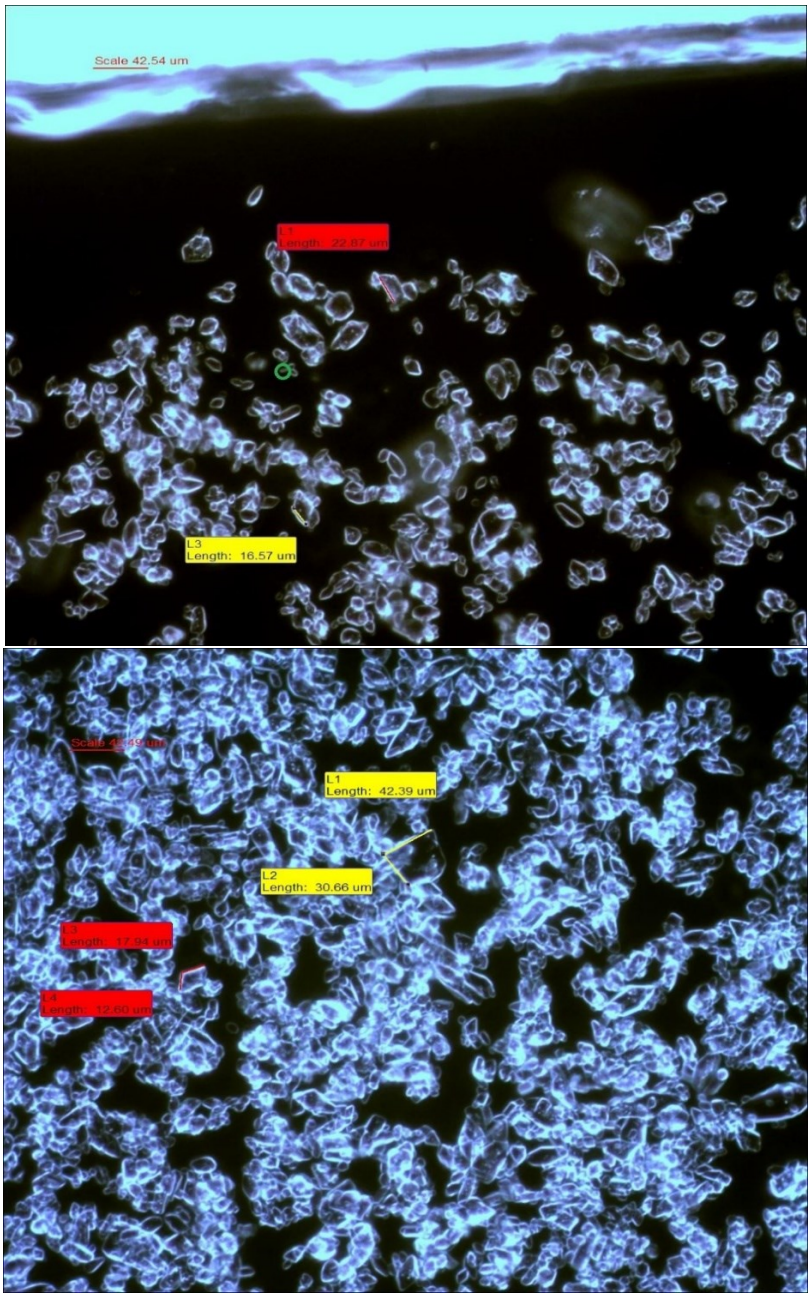

Figure 4.3. Microscopic images of crystals found in a droplet of the second slurry mixture with CO_2-loading 0.38, for which the settling velocity was investigated. The large white region in the top image is the interface of the cover glass. The images were taken with the standard magnification and with the height adjuster in position PM0.

The older solution was also investigated with the microscope. It was seen that the particle size within the older solution was far greater than for the freshly made mixtures. However, their size could not be determined as the crystals needed to be studied with a lower magnification, outside the region of calibration of the microscope. The images of the crystals can be seen in Appendix C.

4.1.2 The stock mixture with a CO_2-loading of 0.50

Three experimental runs were conducted on the stock mixture with a CO_2-loading of 0.50. During the first experimental run, the water level in the water bath hindered an accurate visual reading of the position of the front at 50 °C. This can be seen in Figure A.6, where the first experimental data value could only be registered after around 0.4 hours. Even though enough experimental data points were acquired to perform a linear regression, another experimental run was conducted without switching the position of the measuring cylinders. The settling velocities obtained at 21 °C were, for the two attempts, almost identical at 37.0 and 37.1 mm/h. However, between the two attempts at 50 °C, the settling velocity differed considerably. During the first attempt, the obtained settling velocity was 75.3 mm/h, and for the second attempt it was instead 86.5 mm/h.

Prior to the third experimental run, the position of the measuring cylinders was switched. At 21 °C, the obtained settling velocity during the third experimental run was 47.9 mm/h, 29 % greater than the two previous runs. At 50 °C, the settling velocity was 76.9 mm/h, similar to the settling velocity obtained during the first experimental run.

A drop of the slurry mixture was also studied with the microscope. At the standard magnification, and with the height adjuster in position P25, individual crystals could be clearly visualized. Figure 4.4 shows a large presence of rod-shaped or rectangular crystals, with great differences in the respective side lengths for many of the crystals. Smaller circular structures were also observed, these were deemed to not represent crystals but fluid droplets within air bubbles. The motivation for this can be found in Appendix H.

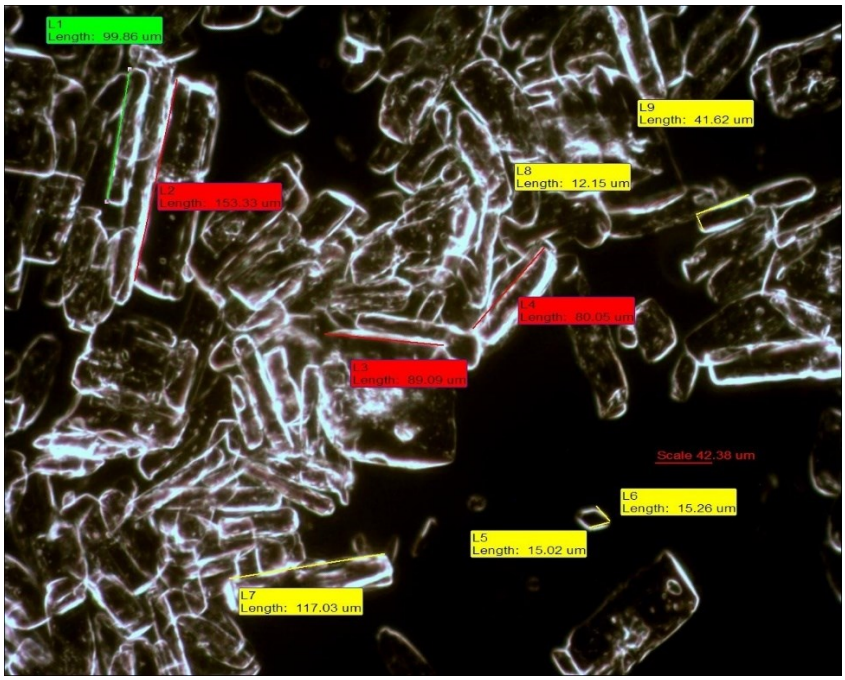

Figure 4.4. Image of the rod-shaped crystals found in a droplet of the 0H25A75D slurry with a CO_2-loading of 0.5. The standard magnification was utilized, and the height adjuster was placed in position P25 during the image capturing.

4.2 Lamella sedimentation experiment

Due to the large volumes of chemicals needed to conduct one lamella sedimentation experiment, it was only performed at one stock mixture concentration. The chosen stock mixture was a 0H25A75D solution, having a CO_2-loading of 0.38, as this is the composition expected for the rich liquid entering the separator within the pilot plant. The qualitative assessment of the separation method was done through visually examining the equipment, and the difference in colour of the inflow and outflow slurry during operation. Qualitative results were also obtained by employing the Nikon Optiphot microscope, where the presence and size of salt crystals within the *Bottom*- and *Effluent slurry* samples could be investigated.

4.2.1 The lamella sedimentation basin

During the experiment with the lamella sedimentation basin, the following observations were made for the in- and outgoing slurry mixtures. The ingoing slurry mixture had a clear white colour, visually resembling milk, see the left image in Figure 4.5, while the effluent was more transparent, seen in the right image in Figure 4.5. Furthermore, the transparency seemingly increased over time.

Figure 4.5. Image showing the ingoing (left) and outgoing (right) mixtures to the lamella sedimentation basin.

During operation, large portions of the precipitate was separated, ending up in the bottom of the lamella sedimentation equipment, see Figure 4.6. There, the precipitate salt crystals formed a thick, solid white layer. Above this layer, a clearer, but slightly opaque liquid, left the channels formed by the inclined plates and flowed out of the lamella sedimentation basin. At the end of operation, samples were collected from the two fractions (the bottom layer and the outgoing liquid) for further evaluation.

Figure 4.6. The lamella sedimentation basin during operation. The interface between the precipitate-enriched slurry and the lean slurry with less salt crystals can clearly be seen at the distinct border between the white and the more transparent liquid phases.

4.2.2 Qualitative results concerning the effluent slurry

After the collection of the *Effluent slurry*, it was investigated with the microscope. The investigation showed that there existed large, polygon-shaped crystals within the *Effluent slurry*, as shown in Figure 4.7. The observed side lengths extended above 20.60 µm. The side lengths were estimated with the calibration done when the height adjuster was in position P20. The image is thought to be representative of the particle concentration, and also the particle sizes observed within the studied droplet of the *Effluent slurry*. However, whether it is representative for the entire *Effluent sample* has not been determined. Small circular structures were also observed during investigation of the *Effluent slurry*. It was deemed that these did not represent crystals, but instead fluid droplets. The motivation can be found in Appendix H.

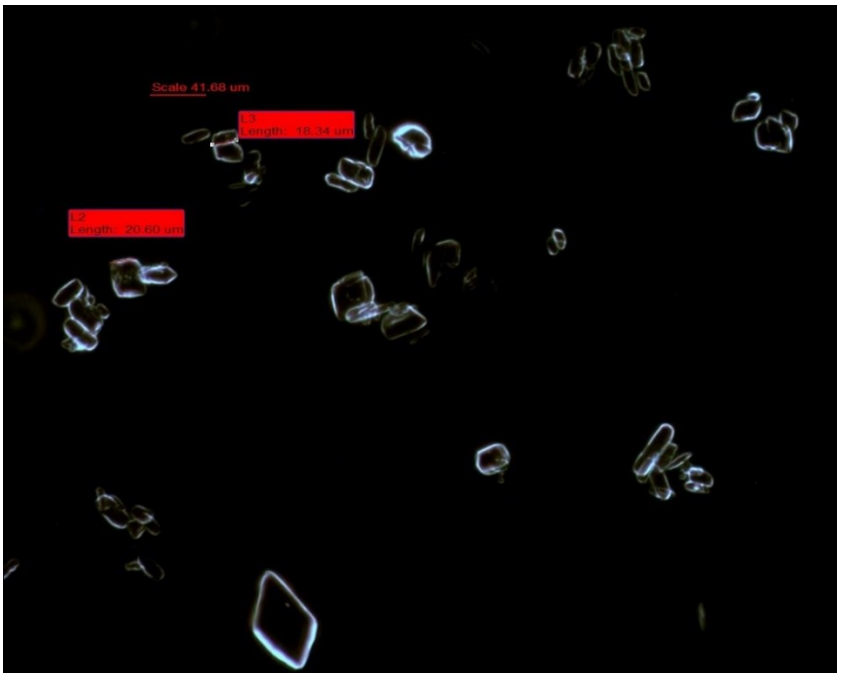

Figure 4.7. Image showing crystals in the Effluent slurry sample, taken with the standard magnification and the height adjuster rotor in position P20.

4.2.3 Qualitative results of the microscope study of the bottom slurry

The microscopic evaluation of the *Bottom slurry* was conducted in two different ways. First, similar to the study of the *Effluent slurry*, a single fluid droplet was investigated. Two representative images of what was seen, is presented in Figure 4.8. The concentration of particles was seemingly very high, with overlapping contours of different carbamate salt crystals throughout the entire image. In addition, the observable crystal shapes are roughly rectangular, rhombic or polygonal. Very large crystals were also observed for the *Bottom slurry*. In the right image of Figure 4.8, two large rhombic-shaped crystal can be seen close to the boundary of the liquid droplet.

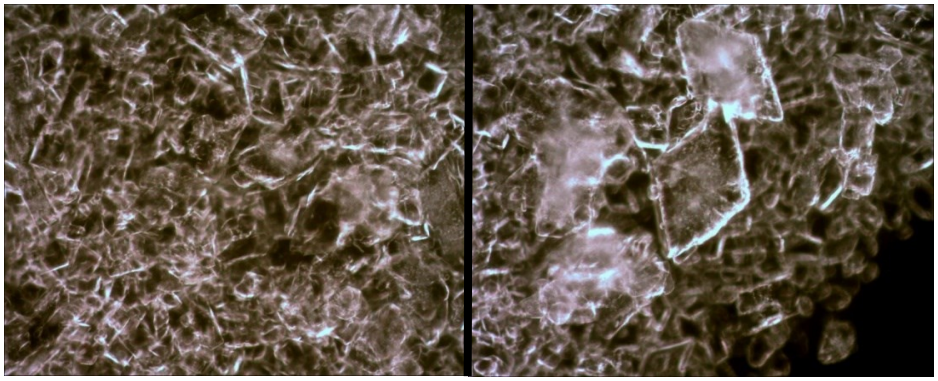

Figure 4.8. Images showing crystals in a droplet of the bottom slurry from the lamella sedimentation experiment. In the images, the standard magnification was utilized, and the height adjuster rotor was in position P95.

However, no size determination could be conducted for the images presented in Figure 4.8, as the height adjuster rotor was in position P95 when utilizing the standard magnification. This position of the height adjuster rotor was far outside the range for which the microscope had been calibrated. Calibrations could only be conducted for height adjuster positions in the range from M30 up to P30, not all the way up to P95. Therefore, an additional approach to studying the *Bottom slurry* was warranted. In the second approach, a small amount of the *Bottom slurry* was added to a Petri dish. The majority of the liquid was allowed to evaporate, under atmospheric conditions, after which a tiny amount of the solid paste left was transferred to a microscope slide. A striking difference in the amount of overlapping of particles was achieved by applying the new approach, which can be seen by the image in Figure 4.9. Clearer crystal edges were also an effect of the new approach. Furthermore, the crystals could also be visualized with the standard magnification and the height adjuster rotor in position PM0. Therefore, the size of the crystals could be measured, with the side lengths of the crystals ranging between 50.64 µm down below 9.3 µm. Smaller circular structures were also observed with the second procedure. It was deemed that these did not represent crystals, but fluid droplets. The motivation can be found in Appendix H.

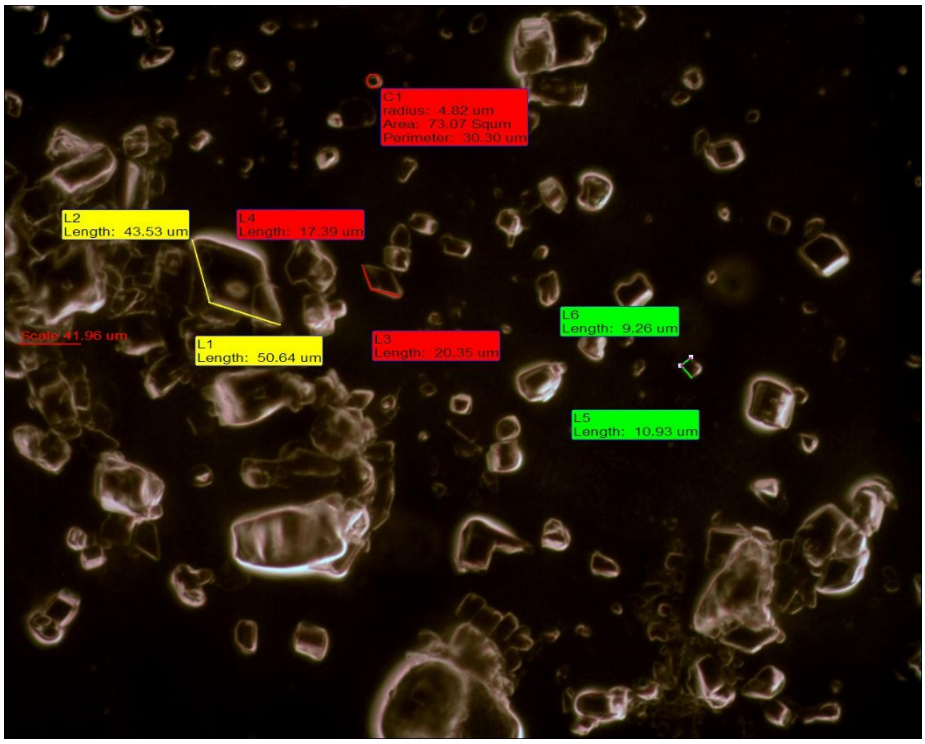

Figure 4.9. Image taken of crystals from the Bottom slurry from the lamella sedimentation experiment with the second approach. The standard magnification was utilized, and the height adjuster rotor was placed in position PM0 during the image capturing.

4.3 Freezing temperature

The freezing temperature was measured for both unloaded and loaded stock mixtures where the weight ratio between DMSO and AMP equalled three, as it is this composition that will be used within the pilot plant. The freezing point was also evaluated for these stock mixtures with addition of either 5 or 10% water. Water accumulation in the non-aqueous systems, during operation of the pilot plant, could happen over time due to humid flue gases or improper storage conditions. All CO2-loadings (0, 0.2, 0.38 and 0.5) were evaluated.

However, reliable results, meaning that a stable temperature value was acquired during testing, were not obtained for all tested mixtures. The obtained freezing temperature, measured as the melting temperature of the stock mixture, for each reliable, individual measurement can be found in Appendix D. In the following sections, the average values of the obtained melting temperatures will be presented, along with the standard deviations. In addition to the stock mixtures that were tested, a reference sample that only contained DMSO was also tested. For DMSO, the highest melting temperature obtained with the employed method was 19.4 °C, while the lowest registered melting temperature was 18.8 °C. Two additional measurements were also conducted, and the average value of the melting temperature was determined to be 19.2 °C, with a standard deviation of 0.3 °C. The average value is similar to the melting temperature of 18.5 °C stated in the literature [15].

4.3.1 0H25A75D mixtures

Six samples from stock mixtures having the composition 0H25A75D were prepared. Table 3.1 shows the meaning behind the abbreviation. Two different samples were prepared from the unloaded stock mixture to see if the registered melting temperature was affected by the

preparation of the sample. The first of these samples was not mixed prior to freezing, thereby acquiring the additional name *Unmixed*. The second sample without any absorbed CO_2 was, along with all the remaining samples, vigorously mixed prior to freezing. Therefore, it was given the additional name *Mixed*. Furthermore, two samples were prepared from stock mixtures with a CO_2-loading of 0.38. One of the samples came from the 8-month old stock mixture with the same composition. As it was found that the older stock mixture had distinguishably larger carbamate salt particles, this sample was given the additional name *LP*. Hence, the name distinguishes that the sample was from the older stock mixture with larger particles. The second sample was given the additional name *SP*, meaning that it stemmed from the newer stock mixture with smaller particles. Single samples with CO_2-loadings of 0.2 and 0.5 were prepared, respectively.

Three to four measurements were conducted for each sample during consecutive days. With the employed method, no representative value could be acquired for the *SP* sample, which had a CO_2-loading of 0.38. Figure 4.10 shows the average melting temperature for the different samples. The standard deviation for each value is indicated with the vertical error bars. The lowest average melting temperature was observed for the sample where the CO_2-loading was 0.2, with the value being 6.3 °C. The standard deviation of the measurements done on the sample is 1 °C. Thereafter, the two stock mixtures without any absorbed CO_2 had the lowest average melting temperatures. The *Unmixed* sample had an average melting temperature of 7.1 °C, compared to 8.5 °C for the *Mixed* sample. The *Unmixed* sample had a roughly three times larger standard deviation of 2 °C than the 0.6 °C obtained for the *Mixed* sample. The *LP* sample, having a CO_2-loading of 0.38, had the second highest average freezing temperature at 9.7 °C, with a standard deviation of 1.4 °C. Lastly, the slurry sample with the highest CO_2-loading had the average melting temperature of 15.8 °C, while the standard deviation amounted to 0.8 °C.

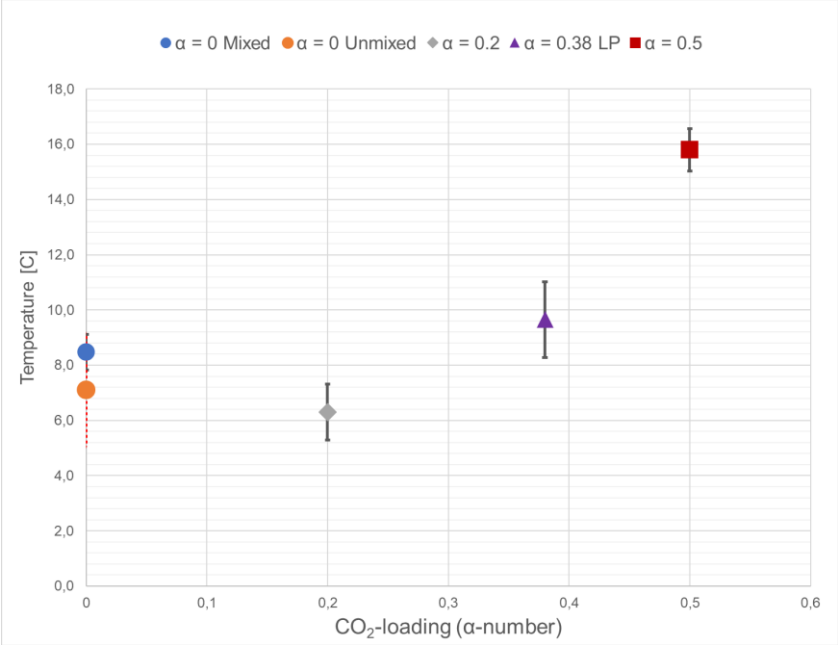

Figure 4.10. Average measured melting temperature of the 0 wt-% water, 25 wt-% AMP, and 75 wt-% DMSO samples with varying CO_2-loading. The error bars indicate the standard deviations of each measurement series. The experimental data for each measurement can be found in Appendix D.

4.3.2 5H24A71D mixtures

Five different samples were prepared with 5 wt-% water. Similar to the 0H25A75D samples, two samples (*SP* and *LP*) with a CO_2-loading of 0.38 were tested. The difference was in the utilized stock mixture, as described in the previous section. However, no representative values were obtained for the *SP* mixture, nor for the sample where the CO_2-loading, was 0.2. Therefore, they are not presented in Figure 4.11.

Three individual measurements were conducted for the two samples where the CO_2-loading was 0 and 0.5. Four individual measurements were conducted for the *LP* sample, where the CO_2-loading was 0.38. In contrast to the results of the 0 wt-% water samples, the *LP* sample had the highest average melting temperature at 3.6 °C. The standard deviations of its four measurements amounted to 1.9 °C, and the consecutive measurements followed a trend of increasing melting temperatures. The sample with a CO_2-loading of 0.5 had a lower average melting temperature at 2.3 °C, and a smaller standard deviation of 1.7 °C. The average freezing temperature for the unloaded sample was negative, at –7.5 °C. Furthermore, the unloaded sample also had the lowest standard deviation of the three samples at 1 °C, which can be seen in Figure 4.11.

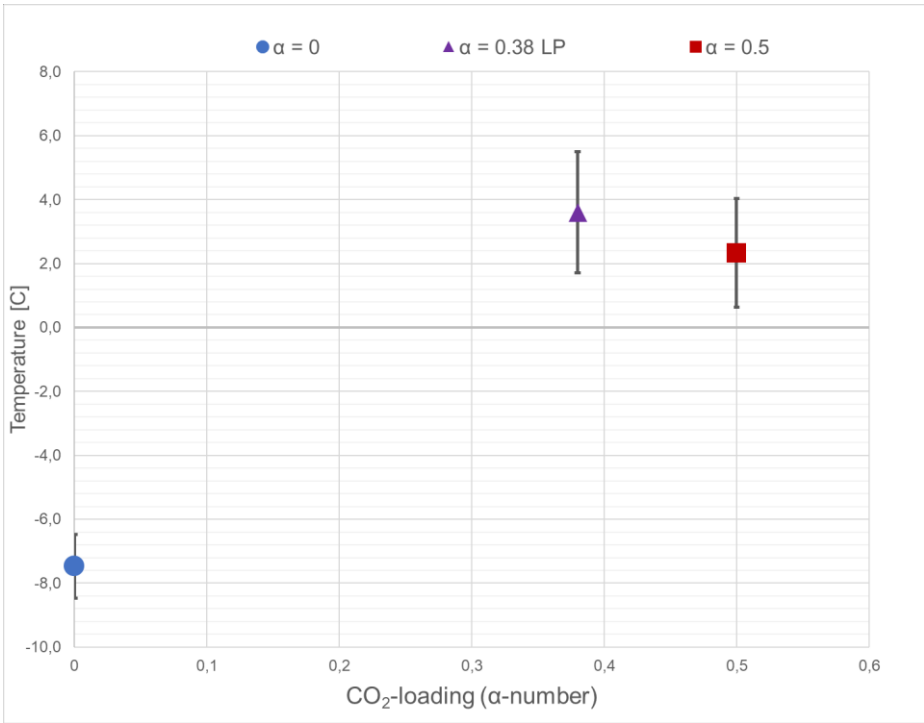

Figure 4.11. Average measured melting temperature of the 5 wt-% water, 24 wt-% AMP, and 71 wt-% DMSO samples with varying CO_2-loading. The error bars indicate the standard deviations of each measurement series. The experimental data for each measurement can be found in Appendix D.

4.3.3 10H22.5A67.5D mixtures

Five samples with 10 wt-% added water, with the same CO_2-loadings as the 5 wt-% water samples, were tested and representative values could be obtained for all tested stock mixtures. Four individual measurements were conducted during consecutive days for all samples except the *LP* sample with a CO_2-loading of 0.38. It was only tested three times, due to time constraints.

In Figure 4.12, the average melting temperatures are showed with the standard deviation for each measurement series. The lowest average melting temperature was -28.8 °C, with a standard deviation of 2.0 °C, which was obtained for the *SP* sample with a CO_2-loading of 0.38. Thereafter, it was the unloaded sample that had the lowest average freezing temperature of –19.6 °C, but the standard deviation of the measurement was 4.3 °C. This is the largest obtained standard deviation, and there was a temperature difference of 10 °C between the highest and lowest observed melting temperatures. The average melting temperature for the *LP* sample and the sample with a CO_2-loading of 0.2 were very close, -12 °C and –11.7 °C respectively. Their respective standard deviations were 2.9 and 2.0 °C. The sample with a CO_2-loading of 0.5 was the one with the lowest standard deviation, 1.8 °C, and the highest average temperature of –9.2 °C of the five tested samples.

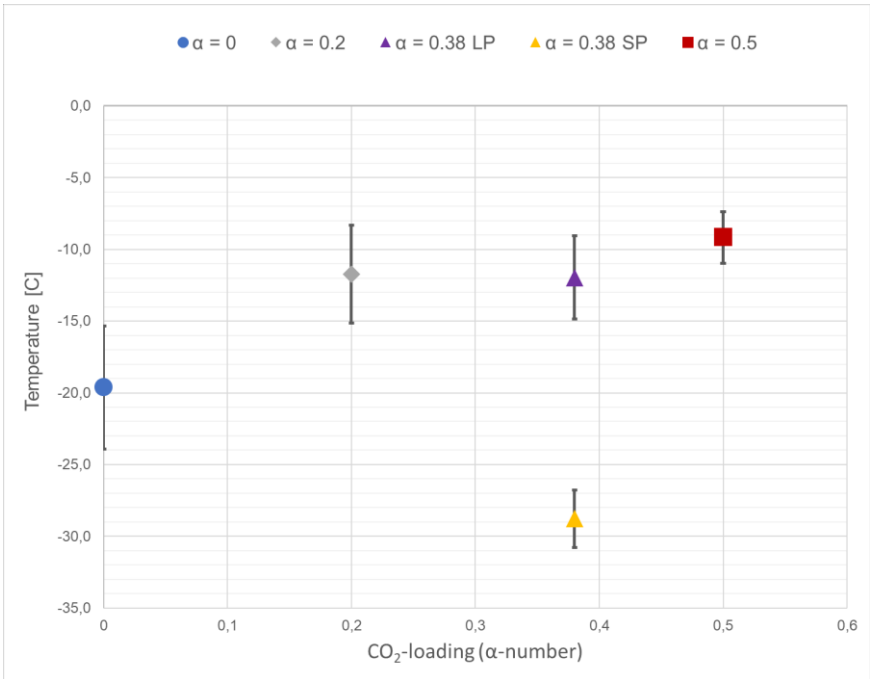

Figure 4.12. Average measured melting temperature of the 10 wt-% water, 22.5 wt-% AMP, and 67.5 wt-% DMSO samples with varying CO_2-loading. The error bars indicate the standard deviations of each measurement series. The experimental data for each measurement can be found in Appendix D.

Summarizing the results, it can be seen that only three CO_2-loadings (0, 0.38 *LP* and 0.5) were tested for all three water contents. In Figure 4.13, the average melting temperatures for these CO_2-loadings are plotted against the water content of the sample. A trend that can be seen in all three cases is that the average melting temperature decreases with the water content in the sample.

At 0-and 10 wt-% water, the order from highest to lowest average melting temperature is the same, but another trend was observed at 5 wt-% water. It can also be seen that for the samples with 0 wt-% water, the *LP* sample with a CO_2-loading of 0.38 is closer in melting temperature to the unloaded sample than the sample with a CO_2-loading of 0.50. But for the 10 wt-% samples, the opposite was instead true.

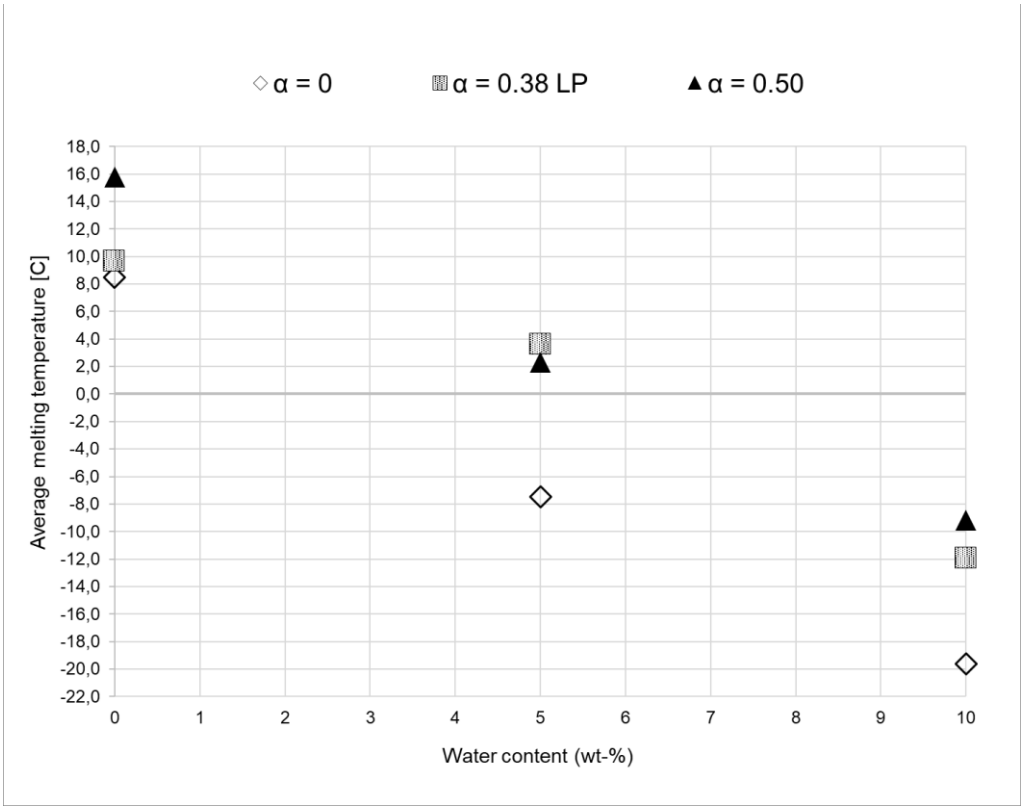

Figure 4.13. The average melting temperature with varying water content. Only the results from the three stock mixtures for which results were obtained at all water contents are shown. The associated error bars have been omitted.

4.4 Density

Two methods, using the hydrometers and a gravimetrical method, were used to evaluate the density for unloaded stock mixtures, having all six investigated compositions of water, AMP, and DMSO. However, to measure the density at an elevated temperature, and for measurements of the CO_2-loaded stock mixtures, only the gravimetric method was employed. It was deemed that utilizing the hydrometer for these experiments would be accompanied with too many sources of error, as the sample would be open to the atmosphere for an extended time period. Five out of eighteen CO_2-loaded stock mixtures could not be tested with the gravimetric method.

4.4.1 Unloaded stock mixtures

Results with the hydrometer at room temperature

Six unloaded stock mixtures could be tested at room temperature, 20 °C, with the hydrometers. Furthermore, the density of pure DMSO was also tested with the same method.

The six unloaded stock mixtures all differed in the weight percentage of water, AMP, and DMSO, and can be split up into two principal groups, which is visualized in Table 3.1.

For all the unloaded stock mixtures within the first group, two different hydrometers could be utilized to determine the density of the stock mixtures within the chosen measuring cylinder. The average experimental value obtained for the density, after five measurements per hydrometer, is presented in the second and third column of Table 4.1. The two hydrometers are labelled after their working range. As can be seen, the values from the different hydrometers differs slightly, but at most 0.003 g/cm^3. Both hydrometers could also be used to measure the density of pure DMSO at room temperature. The obtained densities were 1.100 and 1.099 g/cm^3 which is similar to the value of 1.108 g/cm^3 at 20 °C found in literature [39]. The results of the density experiments with the hydrometer for DMSO are also presented in Table 4.1. The density reading for each separate measurement can be found in Appendix E.

Table 4.1. The table shows the average density from five measurements at a room temperature of 20 °C, utilizing the two hydrometers for the DMSO sample and the three unloaded samples with a weight ratio between DMSO and AMP of three.

	Hydrometer	
	1.000 - 1.150	1.000 - 1.210
Sample Mixture	Average Density [g/cm^3]	Average Density [g/cm^3]
0H25A75D	1.049	1.048
5H24A71D	1.056	1.054
10H22.5A67.5D	1.061	1.058
DMSO	1.100	1.099

It can be seen from Table 4.1 that the density of the unloaded stock mixtures were all smaller than for pure DMSO. The lowest density, obtained with both hydrometers, was found for the 0H25A75D mixture with values of 1.049 and 1.048 g/cm^3, respectively. The density increased with increasing water content, and the results show that the 1.000 – 1.210 hydrometer consistently gave a slightly lower value of the density than the 1.000 – 1.150 hydrometer. For the stock mixtures, the difference in the density values obtained with the different hydrometers increases with the water content of the mixtures.

For the second group of unloaded stock mixtures (with a higher AMP concentration), only the hydrometer with the working range 1.000 – 1.210 g/cm^3 could be utilized, as the larger hydrometer with the working range 1.000 – 1 .150 g/cm^3 was too long to fit within the available measuring cylinder when having to measure in its lowest region, i.e., around 1.000 g/cm^3. Nevertheless, the experimental data acquired with the 1.000 – 1.210 hydrometer is presented in Table 4.2. The density value is the average value from five measurements. The density reading for each measurement can be found in Appendix E.

Table 4.2. The table shows the average density from five measurements at a room temperature of 20 °C, utilizing the 1.000 – 1.210 hydrometer for the three unloaded samples with a weight ratio between DMSO and AMP of one.

	Hydrometer
	1.000 - 1.210
Sample Mixture	Average Density [g/cm^3]
0H50A50D	1.004
5H47.5A47.5D	1.012
10H45A45D	1.019

The higher concentration of AMP, and hence lower concentration of DMSO, has an effect on the density. When comparing the samples with the same water content, it is seen that the mixtures in the second group have a lower density than the mixtures in the first group. The same trend, that the density increases with increasing water content, can also be seen in the experimental data for the second group, see Table 4.2.

Results with the gravimetric density method at room temperature

The densities of the six unloaded stock mixtures were also determined at room temperature, 20 °C, with the gravimetric approach. The density of pure DMSO was also investigated at room temperature with the gravimetric approach. From the experimental data, which can be found in Appendix E, the gravimetrically determined density could be calculated through equation 8.

$$\rho_{gravimetric} = \frac{(m_{V.flask+sol+cap} - m_{V.flask} - m_{cap})}{V} \qquad 8$$

In equation 8, the masses correspond to the average weights over three measurements of the utilized cap, the utilized volumetric flask, and the combination of the two filled with 50 mL of the stock mixture. The volume of mixture, V, equalled 50 ± 0.06 mL for all the measurements of unloaded stock mixtures. Applying equation 8 to the experimental data, it yields the gravimetrically derived density values presented in Table 4.3.

Table 4.3. The table shows the gravimetrically derived density at room temperature for DMSO and the six investigated unloaded stock mixtures.

Sample Mixture	Temperature [°C]	Gravimetrically derived density [g/cm^3]
0H25A75D	20	1.047
5H24A71D	20	1.050
10H22.5A67.5D	20	1.057
0H50A50D	20	1.000
5H47.5A47.5D	20	1.009
10H45A45D	20	1.018
DMSO	20	1.099

The gravimetrically derived density values in Table 4.3.can be compared with values obtained with the hydrometer presented in Table 4.1 and Table 4.2. The two methods yield similar results, with the largest absolute difference between the two methods being for the 5H24A71D sample, where the difference between the gravimetrically derived density and the density obtained with the 1.000 – 1.150 hydrometer amounted to 0.006 g/cm^3. For all measurements, the gravimetrically derived density was slightly smaller than the density obtained with the hydrometers.

Results with the gravimetric density method at an elevated temperature

Gravimetric density determinations were also done for the six unloaded stock mixtures at a higher temperature of 50 °C. From the experimental data, see Appendix E, equation 8 could be used to calculate the gravimetrically determined densities at 50 °C, which are presented in Table 4.4. When comparing the results for the same samples, at different the temperatures, it is seen that the density is decreased for all mixtures when the temperature is elevated to 50 °C. For all samples, the decrease in density was in the interval of 0.025 to 0.027 g/cm^3

Table 4.4. The table shows the gravimetrically derived density for the six investigated unloaded mixtures at an elevated temperature of 50 °C.

Sample Mixture	Temperature [°C]	Gravimetrically derived density [g/cm^3]
0H25A75D	50	1.020
5H24A71D	50	1.025
10H22.5A67.5D	50	1.030
0H50A50D	50	0.974
5H47.5A47.5D	50	0.983
10H45A45D	50	0.992

4.4.2 CO_2-loaded mixtures

The density of the mixtures with CO_2-loadings of 0.20, 0.38, and 0.50 were also investigated gravimetrically. One 0H25A75D stock mixture that had a CO_2-loading of 0.22 was also investigated. The used volume of CO_2-loaded mixture was 50 ± 0.06 mL for all except one sample, the 10H45A45D slurry, for which a smaller volumetric flask with a volume of 25 ± 0.04 mL had to be utilized. This was due to lack of sufficient mixture for the larger volumetric flask to be used. For the two higher CO_2-loadings, 0.38 and 0.50, only one mixture where the weight ratio of DMSO to AMP equalled one could be investigated. The rest of these slurries were hard to transfer into the measuring cylinder, hindering the possibility of acquiring a representative sample and therefore any estimations of the density. However, for the higher CO_2-loadings, all intended experiments could be carried out for the slurry mixtures having a weight ratio between DMSO and AMP of three.

With the experimentally measured weights, see Appendix E, the gravimetrically derived densities can be calculated through equation 8. The resulting, gravimetrically derived densities are presented in Table 4.5. The previously observed trend, increasing density with increasing water content, is also observed at room temperature for the loaded mixtures.

Table 4.5. The table shows the gravimetrically derived density, at room temperature, for the investigated loaded mixtures having a CO_2-loading of 0.20, 0.38 and 0.50. One sample with a CO_2-loading of 0.22 are also included. At the temperature specified in the table, the volume of the mixture was either 25 or 50 mL. The measured temperature is also listed.

Sample mixture	CO_2-loading	Temperature [°C]	Gravimetrically determined density [g/cm^3]
0H25A75D	0.20	20	1.073
0H25A75D	0.22	20	1.075
5H24A71D	0.20	20	1.076
10H22.5A67.5D	0.20	21	1.081
0H50A50D	0.20	21	1.059
5H47.5A47.5D	0.20	20	1.062
10H45A45D	0.20	20	1.078
0H25A75D	0.38	20	1.104
5H24A71D	0.38	21	1.107
10H22.5A67.5D	0.38	22	1.108
0H50A50D	0.38	21	1.115
0H25A75D	0.50	20	1.118
5H24A71D	0.50	21	1.120
10H22.5A67.5D	0.50	21	1.127

Comparing the densities for the loaded mixtures with the densities at room temperature for the unloaded mixtures, the result is that the CO_2-loaded mixtures have a greater density. Also when the CO2-loading was 0.20, it was observed that a greater AMP concentration results in a lower density. However, the difference in density between the two groups is smaller for the CO_2-loaded mixtures than for the unloaded mixtures.

An estimated density for the loaded mixture, based upon the gravimetrically derived density of the unloaded mixtures at 20 °C in Table 4.3, can be calculated given two assumptions. The first assumption is that the volume of the mixture is not altered as a result of the absorbed CO_2. The next assumption is that the same temperature applies for the loaded and the unloaded mixture. The first step of the calculation is to choose a volume V, for example 50 mL. The weight of 50 mL of the mixture, denoted m_1, can be calculated according to equation 9, by using the value of the density of the unloaded mixture in Table 4.3.

$$m_1 = \rho_{unloaded,T} * V \qquad 9$$

Then, the weight of the amine in the mixture, denoted m_{AMP}, can be calculated from equation 10, as the weight percentage of the amine within the mixture is known.

$$m_{AMP} = x_{AMP} m_1 \qquad 10$$

Next, the mass of CO_2, denoted m_{CO2}, required to achieve the correct CO_2-loading, expressed with the α-value, can be calculated by equation 11.

$$m_{CO2} = \frac{m_{AMP}}{M_{AMP}} * \alpha * M_{CO2} \quad (11)$$

In equation 11, M_{AMP} and M_{CO2} are the molar masses of the respective chemicals. The molar mass for AMP is 89.14 g/mole, while the molar mass of CO_2 is 44.01 g/mole. A new total weight of the mixture, denoted as m_2, will be the sum of m_1 and m_{CO2}. If it is assumed that the volume of the mixture does not change during the addition of the CO_2, the estimated density at room temperature, $\rho_{loaded\_est,T}$ for the loaded mixture is given from equation 12.

$$\rho_{loaded_{est},T} = \frac{(m_1 + m_{CO2})}{V} = \frac{m_2}{V} \quad (12)$$

The estimated densities was calculated with equations 9 to 12, with the resulting values presented in Table 4.6. They can be compared to the gravimetrically derived densities for the loaded mixtures, presented in Table 4.5. Although not all gravimetric experiments were carried out at precisely 20 °C, due to temperature fluctuations in the lab, the estimated densities are similar to the experimentally determined results. The estimation was closest to the experimental results for the samples having a weight ratio between DMSO and AMP of three and a CO_2-loading of 0.20, with the largest difference being 0.02 g/cm^3. For the remaining samples, the estimated densities underestimated the values achieved experimentally, and the deviations were, for most, slightly greater in magnitude. The average error between the estimated density and the gravimetrically determined density is 0.5 %.

Table 4.6. The densities estimated using equations 9 to 12 of CO_2-loaded mixtures at room temperature, 20 °C.

Sample mixture	CO_2-loading	Temperature [°C]	Estimated density [g/cm^3]
0H25A75D	0.20	20.0	1.073
0H25A75D	0.22	20.0	1.075
5H24A71D	0.20	20.0	1.076
10H22.5A67.5D	0.20	20.0	1.083
0H50A50D	0.20	20.0	1.049
5H47.5A47.5D	0.20	20.0	1.059
10H45A45D	0.20	20.0	1.068
0H25A75D	0.38	20.0	1.096
5H24A71D	0.38	20.0	1.099
10H22.5A67.5D	0.38	20.0	1.107
0H50A50D	0.38	20.0	1.094
0H25A75D	0.50	20.0	1.112
5H24A71D	0.50	20.0	1.115
10H22.5A67.5D	0.50	20.0	1.122

4.5 Viscosity

The viscosity was evaluated for unloaded stock mixtures at room temperature using three different methods, an Ostwald viscometer, a rheometer and a rotary viscometer. From the Ostwald viscometer, the kinematic viscosities were first obtained, and could then be calculated to dynamic viscosities by using the density results obtained in the previous section. The Anton Paar MCR 302e was also utilized to measure the viscosity of the unloaded stock mixtures at an elevated temperature of 50 °C. Lastly, CO_2-loaded stock mixtures were investigated with the NDJ-8S Digital Rotary Viscometer.

4.5.1 The Ostwald viscometer

Results with the Ostwald viscometer on reference mixtures

Before evaluating the viscosity of the amine mixtures, the Ostwald viscometer was calibrated using deionized water. This was done by measuring the time it took for the water to fall between the upper and lower line of the Ostwald viscometer. The registered temperatures outside the reservoir bulb and the measurement bulb respectively, were both 19.9 °C. The average duration of time required for the water to fall between the two lines, over five measurements, was 80.578 seconds. All the experimental data for each attempt with the Ostwald viscometer can be found in Appendix F. The experimental results obtained for water were used to find the *K*-value for the utilized Ostwald viscometer. The *K*-value can be calculated according to equation 13. The literature value for the kinematic viscosity of water at a temperature of 20 °C, and 1 bar is reported to be $1.004*10^{-6}$ m^2/s [54].

$$K = \frac{\vartheta_{H2O}(lit)}{t_{avg,H2O}} \approx 1.246 * 10^{-8} \left[\frac{m^2}{s^2}\right] \quad 13$$

After having determined the *K*-value of the Ostwald viscometer, the kinematic viscosities of two reference mixtures, DMSO and 1-pentanol, were experimentally determined. The temperatures at the outside the reservoir bulb and the measurement bulb were 20 °C during the both experiments with DMSO and 1-pentanol.

The average duration of time required for DMSO to fall between the lines of the Ostwald viscometer was 157.472 seconds, while a longer time of 388.26 seconds was required for 1-pentanol. By multiplying the average times required for DMSO and 1-pentanol respectively with the *K*-value for the Ostwald viscometer, the kinematic viscosities were acquired, and are presented in Table 4.7. Multiplying with the literature values of the densities of each chemical, 1.1008 g/cm^3 for DMSO [39] and 0.81468 g/cm^3 for 1-pentanol [55] at 20 °C, and converting to the unit to mPa·s by multiplying with a million, the dynamic viscosities in the third column in Table 4.7 are given. The results obtained from the reference mixtures could be compared to viscosities at 20 °C previously presented within the literature, which are 2.191 mPa·s for DMSO [39] and 4.011 mPa·s for 1-pentanol [55].

Table 4.7. The table shows the experimentally determined kinematic viscosity for the two reference chemicals, DMSO and 1-pentanol. The listed dynamic viscosities has been calculated from the kinematic viscosities using literature values of the densities of the chemicals at room temperature, 20 °C.

Chemical	Kinematic viscosity [m^2/s]	Dynamic viscosity [mPa·s]
DMSO	1.962*10^{-6}	2.160
1-pentanol	4.838*10^{-6}	3.941

Results with the Ostwald viscometer on unloaded mixtures of water, AMP, and DMSO

The average time it took for the unloaded mixtures of water, AMP, and DMSO to fall between the two lines of the Ostwald viscometer can be calculated from the experimental data presented in Appendix F. The resulting kinematic viscosities, calculated using the experimentally determined *K*-value from equation 13, are presented in Table 4.8. For the stock mixtures, it can be seen that the kinematic viscosity increases with increasing water content of the mixture. From the results, it can also be seen that when the weight ratio between DMSO and AMP decreases, the kinematic viscosity instead increases. To acquire the experimentally determined dynamic viscosity of the mixtures, utilizing the Ostwald viscometer, the kinematic viscosities must be multiplied with the experimentally determined densities for each mixture at room temperature. The chosen density values, the gravimetrically derived densities, are also reported in Table 4.8.

Table 4.8. The experimentally obtained kinematic and dynamic viscosities from the Ostwald viscometer for the unloaded mixtures of water, AMP, and DMSO are presented.

Mixture	Kinematic viscosity [m^2/s]	Density [g/cm^3] (from Table 4.3)	Dynamic viscosity [mPa·s]
0H25A75D	$3.355*10^{-6}$	1.047	3.513
5H24A71D	$4.140*10^{-6}$	1.050	4.347
10H22.5A67.5D	$5.025*10^{-6}$	1.057	5.306
0H50A50D	$7.900*10^{-6}$	1.000	7.900
5H47.5A47.5D	$10.54*10^{-6}$	1.009	10.64
10H45A45D	$12.53*10^{-6}$	1.018	12.76

4.5.2 The Anton Paar MCR 302e

From the Anton Paar MCR 302e, the regressed values of the viscosity was obtained for 40 different shear rates of the bob. The temperature setpoint during the measurements of the viscosities was 20 °C. At the lowest shear rates, the dynamic viscosity values fluctuated tremendously for all experiments. However, after the initial fluctuations in the viscosity, it eventually stabilized around a single value. For the unloaded 0H25A75D sample at 20 °C the dynamic viscosity value stabilized after ten data points, around 3.745 mPa·s , with a standard deviation of 0.032 mPa·s .

The average temperature was 19.98 °C, with a standard deviation of 0.01 °C. Graphs of the experimental data can be found in Appendix F. Figure A.22 to Figure A.25 indicate that the stock mixtures are Newtonian, as the viscosity does not change drastically in value after the initial period of fluctuating values.Table 4.9 summarizes the average viscosity values and the average temperatures, with their respective standard deviations, for the experiments at room temperature. Table 4.9 also contains a reference measurement that was conducted for a sample of pure DMSO at room temperature.

Table 4.9. The average dynamic viscosity values of different mixtures, obtained using the Anton Paar Rheometer. The standard deviation from the measurements is also included for each of the tested mixtures. The average temperature, with the standard deviation, is also reported and was around 20 °C for all the measurements.

Sample Mixture	Average Temperature [°C]	Average Dynamic Viscosity [mPa·s]
DMSO	19.96 +/- 0.01	2.3200 +/- 0.0458
0H25A75D	19.98 +/- 0.01	3.7455 +/- 0.0324
5H24A71D	19.96 +/- 0.02	4.6418 +/- 0.0362
10H22.5A67.5D	20.04 +/- 0.01	5.7128 +/- 0.0311
0H50A50D	20.03 +/- 0.01	8.3804 +/- 0.0687
5H47.5A47.5D	20.02 +/- 0.01	11.0739 +/- 0.0308
10H45A45D	19.98 +/- 0.01	13.1789 +/- 0.0573

Furthermore, the viscosities of the unloaded mixtures were investigated with the rheometer at a higher temperature of 50 °C. The graphs and the experimental data for the measurements can be found in Appendix F. Table 4.10 summarizes the average viscosity values and the average temperatures, with their respective standard deviations, for the experiments carried out at 50 °C. Table 4.10 also contains a reference measurement that was conducted for a sample of water at 50 °C. By comparing the values in Table 4.9 to Table 4.10, it can be seen that the viscosity decreases for all mixtures with an increased temperature. However at each temperature, the order from lowest to highest viscosity was the same.

Table 4.10. The average dynamic viscosity values, and the standard deviation from the measurements for each of the tested mixtures. The average temperature, with the standard deviation, is also reported and was around 50 °C for all the measurements, with the largest deviation being for the reference test of water.

Sample Mixture	Average Temperature [°C]	Average Dynamic Viscosity [mPa·s]
Water	49.66 +/- 0.18	0.6291 +/- 0.0666
0H25A75D	50.03 +/- 0.02	1.8168 +/- 0.0303
5H24A71D	50.10 +/- 0.06	2.1402 +/- 0.0229
10H22.5A67.5D	50.12 +/- 0.06	2.4197 +/- 0.0625
0H50A50D	50.03 +/- 0.02	3.0752 +/- 0.0293
5H47.5A47.5D	50.13 +/- 0.06	3.6910 +/- 0.0310
10H45A45D	50.12 +/- 0.07	4.1119 +/- 0.0311

4.5.3 The NDJ-8S Digital Rotary Viscometer

Results for the unloaded mixtures

Different rotors, with different working range, were available for the measurements using the NDJ-8S Digital Rotary Viscometer. The dynamic viscosities of the investigated unloaded mixtures were all in the range so that Rotor 0 could be used for the evaluation. The range of Rotor 0 is between 0 to 100 mPa·s, depending on the rotor revolution speed utilized. For Rotor 0, the viscosity measurements could be operated at four different rotational rotor speeds: 6, 12, 30, and 60 revolutions per minute (RPM). For each investigated mixture, at each RPM setting, two or three individual measurements were conducted. The viscosities of deionized water, DMSO, and 1-pentanol were investigated as reference solutions. The unloaded stock mixtures, of each composition seen in Table 3.1, were investigated with the rotary viscometer. The average value of the dynamic viscosity for each mixture at each RPM setting is presented in Table 4.11, together with the percentage of the maximum detectable viscosity value in parenthesis. The maximum value can be found in the last row of Table 4.11. The text OVER signifies that the registered dynamic viscosity was greater than the maximum detectable dynamic viscosity for the chosen RPM setting, and hence, no experimental value could be determined.

For different RPM settings, the average experimental value obtained for the same mixture differs, a result that was observed for all of the investigated mixtures. A trend was observed were the obtained average viscosities increase with decreasing RPM setting. This was observed for all samples except for DMSO at 12 RPM, which showed a lower value than the viscosity obtained at 30 RPM. Values obtained for different mixtures under different RPM settings should hence not be compared. With that in mind, the results show that mixtures with higher water content have a higher viscosity. Another observable result from Table 4.11 is that for stock mixtures with the same water content, the mixtures with a lower weight ratio of DMSO to AMP have a higher viscosity.

Table 4.11. The table shows the measured viscosity using the NDJ-8S Digital Rotary Viscometer for the following mixtures: water, DMSO, 1-pentanol, and the unloaded sample mixtures of water, AMP, and DMSO. The average experimentally determined viscosity is listed for different RPM settings. The value presented within parenthesis is the percentage of the observed viscosity to the maximum viscosity detectable at the specified RPM setting, which is showed in the last row of the table.

Mixture	Rotary Viscometer RPM setting Rotor 0			
	6	12	30	60
	Viscosity [mPa·s]			
Water	1.73 (1.73 %)	1.27 (2.54 %)	1.12 (5.6 %)	1.02 (10.2 %)
DMSO	2.53 (2.53 %)	2.22 (4.44 %)	2.25 (11.25 %)	2.01 (20.1 %)
1-pentanol	5.07 (5.07 %)	4.12 (8.24 %)	3.78 (18.9 %)	3.44 (34.4 %)
0H25A75D	3.80 (3.80 %)	3.45 (6.90 %)	3.17 (15.85 %)	2.98 (29.8 %)
5H24A71D	4.60 (4.60 %)	4.38 (8.76 %)	4.00 (20 5)	3.79 (37.9 %)
10H22.5A67.5D	5.40 (5.40 %)	5.03 (10.06 %)	4.75 (23.75 %)	4.58 (45.8 %)
0H50A50D	8.23 (8.23 %)	7.57 (15.14 %)	7.09 (35.45 %)	6.91 (69.1 %)
5H47.5A47.5D	10.57 (10.57 %)	9.85 (19.70 %)	9.24 (46.2 %)	9.23 (92.3 %)
10H45A45D	12.00 (12.00 %)	11.17 (22.34 %)	10.99 (54.95 %)	OVER
	Maximum detectable dynamic viscosity [mPa·s]			
	100	50	20	10

Results for the loaded mixtures

Although not designed for measuring the viscosity for mixtures containing solid particles, such as the salt particles of the CO_2-loaded mixtures, the NDJ-8S Digital Rotary Viscometer was used to estimate the viscosity for the CO_2-loaded mixtures. In Table 4.12, the sample mixtures for which a stable viscosity value could be obtained, at each rotor setting, are presented.

Table 4.12. The table shows the average dynamic viscosities of CO_2-loaded mixtures utilizing the NDJ-8S Digital Rotary Viscometer for different RPM settings.

Sample mixture	Rotary Viscometer RPM setting Rotor 0			
	6	12	30	60
	Viscosity [mPa·s]			
0H25A75D, α = 0.20	4.80	4.17	3.88	3.65
0H25A75D, α = 0.22	3.93	3.32	3.15	2.93
5H24A71D, α = 0.20	5.87	4.65	4.28	4.06
10H22.5A67.5D α = 0.20	8.63	7.48	6.43	6.22
5H47.5A47.5D α = 0.20	14.3	13.9	13.76	OVER

Several other mixtures were also tested with the NDJ-8S Digital Rotary Viscometer. However, for these mixtures, no single representative value was showed for most of the RPM settings. Instead, the values tended to increase over time. Therefore, as these values are deemed to not be representative, the values are not reported. The measurement log during the experiments can although be found in Appendix F. When trying to conduct the experiment on the 10H45A45D mixture with a CO_2-loading of 0.2, the viscosity was higher than the working range of Rotor 0. Thus, Rotor 1 (100 – 20,000mPas) had to be used for the measurements. Although the results were unreliable, they indicated that the magnitude of the viscosity was much greater, with at least a factor ten, than for the other CO_2-loaded mixtures presented in Table 4.12. Unreliable results were also obtained for the 0H50A50D mixture with a CO_2-loading of 0.38 with Rotor 1. The results indicated that the viscosity was greater than 1000 mPa·s , which corresponds well with the fact that the mixture could not be poured from its reagent bottle and had to be transferred into the measuring beaker with a spatula.

5 Discussion

5.1 Sources of error associated with stock mixture preparation

The preparation of the sample mixtures, including both the mixing of water, AMP, and DMSO, and the loading of the mixture with CO_2 comes with several sources of error. Since the samples have been prepared, and thereafter used to conduct the other experiments, the sources of errors connected with the sample preparation could be applicable to any of the experimental results. However, only sample mixtures that have been deemed representative, and prepared well with regards to the method, have been used for the experimental work.

The largest source of error for the preparation of the unloaded samples has to do with that the scale needed to be placed within a fume hood. The draft of the fume hood could have influenced the weight read from the scale. When the draft velocity changed within the fume hood, the weight the scale showed could vary with up to 0.10 grams. Over time, a strategy to diminish the influence of the draft on the read weight was employed, whereby a large transparent plastic box was placed around the scale. However, for the samples prepared prior to the development of the strategy, slightly incorrect weights of the chemicals could potentially have been read. If that was the case, the chemical composition of the sample would have been slightly different to the one reported. Spilling of the chemicals, either on the scale or on the outside of the reagent bottle, are human errors that would also have affected the composition of the sample.

For the stock mixtures that were to have high CO_2-loadings, especially when the ratio between the weight of DMSO and AMP was one, a mist of fume would start to leave the reagent bottle due to the temperature increase of the exothermic absorption reaction. The composition, nor the weight, of the mist that left the reagent bottle could be determined. Therefore, it was assumed that the mist formation did not change the overall composition, but the validity of the assumption has not been determined. For future experiments, a suggestion would be to cool the sample, especially when trying to reach higher loadings. Another source of error that occurred during loading was that slurry got stuck on the tubing used to transfer the CO_2 into the mixture. However, the amount of sample lost in this way was very small and therefore, the assumption was done that the overall composition was not affected. The composition of the samples could also have been altered through the hygroscopic property of DMSO, and by CO_2 desorbing during the time periods when the cap was taken off the reagent bottle.

5.2 Discussion of settling velocity results

Although the experimental investigation was limited to two CO_2-loadings, the results of the settling velocity experiments can provide insight to the effect of several parameters involved in the sedimentation process.

If the average settling velocities for the two stock mixtures, presented in Figure 4.1, are examined, two conclusions can seemingly be drawn. First, from a quick glance, it seems reasonable to conclude that the settling velocity increases dramatically when the CO_2-loading is increased. The density and viscosity of the surrounding fluid will differ for the slurries with

different CO_2-loadings. The viscosities could not be determined for these two CO_2-loaded stock mixtures, but the drifting measurements did indicate that it could have increased threefold. However, the difference in experimentally obtained densities for the stock mixtures was not large, only around 1 %. This suggests that other factors than the density and viscosity also contribute to the great increase in settling velocity.

Furthermore, that the settling velocity increases with increasing CO_2-loading is not supported by the fact that the sedimentation process proceeded, almost instantaneously, with the old stock mixture, with a CO_2-loading of 0.38. Since the old stock mixture had been stored for a long time, and the container had been open on several occasions, it is likely to have decreased in CO_2-loading through CO_2 desorption (the reverse reaction in reaction equation XVII). If the actual loading of the old stock mixture is lower than 0.38, it would also contradict that a higher CO_2-loading will increase the settling velocity.

Instead, difference in particle sizes could be an explanation for the order of increased settling velocity. The investigations with the microscope indicated that the stock mixture with a CO_2-loading of 0.50 had a much larger crystals present than the stock mixture with a CO_2-loading of 0.38. However, this does not apply to the older stock mixture with a CO_2-loading of 0.38. Although the size of the crystals within the older stock mixture with a CO_2-loading of 0.38 could not be determined, the trend seen during the microscope calibration, see Figure A.1. is that more positive rotations of the height adjuster rotor results in a greater distance per pixel in the captured images. As the resolution of the VisiCam images was kept constant, and hence also the number of pixels, the fact that these crystals were visualized with the height adjuster rotor in position P700 indicates that the older stock mixture had much larger crystals than the other stock mixtures. From these observations, the conclusion is drawn that the particle size that is the dominating factor for determining the magnitude of the settling velocity during zone settling of the carbamate salt particles, not the CO_2-loading of the slurry.

However, it must be noted that for stock mixtures with similar loading but a larger average particle size, there would be a smaller number of particles present, meaning that the particle concentration[N] would decrease. Neither the average particle size nor the concentration of particles were investigated within this master thesis project. Hence, the concentration of particles could be the underlying property determining the magnitude of the settling velocity during zone settling. According to the theory for wastewater treatment plants, it is the particle concentration that is the determining factor, as zone settling will level out the differences caused by different particle sizes. It is thus reasonable to assume that the same should apply for the CO_2-loaded stock mixtures as well, and that the observed differences in particle sizes indirectly results in varying particle concentration. Further experiments, and measurements of the particle concentration would have to be conducted in order to verify this.

The second conclusion that can be drawn from Figure 4.1 is that by increasing the operating temperature, the settling velocity is increased. The obtained settling velocity was almost doubled as the temperature was changed from 21 to 50 °C. However, what is not seen in Figure 4.1 is that another effect also occurred when the temperature was elevated. For the stock mixture with a CO_2-loading of 0.38, the determined settling velocity was 6.2 mm/h during the first experimental run at 50 °C. Between the first and the second experimental run,

[N] The number of particles present per unit volume.

the position of the measuring cylinders was switched, but a similar settling velocity, amounting to 6.5 mm/h was obtained in the other measuring cylinder as well at 50 °C. This would suggest that, initially, the measuring cylinders had had an almost equal particle concentration and liquid composition. The small difference could be explained by small compositional variations between the measuring cylinders, or that there were temperature variations within the water bath during the extent of either of the two experiments. Hence, it could be expected that the settling velocities at 21 °C would also be similar. But for the measuring cylinder that had previously been at 50 °C, its settling velocity at 21 °C was instead 44 % greater than the settling velocity registered during the first experimental run.

For the slurry with a CO_2-loading of 0.50, the two first experimental runs were conducted without switching the position of the measuring cylinders. Then, almost the exact same settling velocity was observed at 21 °C, but not at 50 °C. The determined settling velocity during the second experimental run at 50 °C was 15 % greater than the settling velocity obtained during the first experimental run, even though the same measuring cylinder was used. When the positions of the measuring cylinders were switched, between the second and third experimental run, the observed settling velocity at 21 °C for the measuring cylinder that had previously been at 50 °C was 29 % greater. However, during the third experimental run the settling velocity at 50 °C was similar in magnitude to the settling velocity obtained during the first attempt.

For both CO_2-loadings, there seems to be an effect that when being exposed to the elevated temperature of 50 °C, the stock mixture undergoes either a chemical, and/or a physical change, which results in an increased settling velocity for subsequent experiments. One possible explanations could be that more CO_2 desorbs at 50 °C through the reverse reaction in reaction equation XVII, which could mean that the particle concentration is decreased. As stated above, it is believed that this would result in a higher settling velocity. Another explanation could be that increased crystal growth, or conglomeration of particles occurs at the elevated temperature, with the effective result also being a decreased particle concentration. A more uncertain explanation could be that at the elevated temperature, there is formation of other unknown reaction products could also be the cause.

It must also be discussed that the results could have been influenced by other sources of error. As mentioned, the height of interface was blocked from being read accurately during three attempts for the stock mixture with a CO_2-loading of 0.38. It is possible that the settling proceeded with a different settling velocity during the time when the interface was obstructed from being read. Furthermore, the quality of the images from the camera can also have affected the reading of the height of interface, which could affect the result for specific data points. However, the good fit of the linear regression does indicate that even if specific data points could have been misread, the settling does proceed with a linear behaviour. Errors in reading of the height of interface for a small number of data points would also not alter the slope of the regressed linear equation substantially, given the large number of data points.

5.3 Discussion of lamella sedimentation results

From the visual observation of the lamella sedimentation basin, it can be concluded that the separation method could produce an outgoing mixture lower in precipitate concentration than the incoming slurry. Due to the accumulation of the solid precipitate in the bottom of the

lamella sedimentation basin during operation, it is also believed that a concentrated slurry could have been produced if there had been an outlet pipe in the bottom of the basin. This is supported by the microscope investigation of the *Bottom slurry* where the captured images indicate that there was a greater concentration of crystals in the *Bottom slurry* compared to the *Effluent slurry*. A factor that could have influenced the amount of observed crystals was the manner of mixing of each sample prior to its application to the microscope slide. Furthermore, the sample collection of the *Bottom slurry* from the lamella sedimentation basin can also have been done in a manner resulting in an unrepresentative crystal concentration.

The opaque shade, and the observed crystals for the *Effluent slurry* does indicate that particles are still present in the effluent of the lamella sedimentation basin. Practically, that could cause problems within subsequent unit operations, causing fouling on the surfaces of downstream heat exchangers, abrasion, or clogging. However, the presence of particles within the stream entering into the absorption column could potentially be advantageous. By having small particles entering the absorption column with the liquid, they can act as nucleation points and promote further crystal growth leading to fewer, larger particles instead of many small particles.

5.4 Discussion of the freezing temperature results

Several aspects of the presented results of the melting temperature measurements raises questions. One major aspect of concern was the inability to acquire representative experimental values of the freezing temperature for three of the sixteen investigated samples. The standard deviation of the measurements, extending above that expected from the thermocouple for several measurement series, should also be discussed.

For all of the 0H25A75D measurement series that gave reliable results, with the exception being the *Unmixed* unloaded sample, the standard deviation of the measurements was smaller than 1.5 °C. Therefore, it is reasonable to assume that the variation seen in the experimental data mainly arises from the employed equipment, the model K thermocouple, and not the measurement method. The same conclusion can be drawn from the validation experiment with DMSO, which showed a standard deviation of 0.3 °C. The validation experiment indicated that the melting temperature of DMSO should be 19.2 °C, which is higher than the expected literature value of 18.5 °C. Since the averaged melting temperature is higher than the literature value, it is not believed that the discrepancy is caused by the presence of other components in the sample. All other measurements, where DMSO has been mixed with other components, has indicated that their presence results in freezing point depression, not the uncommon phenomena of giving an increase in the freezing temperature. The difference of the average melting temperature from the literature value although does lie within the range of error expected with the thermocouple.

The difference in standard deviation between the two unloaded samples was substantial, more than three times greater for the unloaded sample. It is reasonable to believe that the difference can be explained by their difference in preparation. The reasonable explanation for the larger standard deviation of the *Unmixed* sample is that it was heterogeneous in composition upon freezing. Different sections of the sample could thereby have different relative concentrations of AMP and DMSO, meaning that melting could take place over a wider range of temperatures. The comparison of the samples shows the importance of acquiring homogeneous samples.

For the 5H24A71D samples, only three of the measurement series tested provided representative values of the melting temperature. The variation, as the standard deviation of the measurement series, was generally higher than for the samples without water. All of the 10H22.5A67.5D samples were frozen at –80 °C. Overall, a greater variation in the representative value for the melting temperature was seen, the largest standard deviation being 4.3 °C, which exceeds the variation that can be expected from the thermocouple. A reason for the increased variation could be that the samples were no longer homogeneous in composition upon being frozen. Sedimentation of the carbamate salt particles until freezing occurred could have led to an uneven distribution of the particles within the sample. For example, it has been shown that sedimentation occurs very differently for the *SP* and *LP* samples with CO_2-loadings of 0.38. It is believed that it is this difference that has manifested itself in that these two 10H22.5A67.5D samples had very different melting temperatures.

Although, it is possible that the variations, including those observed at lower water contents, are inherent to the liquid mixture itself. Experimentally, AMP has showed not to have a clearly defined melting temperature. Hence, an explanation for the variation seen could be that liquid mixtures of water, AMP, and DMSO also exhibit no clear melting temperature, but instead exhibiting an interval of melting temperatures. In that case, the experiments indicate that broader intervals of melting could be expected when the water content increases. Experimental results from three stock mixtures could not be obtained. Two of these stock mixtures were *SP* samples with a CO_2-loading of 0.38, the ones containing zero and five weight percent water respectively. Furthermore, no experimental results were either obtained from the 5H24A71D sample with a CO_2-loading of 0.20. The reason can either have been that melting proceeded too quickly for a melting temperature to be registered with the employed method, or that the samples were too heterogeneous upon being frozen.

Figure 4.13 shows that at 0 and 10 wt-% water, the unloaded stock mixture had the highest melting temperature, but that it was the *LP* sample with a CO_2-loading of 0.38 when the water content was 5 wt-% water. In combination with the lack of experimental results from the three samples discussed above, no clear trend could be identified within the project for how the freezing temperature varies with the CO_2-loading.

5.5 Discussion of the density results

5.5.1 The unloaded stock mixtures

The density of DMSO and the unloaded amine mixtures were experimentally determined at room temperature using both a gravimetric method and hydrometers. Comparing the results from the different methods shows that there is agreement between the obtained values. The largest difference between the experimentally determined densities was found for the unloaded 5H24A71D mixture, being at most 0.006 g/cm^3. For all of the mixtures, including pure DMSO, the largest of the experimentally determined densities was measured with the 1.000 – 1.150 hydrometer. The smallest difference in the experimentally determined density was observed for the 10H45A45D mixture and the sample only containing DMSO, with the registered difference being at most 0.001 g/cm^3. The results indicate that a larger weight ratio between DMSO and AMP results in an increased density of the mixture, a result consistent with the fact that pure DMSO has a large density than pure AMP. Furthermore, increasing the water content for samples containing the same weight ratio between DMSO and AMP also results in an increased density. The similarity between the two experimentally determined densities, with the two different methods, indicates that the actual densities of the liquid

mixtures lie close to the experimentally presented densities herein. This is further supported by the experimentally obtained density of pure DMSO at 20 °C, utilizing both methods, which is very similar to the density value of pure DMSO presented in the literature.

Both of the experimentally determined densities of DMSO were slightly smaller than the value presented in the literature, the difference being around 0.001 g/cm^3. The difference can be explained with the sources of error related to the employed methods. The accuracy of the measured temperature, and small temperature fluctuations during the experiments, are sources of error that would impact the experimentally determined results in both of the methods, since the density is a temperature-dependent property. Temperature fluctuations could also explain the difference in read values for the two different hydrometers. Another potential source of error for the hydrometer experiments could be the reading of the value on the hydrometer, with surface tension effects having potentially complicated the task of correctly reading the hydrometer. Furthermore, inadequate mixing of the mixtures between the measurements, and the hydroscopic nature of DMSO are sources of error that could affect the results. As there was very little variation in the result for measurements on the same mixture, these sources of errors are deemed to not have had a major impact. With the gravimetrical method, there are other sources of error that can impact the results. Any additional volume of the mixture in excess of the desired 50 mL, either on the interior or exterior walls of the volumetric flask, will impact the result.

With the gravimetric approach, the densities of the unloaded mixtures could also be determined at an elevated temperature, as reported in Table 4.4. The results show that at 50 °C, the densities of the unloaded mixtures are lower than at room temperature, as expected from theory. One source of error, that could affect the results for the densities at elevated temperature, is connected to achieving the correct temperature within the sample while changing the volume within the volumetric flask.

5.5.2 The CO_2-loaded stock mixtures

Gravimetric determination of the density of CO_2-loaded amine mixtures were also carried out at temperatures around 20 °C. The experimental results showed that when CO_2 is absorbed and form carbamate salt particles, the density increases compared to the unloaded mixtures with the same composition of water, AMP, and DMSO. From the experimental results on CO_2-loaded stock mixtures, the same trends of higher density with increasing water content and weight ratio between DMSO and AMP were observed, as for the unloaded mixtures.

Additionally, samples with a weight ratio of DMSO to AMP of three were tested with higher CO_2-loadings of 0.38 and 0.50. The density increased with higher CO_2-loading, being around 0.03 and 0.045 g/cm^3 greater, respectively, than the densities of the corresponding stock mixtures with CO_2-loadings of 0.20. Only one CO_2-loaded 0H50A50D sample could be investigated, at a CO_2-loading of 0.38. It had a higher density than any of the other samples with the same CO_2-loading. However, during the sample preparation there was a lot of mist formation during the CO_2-loading process and for some durations of time, the weight did not increase. Therefore, it is possible that the actual CO_2-loading of the 0H50A50D sample was higher than 0.38, potentially even in the range of a CO_2-loading of 0.50. If this was the case, its density would be lower than the corresponding 0H25A75D sample. This would seem reasonable as higher AMP concentration has previously resulted in lower, not higher densities, as seen before at CO_2-loadings of 0 and 0.20.

Besides the error sources connected to sample preparation, additional sources of error connected to the gravimetric method needs to be considered. The formation of a foam top layer was not observed for the samples for which results have been reported. However, it is likely that the carbamate salt particles were not evenly distributed within the stock mixture while being divided into smaller samples. With higher concentration of carbamate particles, larger portions got stuck to the walls of the bottle containing the stock mixture, the walls of the funnel, and the walls of the measuring beaker used to transfer the sample to the volumetric flask. Furthermore, depending on the shape of the utilized volumetric flask (the length of the necks differed), for some measurements, more carbamate particles will have got stuck on the walls of the volumetric flask than for others. This could also be an explanation for the small discrepancies in the density increase for different samples. Differences in temperature could also affect the comparisons done previously. Slightly higher temperatures were measured for several of the CO_2-loaded mixtures, up to 1.0 °C higher than room temperature, which would result in slightly lower densities.

From the experimentally determined densities of the unloaded mixtures, calculated estimations could be made of the densities of the CO_2-loaded mixtures. The estimated and the experimentally determined values corresponded well with each other for the CO_2-loadings of 0.20. The similarity between the estimated values and the experimental values was greatest for the samples where the weight ratio between DMSO and AMP was three. For the rest of investigated samples, the estimation method underestimates the density obtained experimentally. The difference amounted at most to around 0.01 g/cm^3. The reason for the discrepancy could be that more carbamate particles got stuck to the walls of the volumetric flask for higher CO_2-loadings.

5.6 Discussion of the viscosity results

5.6.1 The unloaded stock mixtures

For the unloaded stock mixtures, the highest dynamic viscosity value was registered with the Anton Paar MCR 302e Rheometer. The second highest registered dynamic viscosity was registered with the 6 RPM setting on the NDJ-8S Digital Rotary Viscometer. However, next in order of magnitude came the dynamic viscosity calculated from the experimental results from the Ostwald viscometer and the hydrometer experiments. Thereafter, the additional values registered with the NDJ-8S Digital Rotary Viscometer came in descending order with increasing RPM setting. This trend was seen for all the samples except the 10H45A45D sample, where the dynamic viscosity determined using the Ostwald viscometer was higher than all the values obtained using the NDJ-8S Digital Rotary Viscometer. Nevertheless, two general observations can be identified from the results obtained with any of the three methods. First, an increasing water content increases the viscosity of the mixture, and second, decreasing the weight ratio of DMSO to AMP increases the viscosity of the mixture.

The discrepancy between the results obtained with the Ostwald viscometer and the Anton Paar Rheometer ranges from 0.20 mPa·s to 0.45 mPa·s. One explanation for the differences could be the sources of error connected to the respective methodologies. The results of the Ostwald viscometer could have been affected by temperature fluctuations during the duration of the experiment. Furthermore, as the Ostwald viscometer was open to the atmosphere for the longest period of any experiment, the hygroscopic property of DMSO could have resulted

in composition changes during the duration of the experiment, which, in turn, could have affected the viscosities. However, there was no major difference in results between consecutive measurements, and it is therefore not believed that the composition did change between different measurements due to the hygroscopic nature of DMSO. In addition to the potential sources of error, the reaction speed of the person carrying out the experiment, or inconsistent interpretation of when the liquid reached each line, are human errors that could have affected the results slightly. Different positioning of the Ostwald viscometer, or unintentional movement of the Ostwald viscometer between consecutive measurements could also have affected the results slightly.

Temperature fluctuations could also have affected the results of the rheometer. If the amount of tested mixture differed, the results would also have been affected. Although not disregarding the differences in dynamic viscosity obtained with the different methods, the similarities between the values indicate that the actual viscosities are likely to lie in the region indicated by the results presented herein. This is further supported by the fact that the literature value for the viscosity of pure DMSO at 20 °C, 2.22 mPa·s , lies in between the values provided by the Ostwald viscometer, 2.16 mPa·s, and the rheometer, 2.32 mPa·s [56]. The measurements at an elevated temperature of 50 °C shows an expected behaviour of a lower viscosity at a higher temperature, for all unloaded mixtures.

The results of the NDJ-8S Digital Rotary Viscometer closest to the values of the other two methodologies was primarily given with the 6 RPM setting. However, the registered viscosities were often that low that their percentage value of the maximum detectable viscosity was outside of the range 10 – 100 %. Outside this range, the measurement values were considered unreliable, in accordance with the instrument manual. Furthermore, for measurements conducted with different RPM settings, where the experimental results were within the range of validity, the experimental results did not converge to the same stable value. Therefore, it was deemed that the dynamic viscosity was consistently underestimated with NDJ-8S Digital Rotary Viscometer, although correctly indicating the magnitude of the actual dynamic viscosity of the mixture.

5.6.2 Comparisons of the results for the CO_2-loaded mixtures

Viscosities for the CO_2-loaded mixtures were obtained using the NDJ-8S Digital Rotary Viscometer. However, stable values could not be obtained for all the tested mixtures. For the tested mixtures with a CO_2-loading of 0.20 (that yielded stable values) a higher viscosity than for the corresponding unloaded mixture was registered. However, the 0H25A75D stock mixture with CO_2-loading of 0.22 had a dynamic viscosity similar to the unloaded mixture, a result contrary to all the others. A source of error that could explain this result is that the mixing of the sample was insufficient prior to the transfer of the CO_2-loaded mixture into the measuring beaker. Thus, less carbamate salt particles could have been present in the tested liquid, which, in turn, could explain why the obtained viscosity is similar to the unloaded mixture.

For the majority of the tested mixtures, the dynamic viscosity obtained by the NDJ-8S Digital Rotary Viscometer increased with time. However, the manual states that the reliability for slurries could be poor. The reason that the instrument showed an increasing dynamic viscosity over time could be that the precipitate got stuck and accumulated on the rotor, thereby

affecting the required torque to maintain the rotational speed of the rotor. The torque is the quantity that is measured by a viscometer, which is then translated into a dynamic viscosity for the tested mixture. Another possibility could be that the carbamate salt particles settled in the bottom of the beaker during the measurement. Increasing concentration of carbamate salt particles in the bottom layer would create a greater resistance for the rotor, which could explain the increase in registered dynamic viscosity over time.

However, two of the experiments that showed increasing viscosity values over time did indicate that for higher CO_2-loadings, the viscosity could be drastically greater. For these two stock mixtures, another rotor, suitable for more viscous fluids, had to be used to obtain any values. The drifting measurements also indicated that the viscosities of these two solutions were of a larger magnitude, more in the range of 100 or 1000 mPa·s than around 10 mPa·s as for the other mixtures. An explanation to the sharp increase could be that, for these stock mixtures, the volume of solid carbamate salt particles has become greater than the volume of the liquids water, AMP, and DMSO.

6 Conclusions and future work

Having completed the discussion of the experimental results, the two research questions of this master thesis can be answered. First, the conclusions for each experiment related to the first research question will be presented. Thereafter, the answers from the literature review to the second posed research question will be summarized.

Several conclusions can be drawn from the conducted settling velocity experiments. First, increasing temperature has the effect of increasing the settling velocity for the carbamate salt slurry mixtures. From the other experiments, it has been shown that the viscosity and the density of the CO_2-loaded mixtures decrease with increasing temperature, which is likely the cause of the effect on the settling velocity. Further experiments would have to be conducted to determine whether these effects are the sole reason for the changes in settling velocity with temperature. No clear trend between the CO_2-loading of the slurry and the settling velocity has been identified. Instead, the results showed that particle size, which could translate into the concentration of carbamate salt particles, was the determining factor for the magnitude of the settling velocity. In addition, the experimental results did indicate that after being subjected to the higher temperature of 50 °C for an extended amount of time, the subsequent settling experiment proceeds with a greater settling velocity. Suggestions for the cause of this effect have been posed, such as CO_2 desorption, increased crystal growth, or the formation of other unknown reaction products due to the elevated temperature. But further investigations need to be conducted to reach insight to the cause and the prevalence of the effect.

Through conducting the experimental trial of lamella sedimentation separation upon a CO_2-loaded mixture, it was showed that the separation method could divide the ingoing slurry into two fractions either leaner or richer in carbamate salt particles. However, the experiment showed that the outgoing leaner fraction still contained carbamate salt particles. This could be advantageous, as the remaining particles can act as seeds allowing for the formation of larger particles within the absorption column over time, potentially facilitating the separation before the regeneration step. However, the remaining particles could also be detrimental to the design of the pilot plant through causing fouling, abrasion, or clogging. In order to evaluate these potential outcomes, further investigations are needed.

The experimental results of the freezing temperature experiments have only provided an insight into the effect on the freezing temperature for one of the two investigated parameters. The experimental results show that with an increasing water content, the freezing temperature, measured as the melting temperature, decreases. For the measurements with samples containing water, larger variations, expressed as the standard deviation, were generally registered. The variations could either be caused by the presence of AMP in the mixture or related to the employed equipment and method. No clear trend or conclusion can be drawn from the experimental results on how the CO_2-loading affects the freezing temperature, owning to the failure of the employed method to measure the melting temperature of all the stock mixtures. More experiments, preferably with another method or a more accurate measurement of the temperature, should be conducted to extend the work started herein. Until these experimental results have been presented, the values herein give an estimation of the freezing temperatures that can be expected, but should be used with care. From the

experiments conducted with the reference sample containing pure DMSO, it was shown that either the method or the utilized equipment gives rise to a small systematic error, where the experimentally determined freezing temperature is overestimated. The error was although small enough to be within the range of error expected with the thermocouple.

The density evaluations of the unloaded mixtures showed, using both the experimental methodologies, that a greater weight ratio of DMSO to AMP increases the density of the mixture. The similarity of the values, obtained from the two different methods, implies that the actual density of the unloaded stock mixtures should be close to the values presented herein. It was also shown that if the water content was increased, the density also increased. By increasing the temperature of the mixture, it was observed that the density of the mixture decreased. However, further density experiments for the studied stock mixtures at 50 °C, either with the same or another method, should be conducted to validate the results presented herein. When the mixtures are loaded with CO_2, the density increases. For the mixtures with a CO_2-loading of 0.20, it was also observed that increasing weight ratio of DMSO to AMP, and increasing water content, led to a higher density. An approach to estimate the density for the CO_2-loaded mixtures at 20 °C was also developed. Comparing the estimated values with the experimental results, the approach tends to slightly underestimate the density for the highly CO_2-loaded stock mixtures. Additional research should be conducted to evaluate the density of the CO_2-loaded mixtures with another method, preferably also at an elevated temperature.

Three experimental methods were used to evaluate the viscosity of the unloaded mixtures of water, AMP, and DMSO. Three main trends were identified. Increasing the water content in the sample, increases the viscosity. Increased viscosity is also seen when the weight ratio of DMSO to AMP is decreased. Furthermore, the viscosities for the unloaded mixtures decreased when the temperature was increased. The results from the rheometer showed that the unloaded stock mixtures behave as Newtonian fluids. It is likely that the actual dynamic viscosity lies between the experimental values from the Ostwald viscometer and the rheometer, as was the case for DMSO. Another result from the viscosity experiments was that the investigated CO_2-loaded mixtures had larger dynamic viscosities than the corresponding unloaded mixtures. However, the equipment utilized to acquire the results tended to underestimate the viscosity of the unloaded mixtures. This should be kept in mind for the CO_2-loaded mixtures, which could therefore be slightly underestimated. Furthermore, the equipment could not provide stable or reliable values for several of the investigated stock mixtures. The dynamic viscosity results presented herein for CO_2-loaded mixtures of water, AMP, and DMSO, should hence only be viewed as first estimates and as references for future experiments. New experiments with other equipment and a method designed to get representative viscosity values from slurry mixtures should be conducted, especially for the CO_2-loaded mixtures where no representative value was acquired. The utilized method should enable the particles to be homogeneously distributed within the mixture upon testing, something which the utilized method could not guarantee. The unexpected result of a drastic increase in viscosity seen for some of the samples should also be further investigated. The research should focus on when this drastic increase occurs, and finding the cause of it.

From the conducted literature review, it could be concluded that knowledge of the density, the viscosity, and the freezing temperature of the amine mixtures will be relevant to several design decisions for the pilot plant. The insights gained about the freezing temperature should

be utilized in the design of the chemical storage facilities and to set the limits for cooling within the intercooler. Moreover, knowledge concerning the density and viscosity of the amine mixture will be important when evaluating the performance and when simulating the system, once the pilot plant has been run successfully.

7 References

1. Karayiannis, N. C. H.; Laso, M., Absorption. *Kirk-Othmer Encyclopedia of Chemical Technology* [Online]; Wiley & Sons, Posted 20 December, 2018. https://doi.org/10.1002/0471238961.0102191519201503.a01.pub3, (accessed 27 February 2022)

2. Environmental Protection Agency. Climate Change Indicators: Climate Forcing. https://www.epa.gov/climate-indicators/climate-change-indicators-climate-forcing (accessed 24 January, 2022).

3. Le Quéré, C.; Andres, R. J.; Boden, T.; Conway, T.; Houghton, R. A.; House, J. I.; Marland, G.; Peters, G. P.; van der Werf, G. R.; Ahlström, A.; Andrew, R. M.; Bopp, L.; Canadell, J. G.; Ciais, P.; Doney, S. C.; Enright, C.; Friedlingstein, P.; Huntingford, C.; Jain, A. K.; Jourdain, C.; Kato, E.; Keeling, R. F.; Klein Goldewijk, K.; Levis, S.; Levy, P.; Lomas, M.; Poulter, B.; Raupach, M. R.; Schwinger, J.; Sitch, S.; Stocker, B. D.; Viovy, N.; Zaehle, S.; Zeng, N., The global carbon budget 1959–2011. *Earth Syst. Sci. Data* 2013, *5* (1), 165-185.

4. Rockström, J.; Steffen, W.; Noone, K.; Persson, Å.; Chapin, F. S.; Lambin, E. F.; Lenton, T. M.; Scheffer, M.; Folke, C.; Schellnhuber, H. J.; Nykvist, B.; de Wit, C. A.; Hughes, T.; van der Leeuw, S.; Rodhe, H.; Sörlin, S.; Snyder, P. K.; Costanza, R.; Svedin, U.; Falkenmark, M.; Karlberg, L.; Corell, R. W.; Fabry, V. J.; Hansen, J.; Walker, B.; Liverman, D.; Richardson, K.; Crutzen, P.; Foley, J. A., A safe operating space for humanity. *Nature* 2009, *461* (7263), 472-475.

5. United Nations Framework Convention on Climate Change. The Paris Agreement. https://unfccc.int/process-and-meetings/the-paris-agreement/the-paris-agreement (accessed 28 January, 2022).

6. Energimyndigheten *Processrelaterade och negativa utsläpp – nuläge och förutsättningar för omställning*; Arkitektkopia AB: Bromma, October 2020. ISBN: 978-91-89184-79-4. Number of pages: 96.

7. Naturvårdsverket *Begränsad klimatpåverkan*; Arkitektkopia AB: Bromma, 2019. ISBN: 978-91-620-6859-2. Number of pages: 36

8. Statens Offentliga Utredningar *Vägen till en klimatpositiv framtid*; Elanders Sverige AB: Stockholm, 2020. ISBN: 978-91-38-25019-8. Number of pages: 850.

9. IPCC. Summary for Policymakers. *Global Warming of 1.5°C. An IPCC Special Report on the impacts of global warming of 1.5°C above pre-industrial levels and related global greenhouse gas emission pathways, in the context of strengthening the global response to the threat of climate change, sustainable development, and efforts to eradicate poverty* [Masson-Delmotte, V., P. Zhai, H.-O. Pörtner, D. Roberts, J. Skea, P.R. Shukla, A. Pirani, W. Moufouma-Okia, C. Péan, R. Pidcock, S. Connors, J.B.R. Matthews, Y. Chen, X. Zhou, M.I. Gomis, E. Lonnoy, T. Maycock, M. Tignor, and T. Waterfield (eds.)]. World Meteorological Organization, Geneva, Switzerland. Number of pages: 32.

10. Sifat, N. S.; Haseli, Y., A Critical Review of CO2 Capture Technologies and Prospects for Clean Power Generation. *Energies* 2019, *12* (21).

11. Smith, R. Separation of Heterogeneous Mixtures. *Chemical Process Design and Integration*, 2nd Edition; Wiley: Chichester, West Sussex, United Kingdom, 2016; Vol. pp.125-129.

12. Rochelle Gary, T., Amine Scrubbing for CO2 Capture. *Science* 2009, *325* (5948), 1652-1654.

13. Svensson, H., *Energy efficient processes for the production of gaseous biofuels : reforming and gas upgrading*. Ph.D. Dissertation, Department of Chemical Engineering, Lund University 2014.

14. Karlsson, H., *Precipitating Amine Absorption Systems for Carbon Capture*. Ph.D. Dissertation, Department of Chemical Engineering, Lund University 2021.

15. *DMSO* MSDS No. 102952; MERCK Darmstadt, Germany. 2019.

16. Vega, F.; Cano, M.; Camino, S.; Gallego Fernández, L. M.; Portillo, E.; Navarrete, B., Solvents for Carbon Dioxide Capture. *In Carbon Dioxide Chemistry, Capture and Oil Recovery* [Online]; Karamé, I., Shaya, J., Srour H., Ed. IntechOpen: London, United Kingdom, 2018. DOI: 10.5772/intechopen.68466

17. Sanku, M. G., *Methodologies for non-aqueous systems and precipitating systems as carbon capture technologies : a case-study of AMP-NMP*. Ph.D. Dissertation, Department of Chemical Engineering, Lund University 2020.

18. Rochelle, G. T., 3 - Conventional amine scrubbing for CO2 capture. In *Absorption-Based Post-combustion Capture of Carbon Dioxide* [Online] Feron, P. H. M., Ed. Woodhead Publishing: 2016; pp 35-67. DOI: https://doi.org/10.1016/B978-0-08-100514-9.00003-2

19. Wang, M.; Lawal, A.; Stephenson, P.; Sidders, J.; Ramshaw, C., Post-combustion CO2 capture with chemical absorption: A state-of-the-art review. *Chemical Engineering Research and Design* 2011, *89* (9), 1609-1624.

20. Spietz, T.; Dobras, S.; Więcław-Solny, L.; Krótki, A., Nitrosamines and nitramines in Carbon Capture plants. *Environmental Protection and Natural Resources* 2017, *28* (4), 43-50.

21. Flø, N. E.; Faramarzi, L.; de Cazenove, T.; Hvidsten, O. A.; Morken, A. K.; Hamborg, E. S.; Vernstad, K.; Watson, G.; Pedersen, S.; Cents, T.; Fostås, B. F.; Shah, M. I.; Lombardo, G.; Gjernes, E., Results from MEA Degradation and Reclaiming Processes at the CO2 Technology Centre Mongstad. *Energy Procedia* 2017, *114*, 1307-1324.

22. Oyenekan, B. A.; Rochelle, G. T., Energy Performance of Stripper Configurations for CO2 Capture by Aqueous Amines. *Industrial & Engineering Chemistry Research* 2006, *45* (8), 2457-2464.

23. Aaron, D.; Tsouris, C., Separation of CO2 from Flue Gas: A Review. *Separation Science and Technology* 2005, *40* (1-3), 321-348.

24. Rochelle, G. T., Thermal degradation of amines for CO2 capture. *Current Opinion in Chemical Engineering* 2012, *1* (2), 183-190.

25. Edlund, M. Midroc byter namn till Granitor https://www.granitor.se/nyheter/2021/midroc-byter-namn-till-granitor (accessed 4 April, 2022).

26. Singh, R. P.; Heldman, D. R., Chapter 2 - Fluid Flow in Food Processing. In *Introduction to Food Engineering* 5th Edition, Singh, R. P.; Heldman, D. R., Eds. Academic Press: San Diego, 2014; pp 65-209.

27. Nilsson, B.; Andersson, N., *Applied Transport Phenomena*. Media-Tryck: Lund, 2020.

28. Chhabra, R. P.; Patel, S. A., Fluid Mechanics. *Kirk-Othmer Encyclopedia of Chemical Technology* [Online]; Posted on 8 July, 2020. https://doi.org/10.1002/0471238961.06122109191514.a01.pub3 (accessed April 4, 2022).

29. Pinto, D. D. D.; Johnsen, B.; Awais, M.; Svendsen, H. F.; Knuutila, H. K., Viscosity measurements and modeling of loaded and unloaded aqueous solutions of MDEA, DMEA, DEEA and MAPA. *Chemical Engineering Science* 2017, *171*, 340-350.

30. *AMP* MSDS No. A65182; SIGMA ALDRICH Stockholm, Sweden. 2020.

31. A., D. K.; Sarina, B.; Dirk, S., *Molecular Driving Forces: Statistical Thermodynamics in Biology, Chemistry, Physics, and Nanoscience* 2nd Edition.; Garland Science, Taylor & Francis Group , LLC: Abingdon, United Kingdom, 2010.

32. Amundsen, T. G.; Øi, L. E.; Eimer, D. A., Density and Viscosity of Monoethanolamine + Water + Carbon Dioxide from (25 to 80) °C. *Journal of Chemical & Engineering Data* 2009, *54* (11), 3096-3100.

33. Weiland, R. H.; Dingman, J. C.; Cronin, D. B.; Browning, G. J., Density and Viscosity of Some Partially Carbonated Aqueous Alkanolamine Solutions and Their Blends. *Journal of Chemical & Engineering Data* 1998, *43* (3), 378-382.

34. Haratipour, P.; Baghban, A.; Mohammadi, A. H.; Nazhad, S. H. H.; Bahadori, A., On the estimation of viscosities and densities of CO2-loaded MDEA, MDEA+AMP, MDEA+DIPA, MDEA+MEA, and MDEA+DEA aqueous solutions. *Journal of Molecular Liquids* 2017, *242*, 146-159.

35. Garcia, M.; Knuutila, H. K.; Aronu, U. E.; Gu, S., Influence of substitution of water by organic solvents in amine solutions on absorption of CO2. *International Journal of Greenhouse Gas Control* 2018, *78*, 286-305.

36. Tao, M.; Gao, J.; Zhang, P.; Zhang, W.; Liu, Q.; He, Y.; Shi, Y., Biogas Upgrading by Capturing CO2 in Non-aqueous Phase-Changing Diamine Solutions. *Energy & Fuels* 2017, *31* (6), 6298-6304.

37. Karlsson, H.; Svensson, H., Physical properties of the 2-amino-2-methyl-1-propanol and N-methyl-2-pyrrolidone system. In *14th International Conference on Greenhouse Gas Control Technologies, 2018*, Melbourne, Australia, 2018.

38. Karunarathne, S. S.; Eimer, D. A.; Øi, L. E., Density, viscosity and free energy of activation for viscous flow of CO2 loaded 2-amino-2-methyl-1-propanol (AMP), monoethanol amine (MEA) and H2O mixtures. *Journal of Molecular Liquids* 2020, *311*, 113286.

39. Shi, H.; Ma, L.; Zhao, B.; Pang, Y.; Wu, Z., Density, viscosity and molecular interaction of binary system tetraethylene glycol+dimethyl sulfoxide at T=(293.15 to 318.15)K. *Journal of Molecular Liquids* 2018, *250*, 182-191.

40. Zhao, T.; Zhang, J.; Guo, B.; Zhang, F.; Sha, F.; Xie, X.; Wei, X., Density, viscosity and spectroscopic studies of the binary system of ethylene glycol+dimethyl sulfoxide at T=(298.15 to 323.15) K. *Journal of Molecular Liquids* 2015, *207*, 315-322.

41. LeBel, R. G.; Goring, D. A. I., Density, Viscosity, Refractive Index, and Hygroscopicity of Mixtures of Water and Dimethyl Sulfoxide. *Journal of Chemical & Engineering Data* 1962, *7* (1), 100-101.

42. Havemeyer, R. N., Freezing Point Curve of Dimethyl Sulfoxide—Water Solutions. *Journal of Pharmaceutical Sciences* 1966, *55* (8), 851-853.

43. Ahmed Ibrahim, S., On fluid dynamics of lamella separator modelling and process optimisation. Ph.D. Dissertation, Universität Bremen Produktionstechnik. 2012.

44. Sinnott, R. K., CHAPTER 10 - Equipment Selection, Specification and Design. In *Coulson and Richardson's Chemical Engineering* 2nd Edition, Sinnott, R. K., Ed; Pergamon: Amsterdam, 1993; pp 352-438.

45. Svarovsky, L., Sedimentation. *Kirk-Othmer Encyclopedia of Chemical Technology* [Online]; Posted on 19 May, 2006. https://doi.org/10.1002/0471238961.1905040919220118.a01.pub2 (accessed 28 February, 2022).

46. De, A., *Sedimentation Process And Design of Settling Systems* 1st Edition; Springer: New Delhi, 2017; pp 333.

47. Davis, M. L., *Water and Wastewater Engineering*. The McGraw-Hill Companies, Inc.: 2010.

48. Metcalf & Eddy, I., *Wastewater Engineering: treatment and reuse*. 4th Edition; McGraw-Hill: New York, NY, USA. 2003.

49. Moran, S.; Zimmels, Y., Sedimentation. *Ullmann's Encyclopedia of Industrial Chemistry* [Online]; Posted on 5 December, 2018. https://doi.org/10.1002/9783527306732.b02_12.pub2 (Accessed 28 February, 2022).

50. Kowalski, W. P., The Method of Calculations of the Sedimentation Efficiency in Tanks with Lamella Packets. *Archives of Hydro-Engineering and Environmental Mechanics* 2004, *51* (4), 15.

51. Weiß, G. J., Lamella settlers for treatment of urban storm runoff: Experience with model and prototype tests. *Novatech 2016 - 9ème Conférence internationale sur les techniques et stratégies pour la gestion durable de l'Eau dans la Ville / 9th International Conference on planning and technologies for sustainable management of Water in the City*, June 2016, Lyon, France.

52. Crittenden, J. C.; Trussell, R. R.; Hand, D. W.; Howe, K. J.; Tchobanoglous, G., Gravity Separation. *MWH's Water Treatment: Principles and Design,* 3rd Edition 2012, pp 641-725.

53. TC Ltd. Thermocouple Tolerances. https://www.tc.co.uk/thermocouple-information/thermocouple-tolerances.html (accessed May 30, 2022).

54. Alveteg, M., *Handbook*. Media-Tryck: Lund, 2017.

55. Iglesias-Silva, G. A.; Guzmán-López, A.; Pérez-Durán, G.; Ramos-Estrada, M., Densities and Viscosities for Binary Liquid Mixtures of n-Undecane + 1-Propanol, + 1-Butanol, + 1-Pentanol, and + 1-Hexanol from 283.15 to 363.15 K at 0.1 MPa. *Journal of Chemical & Engineering Data* 2016, *61* (8), 2682-2699.

56. Omota, L. M.; Iulian, O.; Ciocirlan, O.; Nita, I., Viscosity of water, 1,4-dioxane and dimethyl sulfoxide binary and ternary systems at temperatures from 293.15 KTO 313.15 K. *Revue Roumaine de Chimie* 2008, *53*, 977-988.

57. World Health Organization, United Nations Environment Programme Climate Change. https://www.who.int/heli/risks/climate/climatechange/en/ (accessed 4 April, 2022).

58. Medvecky, F.; Lacey, J.; Ashworth, P., Examining the Role of Carbon Capture and Storage Through an Ethical Lens. *Science and Engineering Ethics* 2014, *20* (4), 1111-1128.

59. Linton, M. Ed., *Klimat och moral: nio tankar om hettan*; Natur & Kultur: Stockholm, 2021; p 250.

60. Boucher, P.; Gough, C., Mapping the ethical landscape of carbon capture and storage. *Poiesis Prax* 2012, *9* (3-4), 249-270.

61. Lenzi, D., The ethics of negative emissions. *Global Sustainability* 2018, *1*, (7). doi:10.1017/sus.2018.5

Appendices

Appendix A: Result of the microscope calibration

Eight calibration images were captured, whereby the calibration lines could be precisely placed on images of the calibration slide in accordance with the method. The same standard magnification lens was used for all images presented in this work. The distance between the sample and the lens was instead what was changed. A reference position of the height adjuster rotor was chosen and it was denoted as the PM0 position. “P” stood for plus, and “M” for minus rotations, while the number corresponds to numbers on the height adjuster rotor itself. Four clear calibration images were captured for positive rotations of the height adjuster rotor. These images were taken at rotations denoted as P10, P20, P25, and P30, meaning that the height adjuster rotor had been rotated positively the specified number of steps on its grading. The related calibrations were given the same name. Three clear calibration images were captured for negative rotations of the height adjuster rotor. Hence obtaining negative, or minus, values of rotation, these calibration images and the related calibrations were given the names M10, M20, and M30. Table A.1 showcases the distance per pixel, in µm, for the different positions of the height adjuster rotor obtained from the calibrated images.

Table A.1. In the left column, the positions of the height adjuster rotor are listed. In the right column, the distance, in µm, per pixel for the calibration is reported. The values in the right column where obtained from the VisiCam software after images of the calibration slide had been captured and calibrated in accordance with the method described under section 3.2.

Position of the height adjuster rotor	Distance, in µm, per pixel
P30	0.489203
P25	0.487104
P20	0.486971
P10	0.484616
PM0	0.482281
M10	0.480103
M20	0.477498
M30	0.474794

A linear calibration line was fitted against the experimental results, see Figure A.1, yielding a linear formula for the distance, in µm, per pixel as a function of the position of the height adjuster rotor. The equation became

$$y = 0.0002 * x + 0.4821 \qquad 14$$

with an R^2-value of 0.9944. The y here represents the distance, in µm, per pixel, while x is the position of the height adjuster rotor.

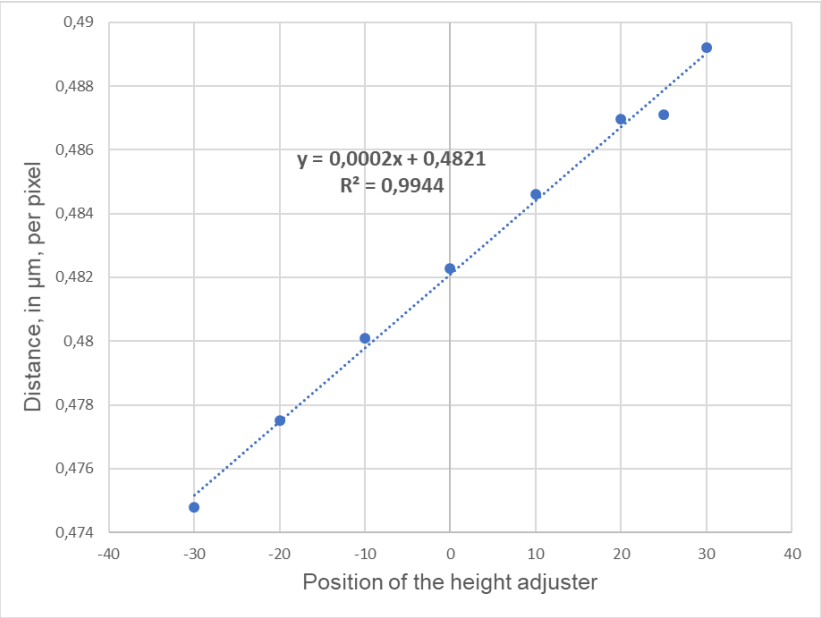

Figure A.1. The experimental data points of the distance, in µm, per pixel for each position of the height adjuster. The values are the same as those reported in Table A.1. The linear regression equation for the data points is also showed within the graph, along with its R^2-value.

Appendix B: Settling velocity experimental data

Experimental data for the 0H25A75D stock mixture with a CO_2-loading of 0.38

In Figure A.2 to Figure A.5, the graphs for the first and second experimental run with the stock mixture having the CO_2-loading of 0.38 are presented. They showcase the height of interface for the precipitate front against the settling time. For three of the graphs, there is a jump in the value of the height of interface, which was caused by the presence of precipitate on top of the liquid layer in the measuring cylinders. The effect was that the correct height of interface could not be read from the images that captured the sedimentation process. Once the correct height of interface of the front could be read, the experimental readings indicate that the height of interface decreased with a linear settling velocity at both temperatures. The linear regression of the experimental data are showed in the graphs.

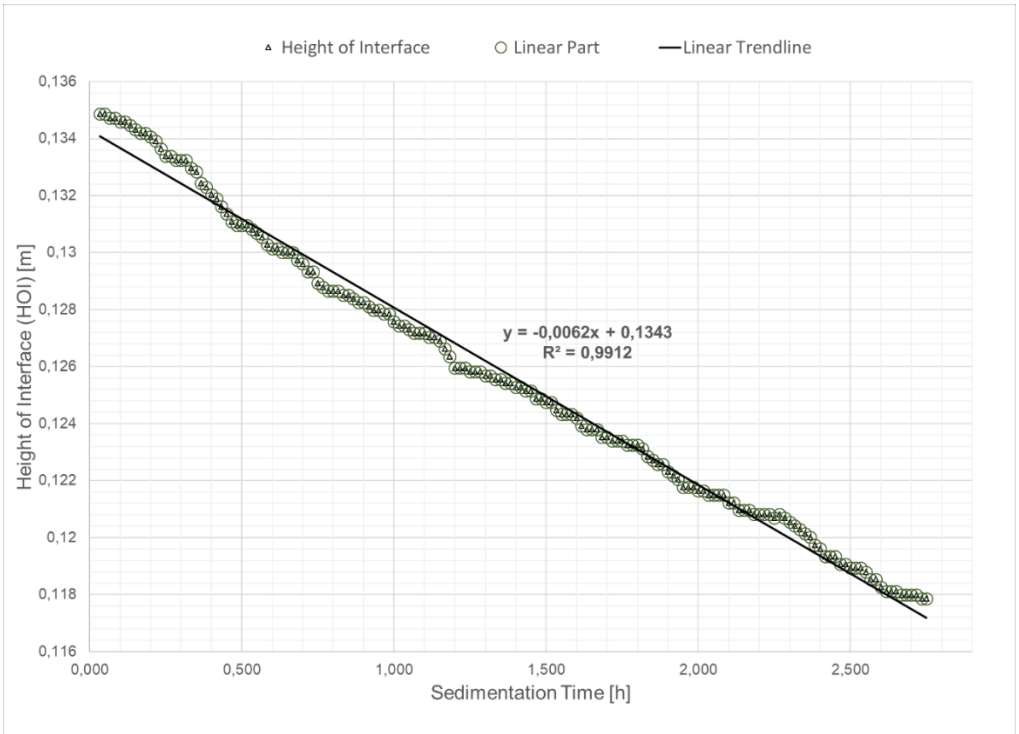

Figure A.2. The graph showcases the experimental data from the 1st settling velocity experiment at 50 °C for the 0H25A75D stock mixture with the CO_2-loading of 0.38. On the y-axis, the height of interface, abbreviated as HOI, is shown in meters. On the x-axis, the settling time is shown in hours.

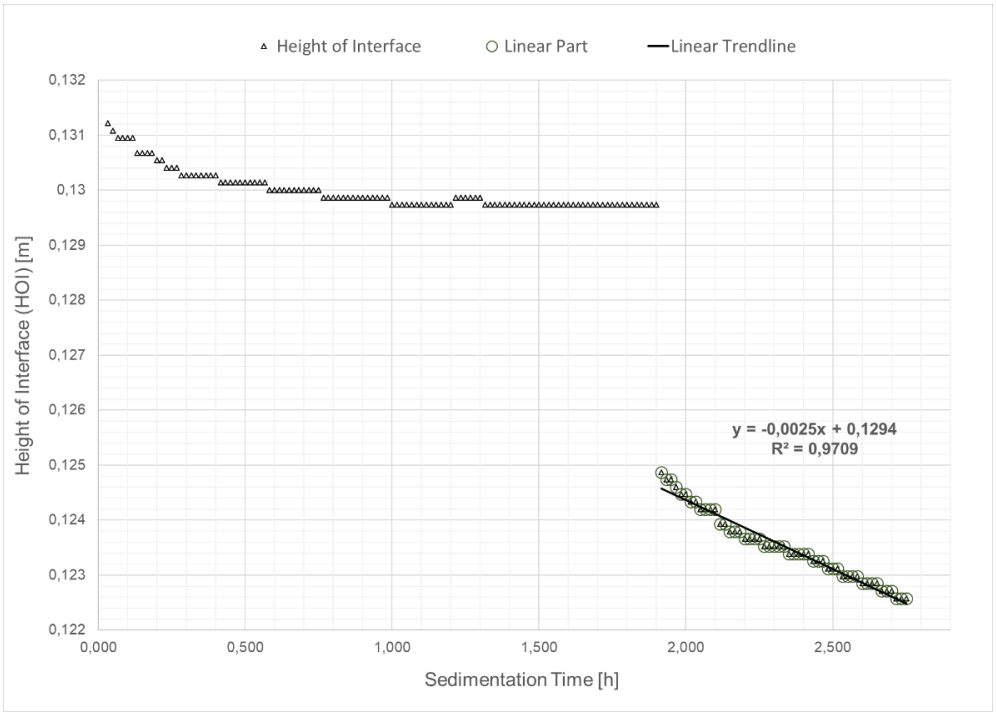

Figure A.3. The graph showcases the experimental data from the 1st settling velocity experiment at 21 °C for the 0H25A75D stock mixture with the CO_2 loading of 0.38. On the y-axis, the height of interface, abbreviated as HOI, is shown in meters. On the x-axis, the settling time is shown in hours.

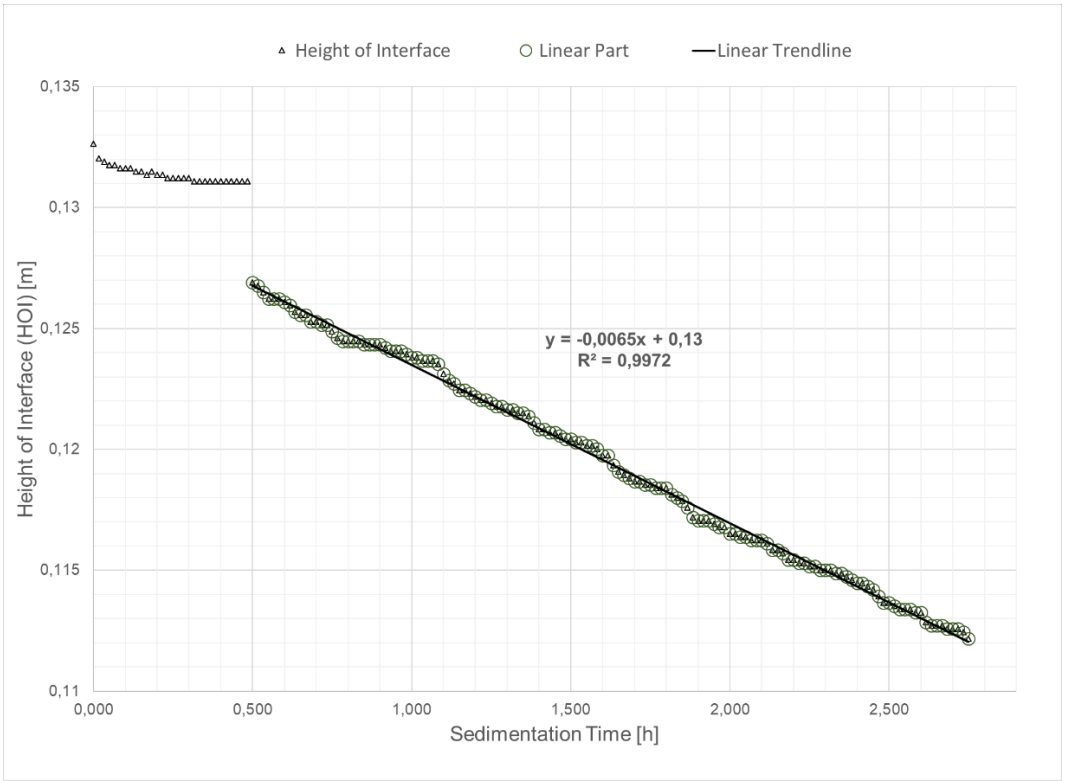

Figure A.4. The graph showcases the experimental data from the 2nd settling velocity experiment at 50 ° for the 0H25A75D stock mixture with the CO_2 loading of 0.38. On the y-axis, the height of interface, abbreviated as HOI, is shown in meters. On the x-axis, the settling time is shown in hours.

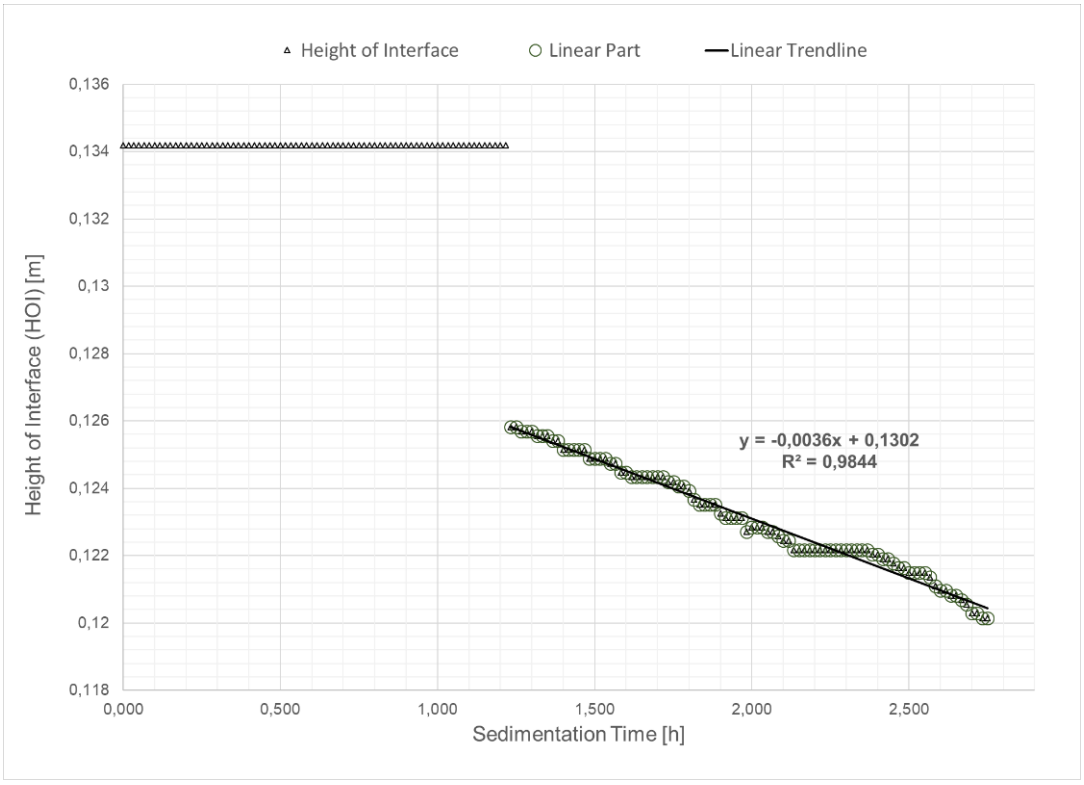

Figure A.5. The graph showcases the experimental data from the 2nd settling velocity experiment at 21 °C for the 0H25A75D stock mixture with the CO_2 loading of 0.38. On the y-axis, the height of interface, abbreviated as HOI, is shown in meters. On the x-axis, the settling time is shown in hours.

Experimental data for the 0H25A75D stock mixture with a CO_2-loading of 0.50

Figure A.6 to Figure A.11 showcase the experimental data from the first, second and third settling velocity experiments for the slurry with a CO_2-loading of 0.50. The linear equation regressed to the initial linear part of the graph is also visible within each figure.

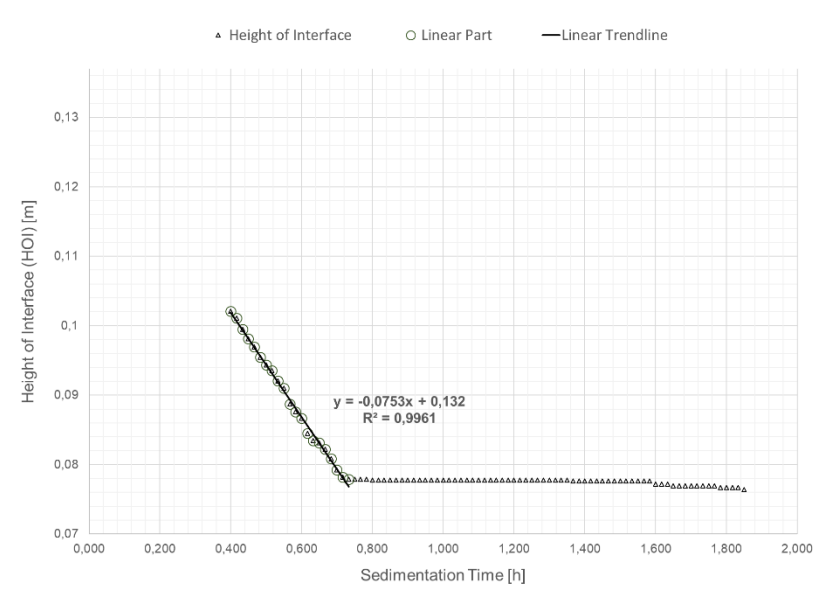

Figure A.6. The graph showcases the experimental data from the 1st settling velocity experiment at 50 °C for the 0H25A75D stock mixture with the CO_2 loading of 0.5. On the y-axis, the height of interface, abbreviated as HOI, is shown in meters. On the x-axis, the settling time is shown in hours.

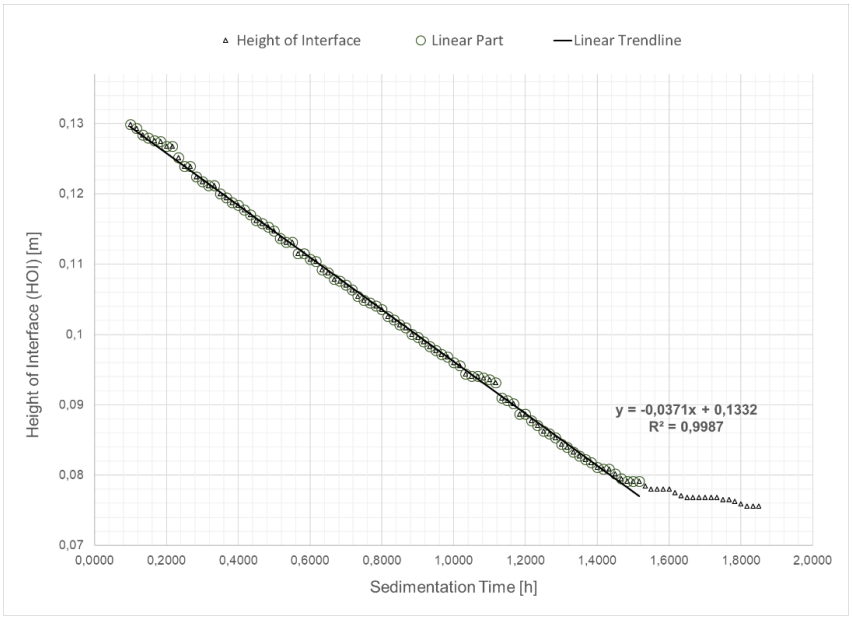

Figure A.7. The graph showcases the experimental data from the 1st settling velocity experiment at 21 °C for the 0H25A75D stock mixture with the CO_2 loading of 0.5. On the y-axis, the height of interface, abbreviated as HOI, is shown in meters. On the x-axis, the settling time is shown in hours.

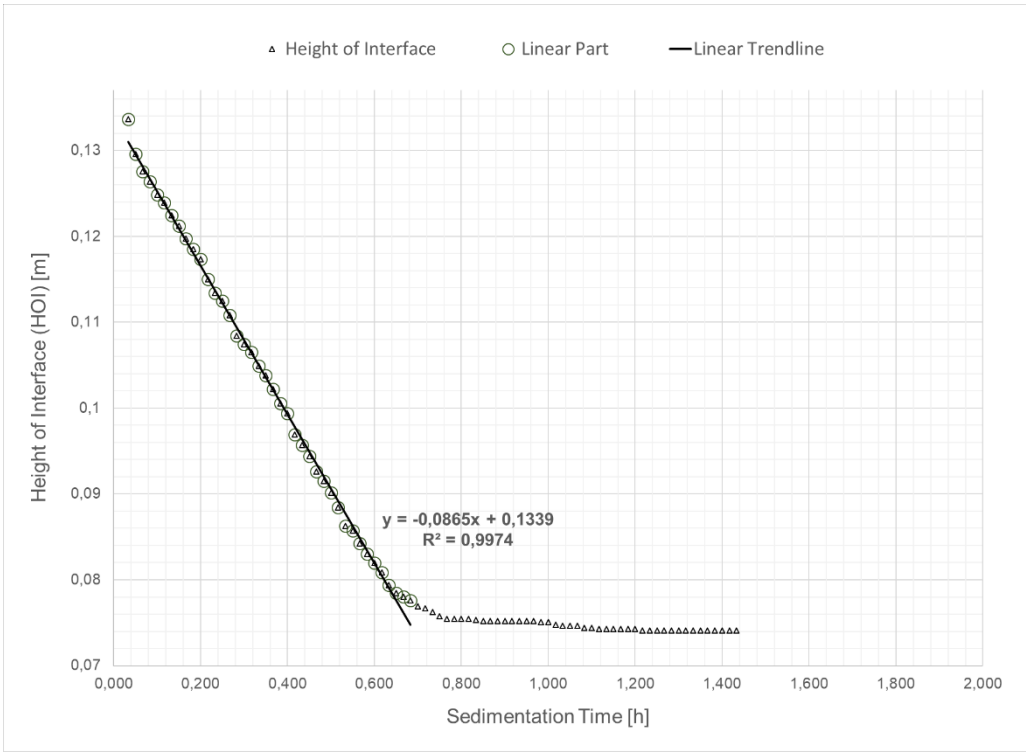

Figure A.8. The graph showcases the experimental data from the 2nd settling velocity experiment at 50 °C for the 0H25A75D stock mixture with the CO_2 loading of 0.5. On the y-axis, the height of interface, abbreviated as HOI, is shown in meters. On the x-axis, the settling time is shown in hours.

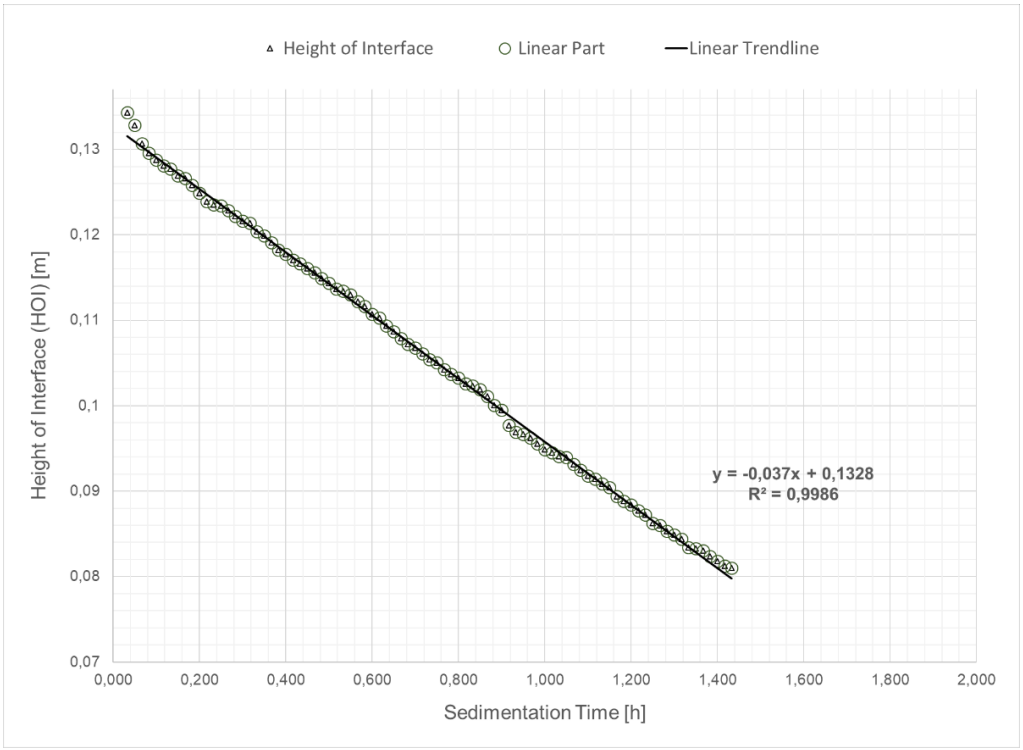

Figure A.9. The graph showcases the experimental data from the 2nd settling velocity experiment at 21 °C for the 0H25A75D stock mixture with the CO_2 loading of 0.5. On the y-axis, the height of interface, abbreviated as HOI, is shown in meters. On the x-axis, the settling time is shown in hours.

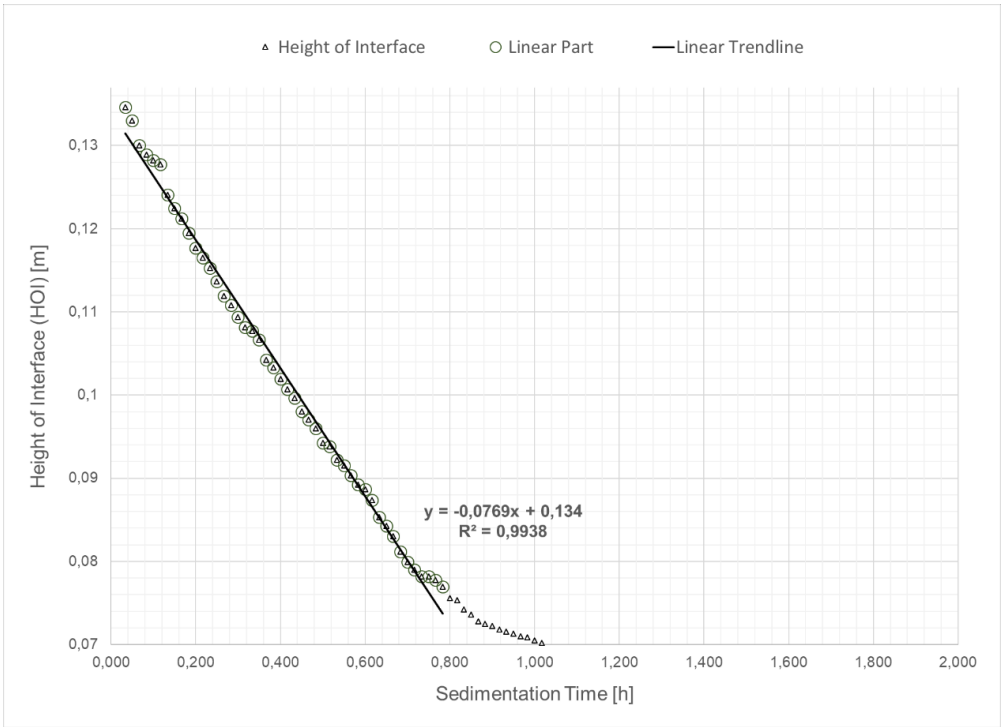

Figure A.10. The graph showcases the experimental data from the 3rd settling velocity experiment at 50 °C for the 0H25A75D stock mixture with the CO_2 loading of 0.5. On the y-axis, the height of interface, abbreviated as HOI, is shown in meters. On the x-axis, the settling time is shown in hours.

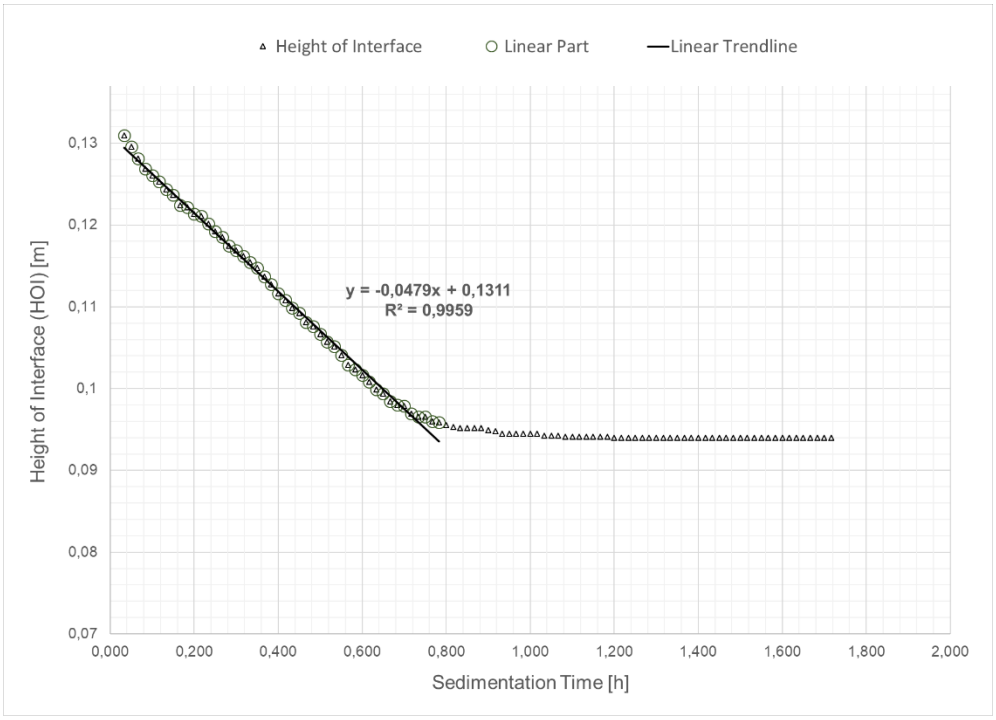

Figure A.11. The graph showcases the experimental data from the 3rd settling velocity experiment at 21 °C for the 0H25A75D stock mixture with the CO_2 loading of 0.5. On the y-axis, the height of interface, abbreviated as HOI, is shown in meters. On the x-axis, the sedimentation time is shown in hours.

Appendix C: Additional microscope images

Figure A.12 shows an image of the crystals found in the old stock mixture with a CO2-loading of 0.38. Experimental runs of the settling velocity were also conducted for this older stock mixture. Its freezing temperature was also investigated, and representative values were obtained for all three investigated water contents.

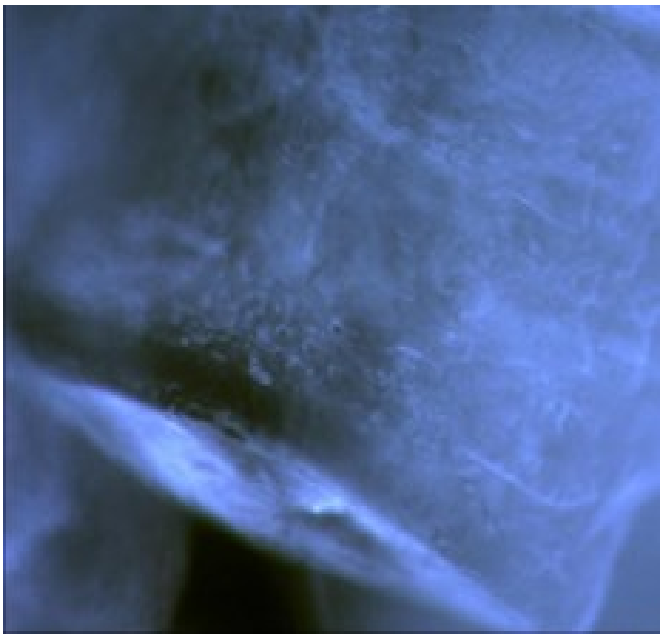

Figure A.12. Contours of the crystal found in the old stock mixture with a CO_2-loading of 0.38. The height adjuster rotor was in position P700 as the image was captured with the standard magnification.

Appendix D: Freezing temperature

Figure A.13 to Figure A.15 shows the registered melting temperatures for all measurements of each measurement series. In Figure A.13, five out of six tested samples with the composition 0H25A75D gave reliable temperature values. For the 5H24A71D samples, presented in Figure A.14, only three of the samples gave reliable temperature values, while all the 10H22.5A67.5D samples did give reliable results, which is seen in Figure A.15.

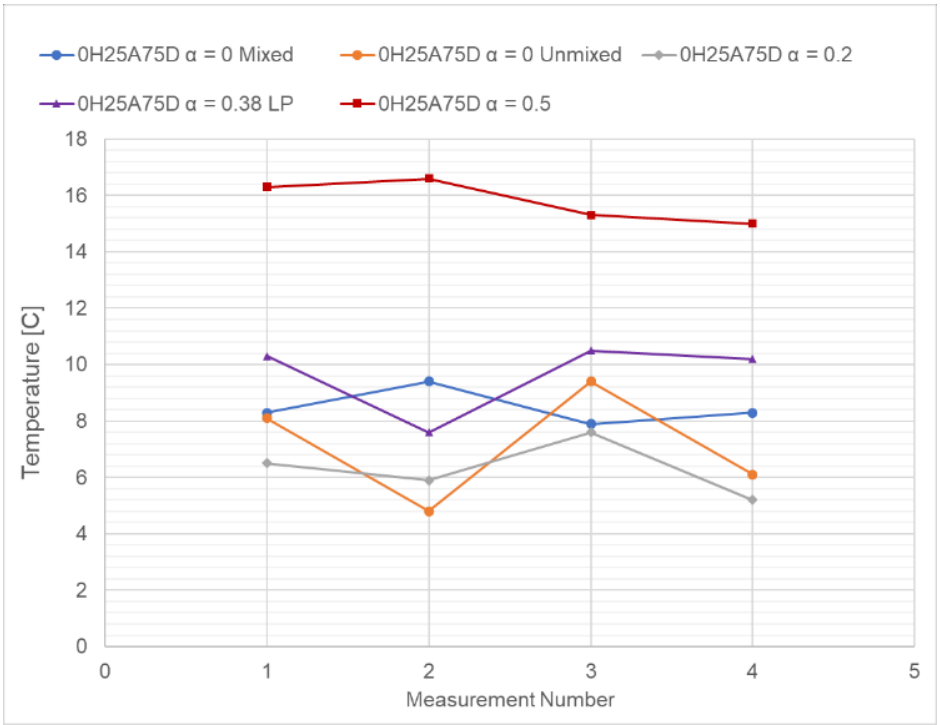

Figure A.13. The registered melting temperature for each reliable measurement for stock mixtures with 0 wt-% water, 25 wt-% AMP, and 75 wt-% DMSO.

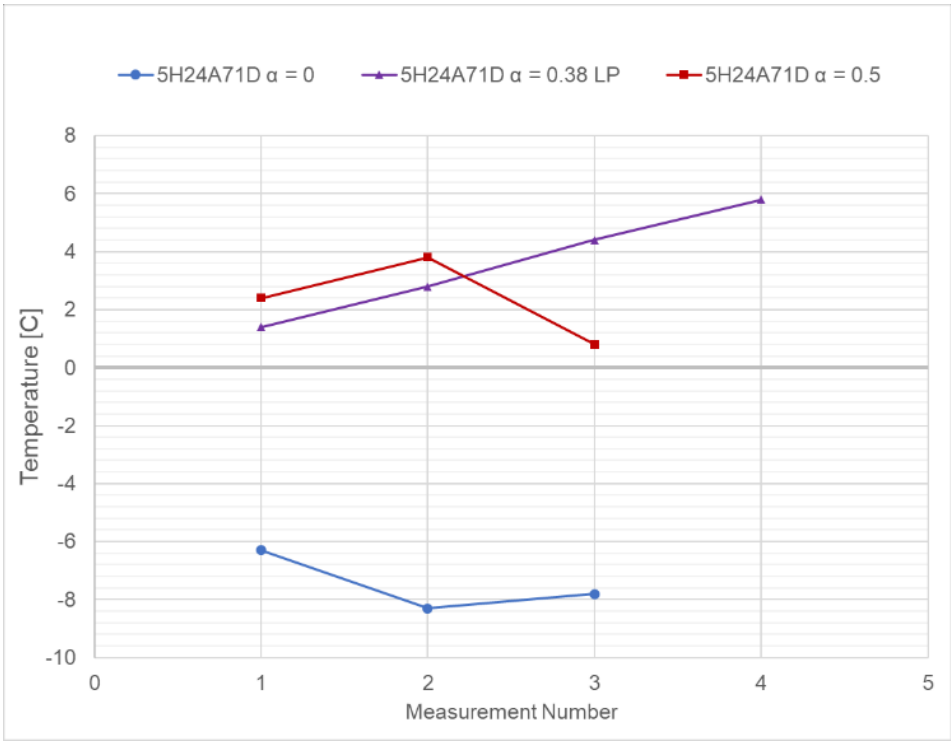

Figure A.14. The registered melting temperature for each reliable measurement for stock mixtures with 5 wt-% water, 24 wt-% AMP, and 71 wt-% DMSO.

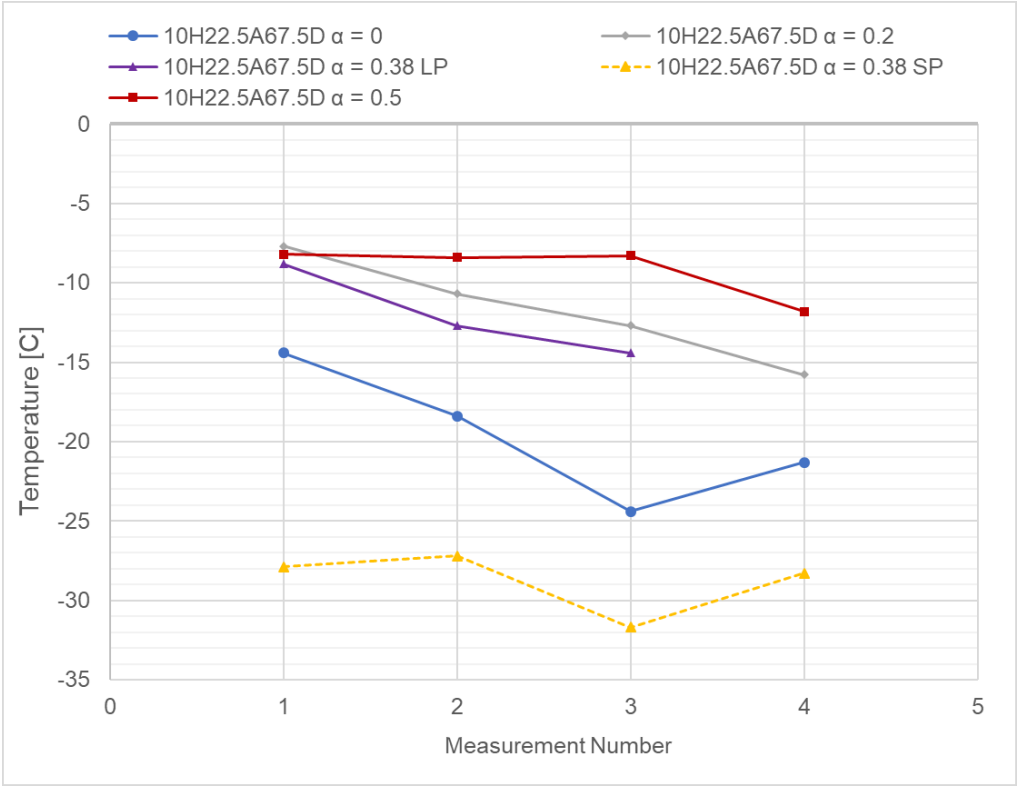

Figure A.15. The registered melting temperature for each reliable measurement for stock mixtures with 10 wt-% water, 22.5 wt-% AMP, and 67.5 wt-% DMSO.

Appendix E: Density Measurements

Figure A.16 shows all the experimental results of the hydrometer experiments, with values reported for each attempt. Figure A.17 and Figure A.18 instead show all the experimental data related to gravimetric density determinations at 20 and 50 °C respectively. All the experimental data for the CO_2-loaded solutions is presented in Figure A.19 and Figure A.20.

0 wt-% H2O/25 wt-% AMP/75 wt-% DMSO α = 0	
Temperature = 20 °C	
Flotation Device 1-1.150	
Attempt	Density [g/cm^3]
1	1.049
2	1.049
3	1.049
4	1.049
5	1.049

0 wt-% H2O/25 wt-% AMP/75 wt-% DMSO α = 0	
Temperature = 20 °C	
Flotation Device 1-1.210	
Attempt	Density [g/cm^3]
1	1.048
2	1.048
3	1.048
4	1.048
5	1.048

5 wt-% H2O/24 wt-% AMP/71 wt-% DMSO α = 0	
Temperature = 20 °C	
Flotation Device 1-1.150	
Attempt	Density [g/cm^3]
1	1.056
2	1.056
3	1.056
4	1.056
5	1.056

5 wt-% H2O/24 wt-% AMP/71 wt-% DMSO α = 0	
Temperature = 20 °C	
Flotation Device 1-1.210	
Attempt	Density [g/cm^3]
1	1.054
2	1.054
3	1.054
4	1.053
5	1.053

10 wt-% H2O/22.5 wt-% AMP/67.5 wt-% DMSO α = 0	
Temperature = 20 °C	
Flotation Device 1-1.150	
Attempt	Density [g/cm^3]
1	1.061
2	1.061
3	1.061
4	1.061
5	1.062

10 wt-% H2O/22.5 wt-% AMP/67.5 wt-% DMSO α = 0	
Temperature = 20 °C	
Flotation Device 1-1.210	
Attempt	Density [g/cm^3]
1	1.058
2	1.058
3	1.058
4	1.059
5	1.058

DMSO	
Temperature = 20 °C	
Flotation Device 1-1.150	
Attempt	Density [g/cm^3]
1	1.1
2	1.1
3	1.1
4	1.1
5	1.1

DMSO	
Temperature = 20 °C	
Flotation Device 1-1.210	
Attempt	Density [g/cm^3]
1	1.099
2	1.099
3	1.099
4	1.099
5	1.099

0 wt-% H2O/50 wt-% AMP/50 wt-% DMSO α = 0	
Temperature = 20 °C	
Flotation Device 1-1.210	
Attempt	Density [g/cm^3]
1	1.004
2	1.004
3	1.004
4	1.004
5	1.004

5 wt-% H2O/47.5 wt-% AMP/47.5 wt-% DMSO α = 0	
Temperature = 20 °C	
Flotation Device 1-1.210	
Attempt	Density [g/cm^3]
1	1.012
2	1.012
3	1.012
4	1.011
5	1.012

10 wt-% H2O/45 wt-% AMP/45 wt-% DMSO α = 0	
Temperature = 20 °C	
Flotation Device 1-1.210	
Attempt	Density [g/cm^3]
1	1.019
2	1.019
3	1.019
4	1.019
5	1.019

Figure A.16. The experimental results of the hydrometer experiments at room temperature, 20 °C, for the unloaded stock mixtures.

DMSO			0 wt-% H2O/25 wt-% AMP/75 wt-% DMSO α = 0		
Temperature = 20 °C			Temperature = 20 °C		
Volume solution = 50 cm^3			Volume solution = 50 cm^3		
Weight cap			**Weight cap**		
Attempt 1	2.0555	[g]	Attempt 1	2.0554	[g]
Attempt 2	2.0555	[g]	Attempt 2	2.0554	[g]
Attempt 3	2.0555	[g]	Attempt 3	2.0555	[g]
Weight measuring flask			**Weight measuring flask**		
Attempt 1	33.3906	[g]	Attempt 1	33.3914	[g]
Attempt 2	33.3903	[g]	Attempt 2	33.3944	[g]
Attempt 3	33.3903	[g]	Attempt 3	33.3967	[g]
Weight measuring flask+cap+solution			**Weight measuring flask+cap+solution**		
Attempt 1	90.3859	[g]	Attempt 1	87.797	[g]
Attempt 2	90.3858	[g]	Attempt 2	87.7969	[g]
Attempt 3	90.3857	[g]	Attempt 3	87.7967	[g]

5 wt-% H2O/24 wt-% AMP/71 wt-% DMSO α = 0			10 wt-% H2O/22.5 wt-% AMP/67.5 wt-% DMSO α = 0		
Temperature = 20 °C			Temperature = 20 °C		
Volume solution = 50 cm^3			Volume solution = 50 cm^3		
Weight cap			**Weight cap**		
Attempt 1	4.7272	[g]	Attempt 1	4.7881	[g]
Attempt 2	4.7268	[g]	Attempt 2	4.7883	[g]
Attempt 3	4.7269	[g]	Attempt 3	4.7885	[g]
Weight measuring flask			**Weight measuring flask**		
Attempt 1	43.3552	[g]	Attempt 1	45.2219	[g]
Attempt 2	43.3555	[g]	Attempt 2	45.2234	[g]
Attempt 3	43.3553	[g]	Attempt 3	45.2168	[g]
Weight measuring flask+cap+solution			**Weight measuring flask+cap+solution**		
Attempt 1	100.6027	[g]	Attempt 1	102.8405	[g]
Attempt 2	100.6031	[g]	Attempt 2	102.8401	[g]
Attempt 3	100.6025	[g]	Attempt 3	102.8401	[g]

0 wt-% H2O/50 wt-% AMP/50 wt-% DMSO α = 0			5 wt-% H2O/47.5 wt-% AMP/47.5 wt-% DMSO α = 0		
Temperature = 20 °C			Temperature = 20 °C		
Volume solution = 50 cm^3			Volume solution = 50 cm^3		
Weight cap			**Weight cap**		
Attempt 1	4.7109	[g]	Attempt 1	3.6447	[g]
Attempt 2	4.7109	[g]	Attempt 2	3.6447	[g]
Attempt 3	4.7109	[g]	Attempt 3	3.6448	[g]
Weight measuring flask			**Weight measuring flask**		
Attempt 1	39.614	[g]	Attempt 1	45.0759	[g]
Attempt 2	39.614	[g]	Attempt 2	45.0752	[g]
Attempt 3	39.614	[g]	Attempt 3	45.0753	[g]
Weight measuring flask+cap+solution			**Weight measuring flask+cap+solution**		
Attempt 1	94.3205	[g]	Attempt 1	99.1935	[g]
Attempt 2	94.3202	[g]	Attempt 2	99.1935	[g]
Attempt 3	94.3198	[g]	Attempt 3	99.1935	[g]

10 wt-% H2O/45 wt-% AMP/45 wt-% DMSO α = 0		
Temperature = 20 °C		
Volume solution = 50 cm^3		
Weight cap		
Attempt 1	9.9042	[g]
Attempt 2	9.9042	[g]
Attempt 3	9.9041	[g]
Weight measuring flask		
Attempt 1	43.8067	[g]
Attempt 2	43.8078	[g]
Attempt 3	43.8078	[g]
Weight measuring flask+cap+solution		
Attempt 1	104.611	[g]
Attempt 2	104.6108	[g]
Attempt 3	104.6108	[g]

Figure A.17. The experimental data for gravimetric density determination at 20 °C for the unloaded stock mixtures.

0 wt-% H2O/25 wt-% AMP/75 wt-% DMSO α = 0		
Temperature = 50 °C		
Volume solution = 50 cm^3		
Weight cap		
Attempt 1	2.0554	[g]
Attempt 2	2.0554	[g]
Attempt 3	2.0555	[g]
Weight measuring flask		
Attempt 1	33.3914	[g]
Attempt 2	33.3944	[g]
Attempt 3	33.3967	[g]
Weight measuring flask+cap+solution		
Attempt 1	86.4645	[g]
Attempt 2	86.4643	[g]
Attempt 3	86.4643	[g]

5 wt-% H2O/24 wt-% AMP/71 wt-% DMSO α = 0		
Temperature = 50 °C		
Volume solution = 50 cm^3		
Weight cap		
Attempt 1	4.7272	[g]
Attempt 2	4.7268	[g]
Attempt 3	4.7269	[g]
Weight measuring flask		
Attempt 1	43.3552	[g]
Attempt 2	43.3555	[g]
Attempt 3	43.3553	[g]
Weight measuring flask+cap+solution		
Attempt 1	99.3499	[g]
Attempt 2	99.3503	[g]
Attempt 3	99.3503	[g]

10 wt-% H2O/22.5 wt-% AMP/67.5 wt-% DMSO α = 0		
Temperature = 50 °C		
Volume solution = 50 cm^3		
Weight cap		
Attempt 1	4.7881	[g]
Attempt 2	4.7883	[g]
Attempt 3	4.7885	[g]
Weight measuring flask		
Attempt 1	45.2219	[g]
Attempt 2	45.2234	[g]
Attempt 3	45.2168	[g]
Weight measuring flask+cap+solution		
Attempt 1	101.504	[g]
Attempt 2	101.5038	[g]
Attempt 3	101.5037	[g]

0 wt-% H2O/50 wt-% AMP/50 wt-% DMSO α = 0		
Temperature = 50 °C		
Volume solution = 50 cm^3		
Weight cap		
Attempt 1	4.7109	[g]
Attempt 2	4.7109	[g]
Attempt 3	4.7109	[g]
Weight measuring flask		
Attempt 1	39.614	[g]
Attempt 2	39.614	[g]
Attempt 3	39.614	[g]
Weight measuring flask+cap+solution		
Attempt 1	93.0435	[g]
Attempt 2	93.0438	[g]
Attempt 3	93.0435	[g]

5 wt-% H2O/47.5 wt-% AMP/47.5 wt-% DMSO α = 0		
Temperature = 50 °C		
Volume solution = 50 cm^3		
Weight cap		
Attempt 1	3.6447	[g]
Attempt 2	3.6447	[g]
Attempt 3	3.6448	[g]
Weight measuring flask		
Attempt 1	45.0759	[g]
Attempt 2	45.0752	[g]
Attempt 3	45.0753	[g]
Weight measuring flask+cap+solution		
Attempt 1	97.8607	[g]
Attempt 2	97.8612	[g]
Attempt 3	97.8613	[g]

10 wt-% H2O/45 wt-% AMP/45 wt-% DMSO α = 0		
Temperature = 50 °C		
Volume solution = 50 cm^3		
Weight cap		
Attempt 1	9.9042	[g]
Attempt 2	9.9042	[g]
Attempt 3	9.9041	[g]
Weight measuring flask		
Attempt 1	43.8067	[g]
Attempt 2	43.8078	[g]
Attempt 3	43.8078	[g]
Weight measuring flask+cap+solution		
Attempt 1	103.3279	[g]
Attempt 2	103.3282	[g]
Attempt 3	103.3283	[g]

Figure A.18. Experimental data for gravimetric density determination at 50 °C for the unloaded stock mixtures.

0 wt-% H2O/25 wt-% AMP/75 wt-% DMSO α = 0.20		
Temperature = 20.4 °C		
Volume solution = 50 cm^3		
Weight cap		
Attempt 1	2.0573	[g]
Attempt 2	2.0575	[g]
Attempt 3	2.0574	[g]
Weight measuring flask		
Attempt 1	35.7604	[g]
Attempt 2	35.7602	[g]
Attempt 3	35.7603	[g]
Weight measuring flask+cap+solution		
Attempt 1	91.4983	[g]
Attempt 2	91.4982	[g]
Attempt 3	91.4981	[g]

0 wt-% H2O/25 wt-% AMP/75 wt-% DMSO α = 0.22		
Temperature = 20.6 °C		
Volume solution = 50 cm^3		
Weight cap		
Attempt 1	2.0574	[g]
Attempt 2	2.0575	[g]
Attempt 3	2.0575	[g]
Weight measuring flask		
Attempt 1	36.6618	[g]
Attempt 2	36.6616	[g]
Attempt 3	36.6616	[g]
Weight measuring flask+cap+solution		
Attempt 1	92.2775	[g]
Attempt 2	92.2768	[g]
Attempt 3	92.7563	[g]

5 wt-% H2O/24 wt-% AMP/71 wt-% DMSO α = 0.20		
Temperature = 20.4 °C		
Volume solution = 50 cm^3		
Weight cap		
Attempt 1	1.9743	[g]
Attempt 2	1.9744	[g]
Attempt 3	1.9744	[g]
Weight measuring flask		
Attempt 1	45.0084	[g]
Attempt 2	45.008	[g]
Attempt 3	45.0077	[g]
Weight measuring flask+cap+solution		
Attempt 1	100.7138	[g]
Attempt 2	100.713	[g]
Attempt 3	100.7131	[g]

10 wt-% H2O/22.5 wt-% AMP/67.5 wt-% DMSO α = 0.20		
Temperature = 20.7 °C		
Volume solution = 50 cm^3		
Weight cap		
Attempt 1	2.0669	[g]
Attempt 2	2.0668	[g]
Attempt 3	2.0667	[g]
Weight measuring flask		
Attempt 1	36.6098	[g]
Attempt 2	36.6099	[g]
Attempt 3	36.6099	[g]
Weight measuring flask+cap+solution		
Attempt 1	92.7486	[g]
Attempt 2	92.7482	[g]
Attempt 3	92.7487	[g]

0 wt-% H2O/50 wt-% AMP/50 wt-% DMSO α = 0.20		
Temperature = 20 .6°C		
Volume solution = 50 cm^3		
Weight cap		
Attempt 1	2.0682	[g]
Attempt 2	2.0683	[g]
Attempt 3	2.0683	[g]
Weight measuring flask		
Attempt 1	44.1418	[g]
Attempt 2	44.1413	[g]
Attempt 3	44.1408	[g]
Weight measuring flask+cap+solution		
Attempt 1	99.1827	[g]
Attempt 2	99.1826	[g]
Attempt 3	99.1828	[g]

5 wt-% H2O/47.5 wt-% AMP/47.5 wt-% DMSO α = 0.20		
Temperature = 20.3 °C		
Volume solution = 50 cm^3		
Weight cap		
Attempt 1	2.0069	[g]
Attempt 2	2.0069	[g]
Attempt 3	2.007	[g]
Weight measuring flask		
Attempt 1	33.0029	[g]
Attempt 2	33.003	[g]
Attempt 3	33.0032	[g]
Weight measuring flask+cap+solution		
Attempt 1	88.0888	[g]
Attempt 2	88.0885	[g]
Attempt 3	88.0885	[g]

10 wt-% H2O/45 wt-% AMP/45 wt-% DMSO α = 0.20		
Temperature = 19.9 °C		
Volume solution = 25 cm^3		
Weight cap		
Attempt 1	2.0778	[g]
Attempt 2	2.0779	[g]
Attempt 3	2.0778	[g]
Weight measuring flask		
Attempt 1	22.9898	[g]
Attempt 2	22.9894	[g]
Attempt 3	22.9898	[g]
Weight measuring flask+cap+solution		
Attempt 1	52.0232	[g]
Attempt 2	52.0234	[g]
Attempt 3	52.0198	[g]

Figure A.19. Experimental data for gravimetric density determination at around 20 °C for the stock mixtures with a CO_2-loading of around 0.20.

0 wt-% H2O/25 wt-% AMP/75 wt-% DMSO α = 0.38		
Temperature = 20.4 °C		
Volume solution = 50 cm^3		
Weight cap		
Attempt 1	2.0667	[g]
Attempt 2	2.0668	[g]
Attempt 3	2.0666	[g]
Weight measuring flask		
Attempt 1	39.5173	[g]
Attempt 2	39.5173	[g]
Attempt 3	39.5169	[g]
Weight measuring flask+cap+solution		
Attempt 1	96.8038	[g]
Attempt 2	96.804	[g]
Attempt 3	96.804	[g]

5 wt-% H2O/24 wt-% AMP/71 wt-% DMSO α = 0.38		
Temperature = 20.9 °C		
Volume solution = 50 cm^3		
Weight cap		
Attempt 1	2.0608	[g]
Attempt 2	2.0607	[g]
Attempt 3	2.0606	[g]
Weight measuring flask		
Attempt 1	36.7466	[g]
Attempt 2	36.7465	[g]
Attempt 3	36.7466	[g]
Weight measuring flask+cap+solution		
Attempt 1	94.167	[g]
Attempt 2	94.1671	[g]
Attempt 3	94.1671	[g]

10 wt-% H2O/22.5 wt-% AMP/67.5 wt-% DMSO α = 0.38		
Temperature = 21.6 °C		
Volume solution = 50 cm^3		
Weight cap		
Attempt 1	2.0729	[g]
Attempt 2	2.0728	[g]
Attempt 3	2.0729	[g]
Weight measuring flask		
Attempt 1	37.44	[g]
Attempt 2	37.4398	[g]
Attempt 3	37.4396	[g]
Weight measuring flask+cap+solution		
Attempt 1	94.919	[g]
Attempt 2	94.9187	[g]
Attempt 3	94.9186	[g]

0 wt-% H2O/50 wt-% AMP/50 wt-% DMSO α = 0.38		
Temperature = 21.1 °C		
Volume solution = 50 cm^3		
Weight cap		
Attempt 1	2.0325	[g]
Attempt 2	2.0323	[g]
Attempt 3	2.0322	[g]
Weight measuring flask		
Attempt 1	33.265	[g]
Attempt 2	33.2651	[g]
Attempt 3	33.2651	[g]
Weight measuring flask+cap+solution		
Attempt 1	91.069	[g]
Attempt 2	91.0692	[g]
Attempt 3	91.0688	[g]

0 wt-% H2O/25 wt-% AMP/75 wt-% DMSO α = 0.50		
Temperature = 20.3 °C		
Volume solution = 50 cm^3		
Weight cap		
Attempt 1	2.0574	[g]
Attempt 2	2.0574	[g]
Attempt 3	2.0573	[g]
Weight measuring flask		
Attempt 1	36.6085	[g]
Attempt 2	36.6084	[g]
Attempt 3	36.6084	[g]
Weight measuring flask+cap+solution		
Attempt 1	94.5478	[g]
Attempt 2	94.5479	[g]
Attempt 3	94.5481	[g]

5 wt-% H2O/24 wt-% AMP/71 wt-% DMSO α = 0.50		
Temperature = 20.6 °C		
Volume solution = 50 cm^3		
Weight cap		
Attempt 1	2.0666	[g]
Attempt 2	2.0667	[g]
Attempt 3	2.0665	[g]
Weight measuring flask		
Attempt 1	36.6609	[g]
Attempt 2	36.6608	[g]
Attempt 3	36.6608	[g]
Weight measuring flask+cap+solution		
Attempt 1	94.7385	[g]
Attempt 2	94.7379	[g]
Attempt 3	94.7374	[g]

10 wt-% H2O/22.5 wt-% AMP/67.5 wt-% DMSO α = 0.50		
Temperature = 21.0 °C		
Volume solution = 50 cm^3		
Weight cap		
Attempt 1	2.0674	[g]
Attempt 2	2.0675	[g]
Attempt 3	2.0673	[g]
Weight measuring flask		
Attempt 1	33.4145	[g]
Attempt 2	33.4142	[g]
Attempt 3	33.4139	[g]
Weight measuring flask+cap+solution		
Attempt 1	91.8547	[g]
Attempt 2	91.8548	[g]
Attempt 3	91.8547	[g]

Figure A.20. Experimental data for gravimetric density determination at around 20 °C for the stock mixtures with a CO_2-loading of 0.38 and 0.50.

Appendix F: Viscosity Measurements

Ostwald viscometer

In Figure A.21, all the experimental data from the Ostwald viscometer experiments are reported. The temperatures stated were registered for the surrounding water close to the respective bulbs prior to the start of the first attempt for each mixture.

Solution	**Water**
Temperature Reservoir Bulb	19.9 [C]
Temperature Measurement Bulb	19.9 [C]
Attempt	Total time [s]
1	80.63
2	80.59
3	80.45
4	80.67
5	80.55

Solution	**0H25A75D**
Temperature Reservoir Bulb	20.0 [C]
Temperature Measurement Bulb	20.0 [C]
Attempt	Total time [s]
1	270.32
2	269.65
3	269.3
4	268.59
5	268.57

Solution	**0H50A50D**
Temperature Reservoir Bulb	20.0 [C]
Temperature Measurement Bulb	20.0 [C]
Attempt	Total time [s]
1	634.96
2	633.42
3	633.55
4	633.57
5	634.5

Solution	**1-pentanol**
Temperature Reservoir Bulb	20.0 [C]
Temperature Measurement Bulb	20.0 [C]
Attempt	Total time [s]
1	388.89
2	389.1
3	388.6
4	387.7
5	387.01

Solution	**5H24A71D**
Temperature Reservoir Bulb	20.0 [C]
Temperature Measurement Bulb	20.0 [C]
Attempt	Total time [s]
1	332.55
2	333.08
3	332.25
4	332.24
5	331.29

Solution	**5H47.5A47.5D**
Temperature Reservoir Bulb	20.0 [C]
Temperature Measurement Bulb	20.0 [C]
Attempt	Total time [s]
1	848.97
2	847.1
3	843.39
4	845.6
5	843.81

Solution	**DMSO**
Temperature Reservoir Bulb	20.0 [C]
Temperature Measurement Bulb	20.0 [C]
Attempt	Total time [s]
1	155.69
2	157.42
3	157.77
4	158.74
5	157.74

Solution	**10H22.5A67.5D**
Temperature Reservoir Bulb	20.0 [C]
Temperature Measurement Bulb	20.0 [C]
Attempt	Total time [s]
1	402.06
2	402.95
3	403.32
4	403.51
5	404.46

Solution	**10H45A45D**
Temperature Reservoir Bulb	20.0 [C]
Temperature Measurement Bulb	20.0 [C]
Attempt	Total time [s]
1	1002.5
2	1004.25
3	1006.52
4	1008.13
5	1007.33

Figure A.21. The total time required for each unloaded stock mixture, for each attempt, to pass between the two test lines on the Ostwald viscometer.

Anton Paar MCR 302e Rheometer Results

Figure A.22 and Figure A.23 showcase the experimental data from the Anton Paar MCR 302e Rheometer for the remaining tested mixtures at temperatures around 20 °C. In Figure A.22, the experimental results for the tested reference mixture, DMSO, is presented along with the experimental results for the unloaded 5H24A71D and 10H22.5A67.5D mixtures. Figure A.23 showcases the dynamic viscosities registered for the unloaded mixtures with a weight ratio between DMSO and AMP of one.

Figure A.24 and Figure A.25 showcases the experimental results for the remaining tested mixtures at temperatures around 50 °C. In Figure A.24, it should be noted that at 50 °C, the tested reference mixture was deionized water, not DMSO. All the experimental data points obtained from the rheometer are also showed in Figure A.26 and Figure A.27.

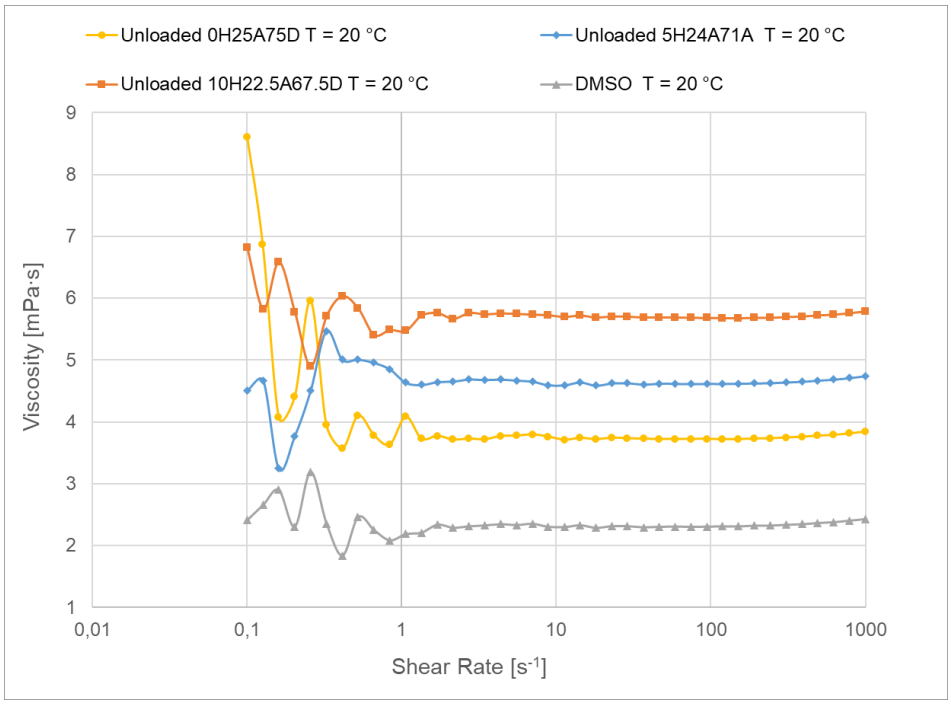

Figure A.22. The graph shows the viscosity results of four unloaded stock mixtures around 20 °C. The mixtures are pure DMSO, the 0H25A75D mixture, 5H24A71D mixture, and the 10H22.5A67.5D mixture.

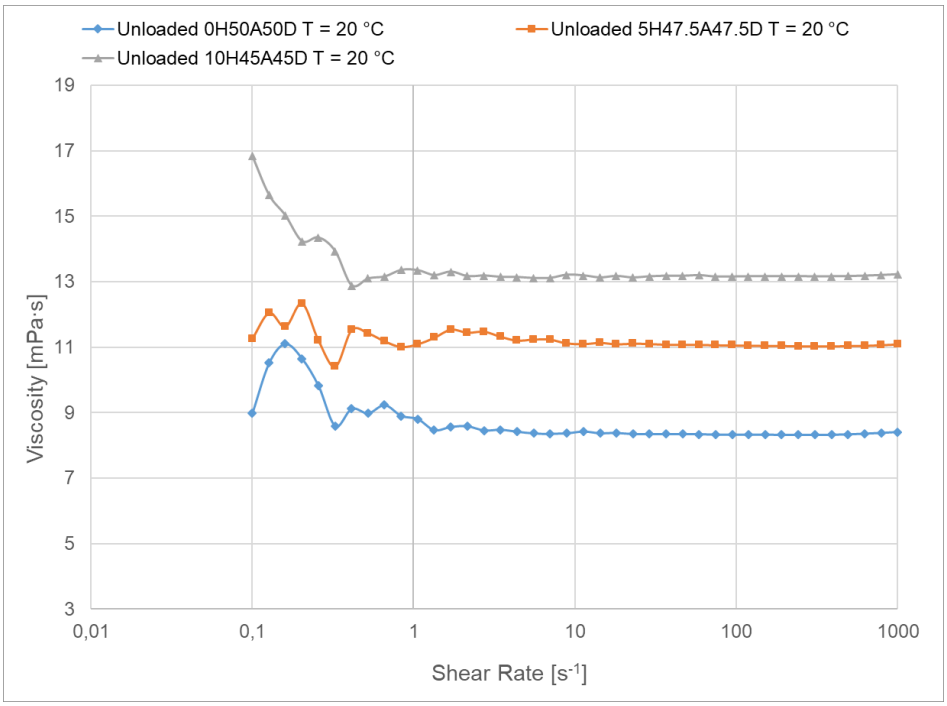

Figure A.23. The graph shows the viscosity results of three sample mixtures around 20 °C. The mixtures are unloaded 0H50A50D, unloaded 5H47.5A47.5D, and unloaded 10H45A45D.

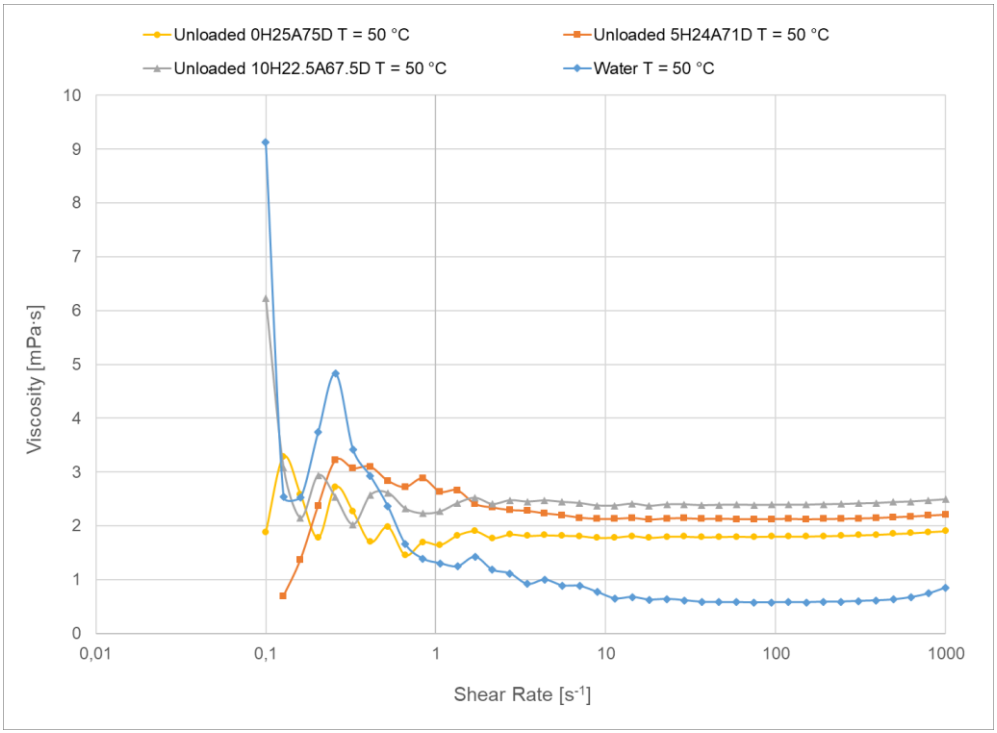

Figure A.24. The graph shows the viscosity results of four sample mixtures around 50 °C. The mixtures are deionized water, unloaded 0H25A75D, unloaded 5H24A71D, and unloaded 10H22.5A67.5D.

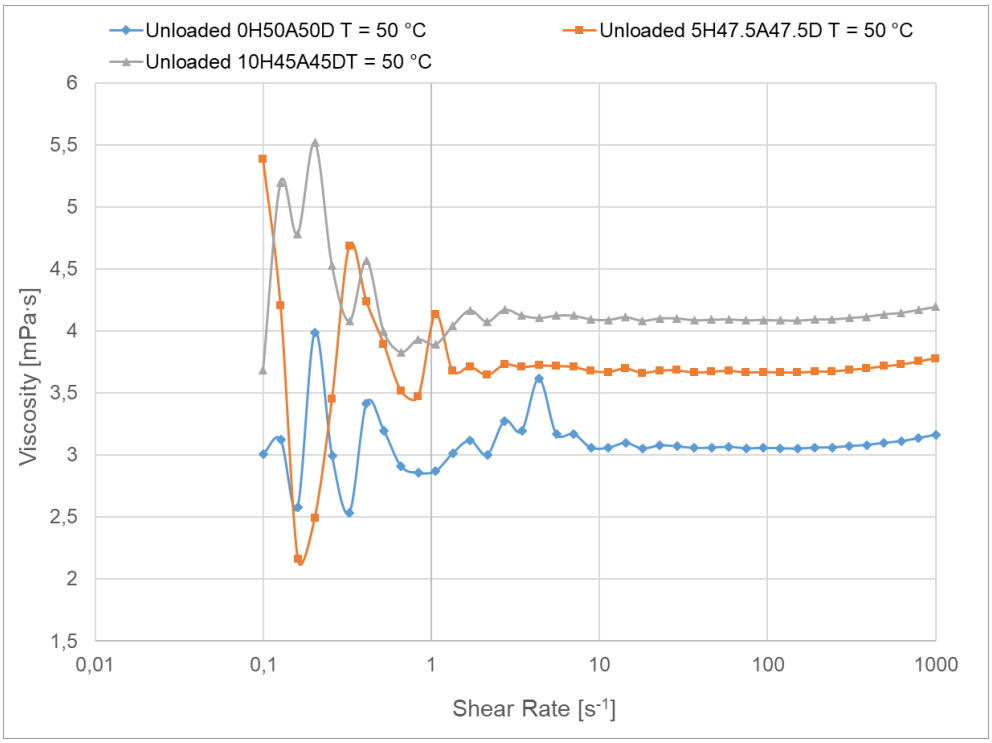

Figure A.25. The graph shows the viscosity results of three sample mixtures around 50 °C. The mixtures are unloaded 0H50A50D, unloaded 5H47.5A47.5D, and unloaded 10H45A45D.

	Solution: DMSO		Solution: 0H25A75D		Solution: 5H24A71D		Solution: 10H22.5A67.5D		Solution: 0H50A50D		Solution: 5H47.5A47.5D		Solution: 10H45A45D	
Point No.	Viscosity [mPa·s]	Temperature [°C]	Viscosity [mPa·s]	Temperature [°C]	Viscosity [mPa·s]	Temperature [°C]	Viscosity [mPa·s]	Temperature [°C]	Viscosity [mPa·s]	Temperature [°C]	Viscosity [mPa·s]	Temperature [°C]	Viscosity [mPa·s]	Temperature [°C]
1	2.4121	19.96	8.6086	19.97	4.5067	19.95	6.813	19.98	8.9757	19.97	11.27	19.95	16.835	19.98
2	2.6628	19.96	6.8637	19.97	4.6663	19.95	5.8259	19.98	10.513	19.98	12.053	19.95	15.642	19.98
3	2.9001	19.96	4.0692	19.97	3.2445	19.94	6.5828	19.99	11.098	19.98	11.628	19.95	15.023	19.98
4	2.3071	19.96	4.4082	19.97	3.7702	19.94	5.7779	19.99	10.651	19.98	12.342	19.96	14.231	19.98
5	3.1947	19.96	5.9563	19.97	5.5038	19.94	4.9032	19.99	9.8159	19.98	11.205	19.96	14.346	19.98
6	2.3573	19.96	3.9469	19.97	5.4707	19.94	5.7118	19.99	8.5905	19.98	10.414	19.96	13.925	19.98
7	1.8392	19.96	3.5673	19.97	5.0069	19.94	6.0297	20,00	9.1167	19.99	11.532	19.96	12.881	19.98
8	2.4635	19.96	4.1006	19.97	5.0103	19.94	5.8363	20,00	8.9813	19.99	11.431	19.97	13.094	19.98
9	2.2528	19.96	3.7826	19.97	4.9561	19.94	5.4078	20,00	9.2295	19.99	11.186	19.97	13.153	19.98
10	2.0854	19.95	3.6335	19.97	4.8529	19.94	5.4872	20.01	8.9	20.00	11.014	19.97	13.354	19.98
11	2.186	19.95	4.0823	19.97	4.636	19.94	5.4729	20.01	8.8029	20.00	11.1	19.98	13.345	19.98
12	2.2086	19.95	3.727	19.97	4.5988	19.94	5.7179	20.01	8.4651	20,00	11.295	19.98	13.195	19.98
13	2.3386	19.95	3.7713	19.97	4.6456	19.94	5.7597	20.02	8.5644	20.01	11.544	19.98	13.302	19.98
14	2.2894	19.95	3.7118	19.98	4.6548	19.94	5.6665	20.02	8.5833	20.01	11.45	19.99	13.164	19.98
15	2.3133	19.95	3.7275	19.98	4.6888	19.94	5.7612	20.02	8.4566	20.01	11.481	19.99	13.181	19.98
16	2.3267	19.95	3.7175	19.97	4.6798	19.95	5.7398	20.03	8.4783	20.02	11.327	19.99	13.14	19.98
17	2.3463	19.95	3.7693	19.97	4.687	19.95	5.7538	20.03	8.4177	20.02	11.209	20,00	13.137	19.98
18	2.3333	19.95	3.7751	19.97	4.6708	19.95	5.7457	20.04	8.3654	20.02	11.244	20,00	13.106	19.98
19	2.3531	19.95	3.7951	19.97	4.6525	19.95	5.7348	20.04	8.3503	20.03	11.237	20.01	13.11	19.98
20	2.3037	19.95	3.7593	19.97	4.5956	19.95	5.7255	20.04	8.3692	20.03	11.123	20.01	13.207	19.98
21	2.3003	19.95	3.7101	19.97	4.594	19.95	5.6975	20.05	8.4228	20.03	11.102	20.01	13.185	19.98
22	2.3302	19.95	3.739	19.97	4.6409	19.95	5.7204	20.05	8.3696	20.04	11.141	20.02	13.123	19.98
23	2.2875	19.95	3.7188	19.97	4.5883	19.96	5.6893	20.05	8.3806	20.04	11.096	20.02	13.168	19.98
24	2.3145	19.95	3.7412	19.97	4.6247	19.96	5.7045	20.05	8.346	20.04	11.115	20.03	13.122	19.98
25	2.3147	19.95	3.7331	19.97	4.6276	19.96	5.702	20.05	8.3466	20.04	11.105	20.03	13.158	19.98
26	2.2962	19.95	3.7248	19.97	4.6065	19.96	5.6882	20.06	8.3463	20.04	11.082	20.03	13.176	19.98
27	2.3043	19.95	3.7199	19.97	4.6204	19.96	5.6894	20.06	8.3478	20.04	11.082	20.03	13.171	19.98
28	2.3086	19.96	3.72	19.98	4.6191	19.97	5.6895	20.06	8.3399	20.05	11.077	20.03	13.193	19.98
29	2.3037	19.96	3.7222	19.98	4.6131	19.97	5.6823	20.06	8.3298	20.05	11.067	20.03	13.148	19.98
30	2.3069	19.96	3.724	19.98	4.6177	19.97	5.6809	20.05	8.324	20.04	11.061	20.03	13.151	19.99
31	2.312	19.96	3.7166	19.98	4.6168	19.98	5.6796	20.05	8.3298	20.04	11.054	20.03	13.158	19.99
32	2.3107	19.97	3.7189	19.98	4.6206	19.98	5.6751	20.05	8.3269	20.04	11.045	20.03	13.159	19.99
33	2.3233	19.97	3.7279	19.98	4.625	19.98	5.684	20.05	8.3202	20.04	11.046	20.03	13.159	19.99
34	2.3247	19.97	3.7322	19.98	4.6283	19.98	5.6839	20.05	8.3213	20.04	11.036	20.03	13.16	19.99
35	2.3365	19.98	3.7462	19.98	4.6412	19.99	5.6954	20.04	8.318	20.04	11.035	20.03	13.157	19.99
36	2.3463	19.98	3.7568	19.99	4.6511	19.99	5.7045	20.04	8.3259	20.03	11.033	20.02	13.159	19.99
37	2.366	19.98	3.7736	19.99	4.6702	19.99	5.7224	20.03	8.3359	20.03	11.041	20.02	13.163	19.99
38	2.3796	19.98	3.7875	19.99	4.6856	19.99	5.734	20.03	8.3581	20.03	11.049	20.02	13.178	19.99
39	2.4039	19.99	3.8112	19.99	4.7105	19.99	5.7585	20.03	8.3811	20.03	11.069	20.02	13.196	19.99
40	2.4296	19.99	3.8413	19.99	4.7422	19.99	5.7857	20.03	8.4103	20.02	11.092	20.02	13.222	20,00

Figure A.26. All experimental data of the registered dynamic viscosity and the temperature for all experiments carried out around 20 °C with the Anton Paar MCR 302e.

	Solution: Water		Solution: 0H25A75D		Solution: 5H24A71D		Solution: 10H22.5A67.5D		Solution: 0H50A50D		Solution: 5H47.5A47.5D		Solution: 10H45A45D	
Point No.	Viscosity	Temperature	Viscosity	Temperature	Viscosity	Temperature	Viscosity	Temperature	Viscosity	Temperature	Viscosity	Temperature	Viscosity	Temperature
1	9.1259	49.73	1.8865	50.09	-5.6794	50.16	6.2288	50.13	3.0044	50.09	5.3817	50.17	3.6842	50.18
2	2.5449	49.72	3.2818	50.09	0.69028	50.17	3.0885	50.14	3.1236	50.09	4.2049	50.17	5.1988	50.18
3	2.5219	49.71	2.5901	50.08	1.3736	50.17	2.1479	50.14	2.5752	50.09	2.1621	50.17	4.7818	50.18
4	3.739	49.70	1.7795	50.08	2.3695	50.17	2.9382	50.14	3.9891	50.08	2.494	50.18	5.5207	50.18
5	4.83	49.68	2.7224	50.08	3.2169	50.17	2.5311	50.14	2.9965	50.08	3.4519	50.18	4.5291	50.18
6	3.4155	49.67	2.2686	50.08	3.0717	50.18	2.0238	50.14	2.5335	50.08	4.687	50.18	4.0784	50.18
7	2.9247	49.66	1.7023	50.08	3.0999	50.18	2.5731	50.15	3.416	50.08	4.2367	50.18	4.5671	50.19
8	2.3619	49.64	1.9847	50.07	2.8406	50.18	2.6132	50.15	3.1977	50.08	3.8937	50.18	3.9931	50.19
9	1.6608	49.62	1.4586	50.07	2.721	50.19	2.3215	50.15	2.9081	50.07	3.5162	50.18	3.8287	50.19
10	1.3908	49.61	1.6955	50.07	2.8826	50.19	2.2299	50.16	2.8554	50.07	3.4705	50.18	3.931	50.19
11	1.3046	49.59	1.6473	50.06	2.6363	50.19	2.266	50.16	2.8685	50.07	4.1338	50.19	3.8896	50.19
12	1.2479	49.57	1.8232	50.06	2.6601	50.19	2.4225	50.16	3.0122	50.07	3.6766	50.19	4.0398	50.19
13	1.4246	49.55	1.9022	50.06	2.409	50.20	2.5201	50.17	3.1163	50.07	3.7105	50.19	4.1658	50.20
14	1.1834	49.53	1.7738	50.06	2.3404	50.20	2.4053	50.17	3.001	50.07	3.6439	50.19	4.074	50.19
15	1.1144	49.52	1.8408	50.06	2.2943	50.20	2.4744	50.17	3.2757	50.07	3.7276	50.19	4.1715	50.20
16	0.91901	49.50	1.8151	50.06	2.2778	50.20	2.4498	50.17	3.1926	50.06	3.7076	50.19	4.124	50.20
17	0.9989	49.49	1.8279	50.05	2.2321	50.20	2.4717	50.18	3.6147	50.06	3.7205	50.20	4.1043	50.19
18	0.89277	49.47	1.8189	50.05	2.1986	50.21	2.4445	50.18	3.1667	50.06	3.7156	50.20	4.124	50.19
19	0.88235	49.46	1.8116	50.05	2.1518	50.20	2.4228	50.18	3.1699	50.06	3.7088	50.19	4.1233	50.19
20	0.7718	49.45	1.7797	50.05	2.129	50.20	2.3767	50.18	3.0583	50.06	3.6758	50.19	4.0935	50.19
21	0.65179	49.45	1.7849	50.05	2.1287	50.19	2.3763	50.18	3.0576	50.06	3.6682	50.19	4.089	50.18
22	0.67721	49.45	1.8117	50.05	2.1452	50.19	2.4121	50.17	3.0969	50.06	3.6964	50.19	4.1117	50.17
23	0.62883	49.46	1.7797	50.05	2.1167	50.18	2.3722	50.17	3.0514	50.06	3.661	50.18	4.0825	50.17
24	0.64153	49.46	1.8008	50.05	2.1366	50.18	2.3989	50.16	3.0761	50.05	3.6796	50.17	4.1019	50.16
25	0.61762	49.48	1.8027	50.04	2.1406	50.17	2.3993	50.15	3.0694	50.05	3.6819	50.16	4.1008	50.16
26	0.58647	49.49	1.7898	50.04	2.1276	50.13	2.3825	50.14	3.0555	50.05	3.6634	50.16	4.0868	50.15
27	0.58211	49.51	1.7961	50.04	2.1318	50.12	2.3893	50.13	3.0583	50.04	3.6698	50.14	4.0905	50.14
28	0.58145	49.54	1.8009	50.03	2.1254	50.11	2.3931	50.12	3.0647	50.04	3.6776	50.12	4.093	50.14
29	0.57568	49.57	1.797	50.03	2.124	50.10	2.3881	50.11	3.0534	50.04	3.6644	50.12	4.0872	50.13
30	0.57947	49.61	1.8035	50.03	2.1243	50.09	2.3903	50.10	3.0558	50.04	3.6659	50.11	4.0883	50.11
31	0.58057	49.65	1.8031	50.03	2.1297	50.09	2.3915	50.08	3.0536	50.03	3.6654	50.10	4.0862	50.09
32	0.57987	49.70	1.8025	50.02	2.1209	50.08	2.3906	50.06	3.05	50.03	3.6625	50.09	4.0838	50.07
33	0.58975	49.75	1.8133	50.02	2.1269	50.07	2.4022	50.04	3.0592	50.00	3.6717	50.08	4.0924	50.06
34	0.5911	49.79	1.8154	50.02	2.129	50.06	2.4038	50.03	3.0603	50.00	3.6725	50.06	4.0934	50.05
35	0.60341	49.84	1.8267	50.02	2.1353	50.05	2.4152	50.02	3.0714	50.01	3.6856	50.06	4.1052	50.04
36	0.61308	49.89	1.8349	50.01	2.1438	50.04	2.4233	50.02	3.0803	50.02	3.6966	50.05	4.1151	50.03
37	0.63172	49.92	1.8514	50.01	2.1592	50.03	2.4402	50.02	3.0972	50.02	3.7143	50.04	4.1346	50.02
38	0.67435	49.91	1.8642	50.01	2.1723	50.03	2.4516	50.03	3.1106	50.01	3.7279	50.04	4.1463	50.02
39	0.74297	49.91	1.8849	50.01	2.1903	50.03	2.4718	50.03	3.1353	50.01	3.753	50.03	4.1699	50.02
40	0.85355	49.91	1.9043	50.01	2.2069	50.03	2.4926	50.02	3.1632	50.01	3.7786	50.03	4.1949	50.02

Figure A.27. All experimental data of the registered dynamic viscosity and the temperature for all experiments carried out around 50 °C with the Anton Paar MCR 302e.

NDJ-8S Digital Rotary Viscometer Results

Figure A.28 showcases all the experimental data obtained from the experiments done with reference liquids and unloaded stock mixtures. In Figure A.29 and Figure A.30, the experimental data for measurements done on CO_2-loaded stock mixtures are presented.

Temperature = 20.0 °C	Rotor 0	6	12	30	60	RPM
0 wt-% H2O/25 wt-% AMP/75 wt-% DMSO α = 0						
Attempt 1. Dynamic viscosity (mPa*s)		3.8	3.5	3.18	2.97	
Attempt 2. Dynamic viscosity (mPa*s)		3.8	3.4	3.16	2.99	
Temperature = 20.0 °C	Rotor 0	6	12	30	60	RPM
5 wt-% H2O/24 wt-% AMP/71 wt-% DMSO α = 0						
Attempt 1. Dynamic viscosity (mPa*s)		4.6	4.4	4	3.78	
Attempt 2. Dynamic viscosity (mPa*s)		4.6	4.35	4	3.8	
Temperature = 20.0 °C	Rotor 0	6	12	30	60	RPM
10 wt-% H2O/22.5 wt-% AMP/67.5 wt-% DMSO α = 0						
Attempt 1. Dynamic viscosity (mPa*s)		5.3	5.05	4.74	4.55	
Attempt 2. Dynamic viscosity (mPa*s)		5.5	5.05	4.76	4.59	
Attempt 3. Dynamic viscosity (mPa*s)		5.4	5	4.76	4.6	
Temperature = 20.1 °C	Rotor 0	6	12	30	60	RPM
0 wt-% H2O/50 wt-% AMP/50 wt-% DMSO α = 0						
Attempt 1. Dynamic viscosity (mPa*s)		8.3	7.65	7.08	6.9	
Attempt 2. Dynamic viscosity (mPa*s)		8.2	7.55	7.08	6.91	
Attempt 3. Dynamic viscosity (mPa*s)		8.2	7.5	7.1	6.92	
Temperature = 20.1 °C	Rotor 0	6	12	30	60	RPM
5 wt-% H2O/47.5 wt-% AMP/47.5 wt-% DMSO α = 0						
Attempt 1. Dynamic viscosity (mPa*s)		10.6	9.85	9.23	9.21	
Attempt 2. Dynamic viscosity (mPa*s)		10.5	9.85	9.23	9.23	
Attempt 3. Dynamic viscosity (mPa*s)		10.6	9.85	9.26	9.25	
Temperature = 20.1 °C	Rotor 0	6	12	30	60	RPM
10 wt-% H2O/45 wt-% AMP/45 wt-% DMSO α = 0						
Attempt 1. Dynamic viscosity (mPa*s)		12.2	11.15	10.98	OVER	
Attempt 2. Dynamic viscosity (mPa*s)		11.7	11.2	11	OVER	
Attempt 3. Dynamic viscosity (mPa*s)		12.1	11.15	11	OVER	
Temperature = 20.0 °C	Rotor 0	6	12	30	60	RPM
DMSO						
Attempt 1. Dynamic viscosity (mPa*s)		2.6	2.2	2.24	2.01	
Attempt 2. Dynamic viscosity (mPa*s)		2.6	2.2	2.24	2.01	
Attempt 3. Dynamic viscosity (mPa*s)		2.4	2.25	2.26	2.02	
Temperature = 20.0 °C	Rotor 0	6	12	30	60	RPM
1-pentanol						
Attempt 1. Dynamic viscosity (mPa*s)		5	4.1	3.74	3.42	
Attempt 2. Dynamic viscosity (mPa*s)		5.1	4.15	3.8	3.44	
Attempt 3. Dynamic viscosity (mPa*s)		5.1	4.1	3.8	3.45	
Temperature = 20.0 °C	Rotor 0	6	12	30	60	RPM
Deionized Water						
Attempt 1. Dynamic viscosity (mPa*s)		1.9	1.15	1.16	0.99	
Attempt 2. Dynamic viscosity (mPa*s)		1.9	1.35	1.08	1.01	
Attempt 3. Dynamic viscosity (mPa*s)		1.4	1.3	1.13	1.05	

Figure A.28. All the experimental data for the viscosity experiments carried out with the NDJ-8S Digital Rotary Viscometer on unloaded amine mixtures and reference liquids.

Temperature = 20.3 °C	Rotor 0	6	12	30	60	RPM
0 wt-% H2O/25 wt-% AMP/75 wt-% DMSO α = 0.20						
Attempt 1. Dynamic viscosity (mPa*s)		5.2	4.2	3.88	3.68	
Attempt 2. Dynamic viscosity (mPa*s)		4.6	4.15	3.86	3.65	
Attempt 3. Dynamic viscosity (mPa*s)		4.6	4.15	3.9	3.63	
Temperature = 20.3 °C	Rotor 0	6	12	30	60	RPM
0 wt-% H2O/25 wt-% AMP/75 wt-% DMSO α = 0.22						
Attempt 1. Dynamic viscosity (mPa*s)		3.9	3.25	3.16	2.97	
Attempt 2. Dynamic viscosity (mPa*s)		3.9	3.35	3.16	2.92	
Attempt 3. Dynamic viscosity (mPa*s)		4	3.35	3.14	2.89	
Temperature = 20.6 °C	Rotor 0	6	12	30	60	RPM
5 wt-% H2O/24 wt-% AMP/71 wt-% DMSO α = 0.20						
Attempt 1. Dynamic viscosity (mPa*s)		5.9	4.65	4.26	4.06	
Attempt 2. Dynamic viscosity (mPa*s)		6	4.65	4.28	4.06	
Attempt 3. Dynamic viscosity (mPa*s)		5.7	4.65	4.3	4.05	
Temperature = 20.6 °C	Rotor 0	6	12	30	60	RPM
10 wt-% H2O/22.5 wt-% AMP/67.5 wt-% DMSO α = 0.20						
Attempt 1. Dynamic viscosity (mPa*s)		8.5	7.44	6.34	6.28	
Attempt 2. Dynamic viscosity (mPa*s)		8.6	7.44	6.44	6.22	
Attempt 3. Dynamic viscosity (mPa*s)		8.8	7.55	6.5	6.17	
Temperature = 20.6 °C	Rotor 0	6	12	30	60	RPM
0 wt-% H2O/50 wt-% AMP/50 wt-% DMSO α = 0.20						
Attempt 1. Dynamic viscosity (mPa*s)		37.4	31.05	OVER	OVER	
Attempt 2. Dynamic viscosity (mPa*s)		40.2	32	OVER	OVER	
Attempt 3. Dynamic viscosity (mPa*s)		41.5	32.6	OVER	OVER	
Temperature = 20.0 °C	Rotor 0	6	12	30	60	RPM
5 wt-% H2O/47.5 wt-% AMP/47.5 wt-% DMSO α = 0.20						
Attempt 1. Dynamic viscosity (mPa*s)		14.6	14	13.78	OVER	
Attempt 2. Dynamic viscosity (mPa*s)		14.3	13.85	13.78	OVER	
Attempt 3. Dynamic viscosity (mPa*s)		14	13.85	13.72	OVER	
Temperature = 20.6 °C	Rotor 0	6	12	30	60	RPM
10 wt-% H2O/45 wt-% AMP/45 wt-% DMSO α = 0.20						
Attempt 1. Dynamic viscosity (mPa*s)		OVER	OVER	OVER	OVER	
Attempt 2. Dynamic viscosity (mPa*s)		OVER	OVER	OVER	OVER	
Attempt 3. Dynamic viscosity (mPa*s)		OVER	OVER	OVER	OVER	
Temperature = 20.6 °C	Rotor 1	3	6	12	30	RPM
10 wt-% H2O/45 wt-% AMP/45 wt-% DMSO α = 0.20						
Attempt 1. Dynamic viscosity (mPa*s)		460	348	272.5	160	
Attempt 2. Dynamic viscosity (mPa*s)		444	357	273	172.6	
Attempt 3. Dynamic viscosity (mPa*s)		424	344	260	176	

Figure A.29. All the experimental data for the viscosity experiments carried out with the NDJ-8S Digital Rotary Viscometer on amine mixtures with a CO_2-loading of 0.20. Highlighted values were unstable values where the value changed with the time of the experiment

Temperature = 20.4 °C	Rotor 0	6	12	30	60	RPM
0 wt-% H2O/25 wt-% AMP/75 wt-% DMSO α = 0.38						
Attempt 1. Dynamic viscosity (mPa*s)		7.8	4.5	4.92	5.11	
Attempt 2. Dynamic viscosity (mPa*s)		10.7	4.6	4.9	4.99	
Attempt 3. Dynamic viscosity (mPa*s)		13.3	5.3	4.76	4.84	
Temperature = 20.6 °C	Rotor 0	6	12	30	60	RPM
0 wt-% H2O/25 wt-% AMP/75 wt-% DMSO α = 0.50						
Attempt 1. Dynamic viscosity (mPa*s)		27.3	19.4	15.4	OVER	
Attempt 2. Dynamic viscosity (mPa*s)		30	20.95	16.18	OVER	
Attempt 3. Dynamic viscosity (mPa*s)		32.1	22.35	16.8	OVER	
Temperature = 20.6 °C	Rotor 0	6	12	30	60	RPM
5 wt-% H2O/24 wt-% AMP/71 wt-% DMSO α = 0.38						
Attempt 1. Dynamic viscosity (mPa*s)		8.6	8.85	8.64	9	
Attempt 2. Dynamic viscosity (mPa*s)		8.2	8.65	8.6	8.79	
Attempt 3. Dynamic viscosity (mPa*s)		7.9	8.2	8.54	8.68	
Temperature = 20.6 °C	Rotor 0	6	12	30	60	RPM
5 wt-% H2O/24 wt-% AMP/71 wt-% DMSO α = 0.50						
Attempt 1. Dynamic viscosity (mPa*s)		22.7	18.6	17.12	OVER	
Attempt 2. Dynamic viscosity (mPa*s)		24.6	19.5	17.4	OVER	
Attempt 3. Dynamic viscosity (mPa*s)		25.4	20.15	17.72	OVER	
Temperature = 20.4 °C	Rotor 0	6	12	30	60	RPM
10 wt-% H2O/22.5 wt-% AMP/67.5 wt-% DMSO α = 0.38						
Attempt 1. Dynamic viscosity (mPa*s)		66.5	33.75	17.3	9.89	
Attempt 2. Dynamic viscosity (mPa*s)		91.9	42.45	OVER	OVER	
Attempt 3. Dynamic viscosity (mPa*s)		98.1	OVER	OVER	OVER	
Temperature = 20.6 °C	Rotor 0	6	12	30	60	RPM
10 wt-% H2O/22.5 wt-% AMP/67.5 wt-% DMSO α = 0.50						
Attempt 1. Dynamic viscosity (mPa*s)		47.8	24.25	10.44	6.28	
Attempt 2. Dynamic viscosity (mPa*s)		62.2	28.2	13.44	5.93	
Attempt 3. Dynamic viscosity (mPa*s)		62.1	32.25	15.78	6.35	
Temperature = 20.2 °C	Rotor 0	6	12	30	60	RPM
0 wt-% H2O/50 wt-% AMP/50 wt-% DMSO α = 0.38						
Attempt 1. Dynamic viscosity (mPa*s)		OVER	OVER	OVER	OVER	
Attempt 2. Dynamic viscosity (mPa*s)		OVER	OVER	OVER	OVER	
Attempt 3. Dynamic viscosity (mPa*s)		OVER	OVER	OVER	OVER	
Temperature = 20.3 °C	Rotor 1	0.3	0.6	1.5	3	RPM
0 wt-% H2O/50 wt-% AMP/50 wt-% DMSO α = 0.38						
Attempt 1. Dynamic viscosity (mPa*s)		1879	1150	1208	1234	
Attempt 2. Dynamic viscosity (mPa*s)		2460	1220	1084	1154	
Attempt 3. Dynamic viscosity (mPa*s)		2685	1250	1048	1092	

Figure A.30. All the experimental data for the viscosity experiments carried out with the NDJ-8S Digital Rotary Viscometer on amine mixtures with a CO_2-loading of 0.38 or 0.50. Highlighted values were unstable values where the value changed with the time of the experiment

Appendix G: Ethical considerations

During the conduction of the master thesis project, ethical considerations have had to be done related to the project. The ethical considerations have been divided into two primary parts. The first part is related to the different aspects of work done within the project ranging from research and scientific writing to experimental work. The second part encompasses the ethical considerations related to climate change abatement, specifically with CCS technologies such as BE-CCS.

Ethical considerations concerning the conducted work

The experimental work that has been conducted through the master thesis project has warranted ethical considerations prior and during its completion. To work safely according to the relevant risk assessments, good laboratory practice, and local rules has been of importance to not put others or oneself in danger. The utilization of the employed chemicals, and their disposal, is another ethical consideration that has been done. The toxicity to aquatic life of AMP, its possibility of causing irritation upon contact, and the fact that its toxic properties is not fully researched has warranted correct disposal of solutions containing AMP in designated containers. Furthermore, the same factors have restricted the amounts of the utilized AMP, and unnecessary wasting of both AMP and other utilized chemicals.

Regarding the scientific writing of the master thesis project, the aim has been to document the method and the experimental results with integrity and honesty. Furthermore, the scientific writing has aimed to spread and contextualize the incorporated information from other sources in accordance with the chosen method of citation and without plagiarizing.

The research has been done with the intention of furthering life of humankind and has been conducted without a conflict of interest or hidden agenda.

Ethical considerations concerning the researched technology

It is easy to misinterpret the problem of climate change and the abatement of it as purely technical or scientific problems that are yet to be solved. But, climate change is a multifaceted problem that also extends into the political, juridical, and economic spheres. Lastly, due to the enormous consequences of climate change that already causes the death of 150,000 persons annually, climate change and mitigation strategies raise several ethical questions for the world population, especially those living in the Global North [57].

The first and overarching question concerning climate change is whether there is a responsibility to mitigate climate change. Principles such as justice and well-being are just a few aspects that have been accounted for in the ethical considerations done regarding climate change. The ethical consensus is that there is a moral responsibility to act against climate change, primarily since it is, and will be, the root cause of suffering for other people [58]. The different response strategies either fall into the broad categories of adaption or mitigation. Adaption would entail that the policies would be enacted to limit the dangerous consequences of climate change from causing harm, but not the cause of the problem. Mitigation strategies instead address the greenhouse gas emissions, the largest anthropogenic contribution to climate change. The spatial and temporal complexity of climate change, whereby the people that are hurt either do not yet exist or live on another side of the world, has proven that a moral responsibility factor is a poor motivator for change [59]. These complex dimensions also

complicate the applicability and suitability of only implementing adaption strategies and warrant that mitigation strategies will also be needed to a large extent [58]. However, the alarming rate of climate change causes a large ethical responsibility related to the choices of achieving mitigation. The causes for ethical reflection for carbon capture and storage (CCS) technologies will be presented below, along with ethical considerations from the literature and the author.

The class of technologies that the studied novel alkanolamine absorption system is a part of, CCS technologies, is a mitigation strategy, although different from many other technologies. CCS addresses the emissions of CO_2 to the atmosphere, not its production as other energy generation technologies. Renewable energy sources, such as wind power, produce electrical energy without the energy harvesting technology leading to direct emissions of CO_2. Thereby, CCS requires that the direct emissions of CO_2 related to the energy production is captured and that storage of the captured CO_2 can be maintained [60]. Storage of CO_2 geologically comes with potential local risks, both at the storage site and during transportation. Probable risks such as leakage could lead to suffocation, while potential larger scale problems could be ground water contamination and increased seismic activity around the storage site [58]. These local risks, which would arise by implementing CCS, come in conflict with the potential global risks of instead allowing the CO_2 to enter the atmosphere. The local risks cause a reluctance into taking responsibility for establishing storage sites [58]. But as Medvecky et al argues, the discussions of the technical risks of CO_2 storage, although important, cannot be allowed to halt humanity from performing its moral duty to combat climate change [58].

Another aspect of contention is if leakage can be prevented indefinitely by geological storage or if it is just a short-term fix for reducing the greenhouse-gas emission. Furthermore, geological CO_2 storage will place an economical burden upon future generations in the form of having to maintain storage sites and re-sequestrate CO_2 that has leaked, a possible intergenerational injustice about which only the current generations can decide [58]. Even small leakage rates of 1 % per 1000 years could mean that the CO_2 emissions have only been displaced in time and will come back to haunt future generations as delayed global warming [58]. The risk of sequestration of CO_2 only being a short-term solution for reducing CO_2 emission is a disheartening thought. However, investment into CCS technologies could still be warranted. In the book “Klimat och Moral - Nio tankar om hettan”, Karim Jebari argues that reasoning that can be seen as “unsustainable”, that humanity solves it current, pressing problems, such as in the short-term reducing the greenhouse gas emissions, and leave less pressing problems to coming generations, such as maintaining storage site, might be the most logical approach. Jebari argues that the use of solutions that work over a longer timescale will be nullified if they do not aid us enough short-term for us to survive. [59]

The relevant question at hand is hence whether CCS technologies are a relevant solution for the short-term. Many presented CCS technologies are hampered by several technical problems such as large energy penalties and requiring process redesign [61]. All of them are also facing the practical problems of a global lack of legal and regulatory frameworks for dealing with CCS technologies [61]. The problems have collectively hindered enough CCS plants, according to earlier estimations of the required capacity today, from being reached [61]. It is not unlikely that overestimation and hubris of the technological aspects can have grave consequences, whereby money and resources will be diverted to a technology for which the

necessary capacity cannot be realized [61]. Lenzi raises that the projected needed scale of BE-CCS plants, if met, would threaten food security and biodiversity due to the land requirement for the required biomass [61]. Negative emission technologies (NETs) can also become an excuse for politicians to not diminish emissions in the short-term [61]. Arguments have also been raised that the CCS technologies divert investments away from better short-term mitigation strategies and will extend the lifetime of fossil fuels [60]. However, the heavy reliance of greenhouse gas emission technologies of our current societies should not be forgotten [58]. CCS does provide, from a technological perspective, a pathway for response to climate change without completely changing the primary utilized energy sources [58].

Given this complex background, a number of ethical considerations has been done by the author. First and foremost, the use of fossil fuels is detrimental to the climate, and the use of fossil fuels should not be unnecessarily extended. Instead, its unnecessary use should be terminated. But what must be considered is that poorer countries will not have the possibility of ceasing their fossil fuel usage within the same timeframe as richer countries. Poorer countries will, paradoxically, have to emit more greenhouse gas emissions to be able to protect their people from climate change, much less develop, over the coming years [59]. Hence, fossil fuel usage is likely to continue, with or without CCS implementation, in the coming decades. CCS, and BE-CCS will thereby be a good alternative among an arsenal of mitigation strategies. It would be unethical to utilize CCS technologies to mask the problems with fossil fuels. It will also be unethical to rely too much upon the technological promises of the technologies to not implement other large-scale mitigation strategies, political changes, and adaption policies. Furthermore, the development of the technology could also be another technical advantage over the Global North against the Global South, with the Global South in the future being required to pay for CCS mitigation technology for a problem mainly caused by the Global North. Furthermore, it is likely that energy companies, major producers of greenhouse gas emission, will benefit from CCS implementation. The unethical aspects would be immense, but the problem of climate change would still be addressed, as explained by John Broome in his chapter in “Klimat och Moral - Nio tankar om hettan” [59].

Through my contribution to trying to implement a novel CCS technology, I do not disregard the problems with the studied technology nor rank it superior to other mitigation strategies. However, I make the ethical consideration that the utilization of CCS technologies will benefit the mitigation of greenhouse gas emissions, especially in the short-term, and that this is the most ethical decision today with regards to the technology and the pressing problem of climate change.

Appendix H. Circular structure results

For three of the four stock mixtures that were investigated with the microscope, different circular structures were seen during the investigation. Within this section, images of these circular structures will be presented. Furthermore, the conclusion that the circular structures did not represent carbamate salt particles will be discussed and supported.

For the stock mixture with a CO_2-loading of 0.50, circular structures, although with holes in their perimeter, were seen. An image is shown in Figure A.31. The image was captured with the height adjuster rotor in position P80, different from the setting whereby the carbamate salt crystals were visualized. The region with these circular structures also appeared outside of the main droplet on the microscope slide, and there are clear straight lines separating regions of the circular structures. Similar circular structures were also observed when the *Bottom slurry* was investigated with the second method, where the solvent had been allowed to evaporate from the bottom slurry.

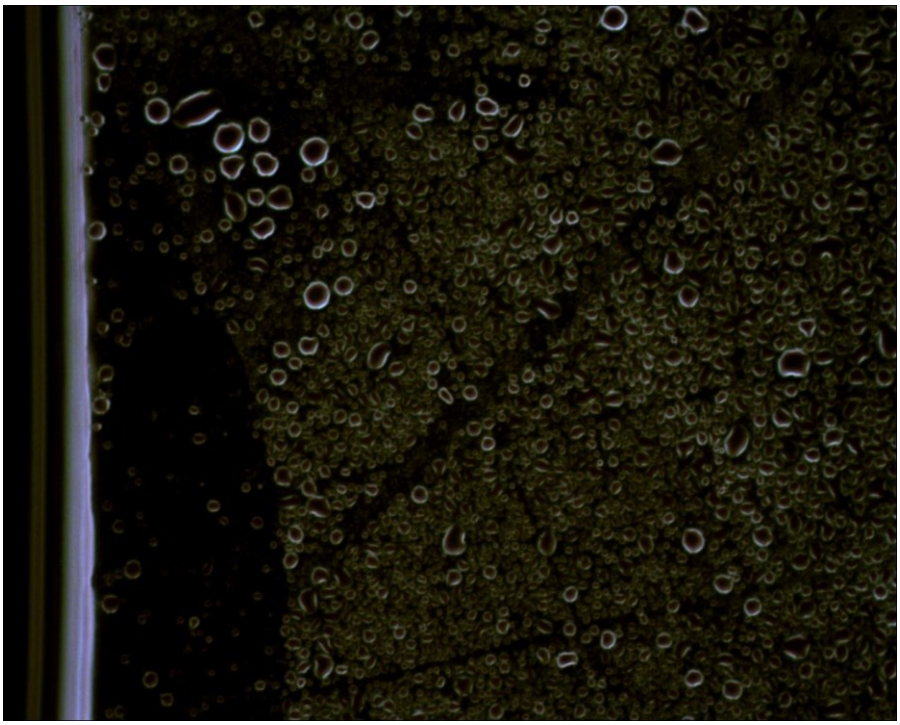

Figure A.31. The small circular structures observed in a minor region of the microscope slide during the investigation of a droplet of the slurry with CO_2-loading of 0.5. The standard magnification was utilized, and the height adjuster was placed in position P80 during the image capturing.

During the investigation of the *Effluent slurry*, circular structures, resembling bubbles, were visible on the microscope slide, which can be seen in the left image of Figure A.32. These were more intensively bright, and did not have holes within their perimeters, in contrast to the ones seen in Figure A.31.

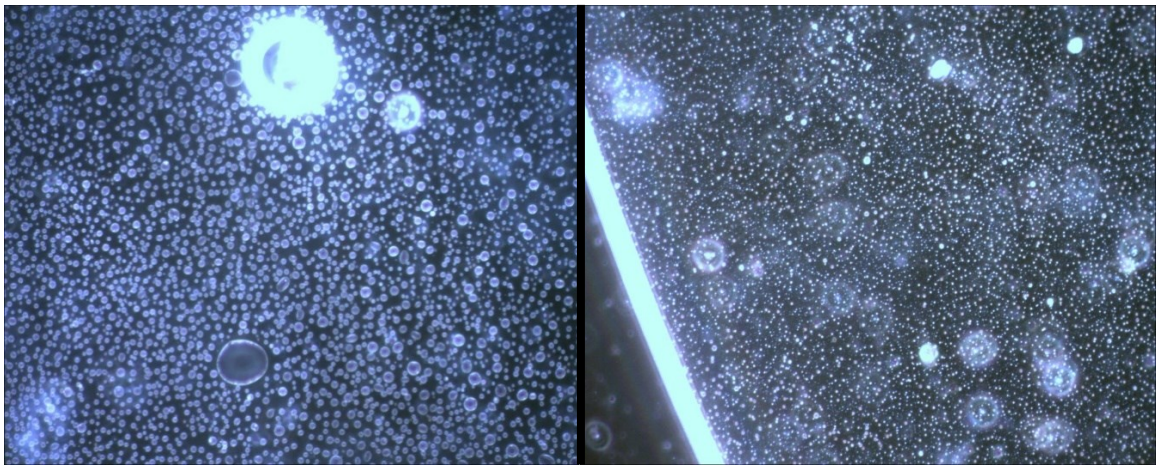

Figure A.32. Images of different circular structures seen in the Effluent slurry from the lamella sedimentation experiment. The standard magnification was utilized, and the height adjuster rotor was placed in position P35 during the image capturing. The bottom image shows two types of spots that were observed within the microscope.

When another amine mixture, studied outside of the master thesis project was investigated with the microscope both these circular structures were found within air bubbles. The interface of the air bubbles can be seen as the double solid, white lines in left and right images of Figure A.33. Within the air bubbles, small circular structures, varying in brightness can be seen. A portion, but not all, of the circular structures in the right image of Figure A.33 have lower light intensity and hole-filled perimeters These images were captured with the same method as the images captured within the master thesis project. In the middle of the left image in Figure A.33, polygon-shaped crystals with straight edges can be seen. However, the polygon-shaped crystals do not extend fully to the other side of the air bubble interface, where only circular structures are visible. The results correspond well to what was seen of circular structures for the mixtures investigated within the master thesis project. Hence, it was deemed that the circular structures did not represent carbamate salt crystals. Instead, it is believed that they were fluid droplets dispersed within air bubbles present under the cover glass.

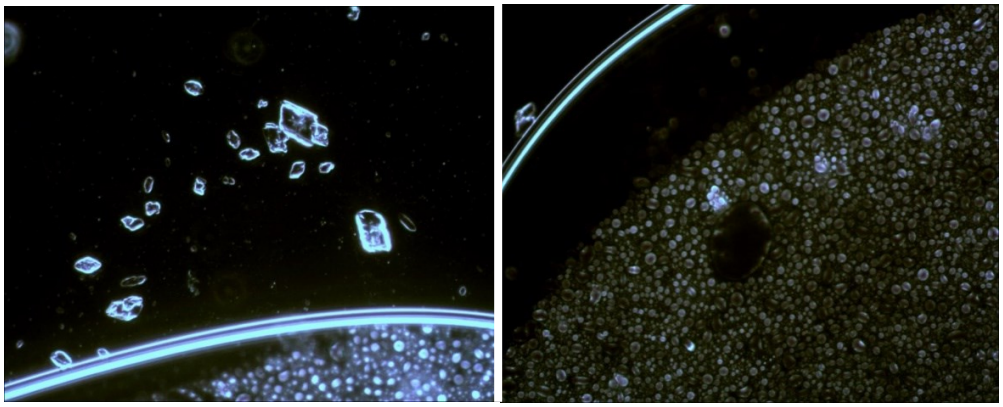

Figure A.33. An image captured with the microscope, using the same method, of an amine slurry studied outside of the scope of the master thesis project. Crystals, with straight edges and polygon-shaped, are seen in the middle of the image. In the bottom of the image, the interface of an air bubble is shown. Within the air bubble, smaller circular structures are visible. Utilized to capture the image was the standard magnification, and the height adjuster was placed in position M10.

In the right image of Figure A.32, there are larger circles with a dot within them, which were inherent to the instrument, and do not represent any object upon the microscope slide itself.

Small, very bright spots are also visible, which are different to the circular structures in the left image of Figure A.32 that were previously discussed. It is believed that these bright spots are not crystals, but that they appear upon a certain magnification due to dust being present upon either the covering glass, the lens, or the illuminator. This is supported by images taken with different magnification of the same location within one sample, see Figure A.34.

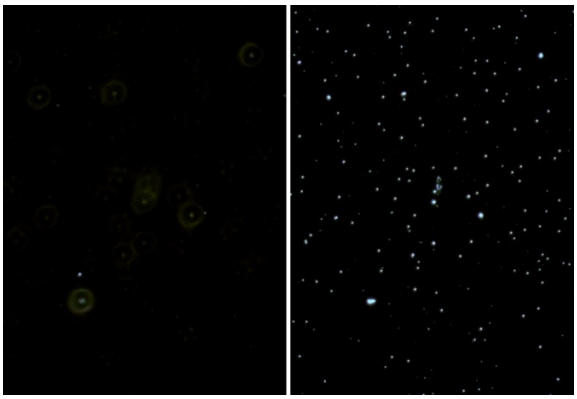

Figure A.34. The images showcase the same location on a microscope slide with effluent slurry upon using different magnifications. In the left image, the standard magnification has been utilized and the height adjuster rotor was in position PM0. In the right image, the height adjuster rotor had instead been rotated into position P90. The light intensity was also adjusted for the second image.